University of Miami
Scholarly Repository

Open Access Dissertations | Electronic Theses and Dissertations

2015-07-27

# Development of Virtual Air/Water Flow Meters Using Fan / Pump Head and Motor Power

Esber Andiroglu
*University of Miami*, e.andiroglu@miami.edu

Follow this and additional works at: https://scholarlyrepository.miami.edu/oa_dissertations

Recommended Citation
Andiroglu, Esber, "Development of Virtual Air/Water Flow Meters Using Fan / Pump Head and Motor Power" (2015). *Open Access Dissertations*. 1467.
https://scholarlyrepository.miami.edu/oa_dissertations/1467

This Open access is brought to you for free and open access by the Electronic Theses and Dissertations at Scholarly Repository. It has been accepted for inclusion in Open Access Dissertations by an authorized administrator of Scholarly Repository. For more information, please contact repository.library@miami.edu.

UNIVERSITY OF MIAMI

# DEVELOPMENT OF VIRTUAL AIR / WATER FLOW METERS USING FAN / PUMP HEAD AND MOTOR POWER

By

Esber Andiroglu

A DISSERTATION

Submitted to the Faculty
of the University of Miami
In partial fulfillment of the requirements for
the degree of Doctor of Philosophy

Coral Gables, Florida

August 2015

©2015

Esber Andiroglu

All Rights Reserved

UNIVERSITY OF MIAMI

A dissertation submitted in partial fulfillment of
the requirements for the degree of
Doctor of Philosophy

# DEVELOPMENT OF VIRTUAL AIR / WATER FLOW METERS USING FAN / PUMP HEAD AND MOTOR POWER

Esber Andiroglu

Approved:

| | |
|---|---|
| _____<br>Gang Wang, Ph.D., P.E.<br>Assistant Professor of Civil, Architectural, and Environmental Engineering | _____<br>Antonio Nanni, PhD., P.E.<br>Lester and Gwen Fisher Endowed Scholar, Professor and Chair of Civil, Architectural, and Environmental Engineering |
| _____<br>Wangda Zuo, Ph.D.<br>Assistant Professor of Civil, Architectural, and Environmental Engineering | _____<br>Dean of the Graduate School |
| _____<br>John Onyango, Ph.D.<br>Assistant Professor of Architecture<br>School of Architecture | |

ANDIROGLU, ESBER (Ph.D., Architectural Engineering)

Development of Virtual Air/Water Flow Meters Using Fan / Pump Head and Motor Power (August 2015)

Abstract of a dissertation at the University of Miami

Dissertation supervised by Professor Gang Wang.
No. of pages in text (156)

Air and water flow rates are key controlled variables in heating, ventilation and air conditioning (HVAC) systems and can have significant impact on overall system performance and efficiency. However, space limitations and expensive installation costs prohibit physical flow meter installations. On the other hand, motor driven fans and pumps are essential components installed in HVAC systems. Since air or water flow rate, fan or pump head and power have correlations, which are determined by fan or pump performance, theoretically the flow rate can be virtually determined by either head, shaft power, or both. Head-power-based virtual flow meters provide more accurate results by eliminating the error caused by the flat section of head and power curves. The available power is either the motor input power obtained from the connected variable frequency drive (VFD) control panel or the VFD input power measured by a power meter. In both cases, the motor efficiency has to be applied to obtain the shaft power. In current head-power-based virtual meter development, motor efficiency is simply chosen as the motor efficiency under a rated frequency fed by sinusoidal power, In fact, the power frequency and harmonic created by the VFD will impact the actual motor efficiency.

The purpose of this study is to develop head-power-based virtual air / water flow meters using the power obtained from either VFD or power meter with precise motor efficiency model. To achieve this purpose, the objectives are: to project motor efficiency

using equivalent circuit theory with the variable frequency impact; to identify the impact of VFD-induced harmonics on the motor efficiency; to validate flow meter using motor efficiency with consideration of both frequency and harmonics impact from both a power meter and VFD output data, and finally verify the developed meter by comparing outcome of each developed model.

Approaches followed to achieve these objectives are: investigation of work conducted by others to date; exploration of a theoretical model for virtual air / water flow meter in order to identify the relationship of fan / pump flow rate with measurable fan / pump head, motor power, power frequency and voltage; application of equivalent circuit theory for motor efficiency estimation; consideration of VFD induced energy losses including harmonic motor losses and investigation of their impact on motor efficiency calculations, and finally application of these explorations for the development of multiple theoretical models for the implementation of virtual air / water flow meters along with their validation through experiments. Comparison of outcomes from different meter models developed showed that the water flow rates determined using the model with impact of VFD induced harmonics degradation considered on VFD and motor efficiencies, proved to yield consistently most reliable results for full range of operating speeds, indicated by the R-square of 0.97 for instant measurement.

# ACKNOWLEDGEMENTS

I would like to express my special appreciation and thanks to my advisor and committee chair, Professor Gang Wang; you have been a tremendous mentor for me. I would like to thank you for guiding and encouraging my research and for allowing me to grow as a research scientist. Your patience and dedication along the process has truly inspired and enabled me.

I would also like to thank my committee members, Professor Wangda Zuo and Professor John Onyongo for serving as my committee members, and Mr. James Sprinkle of the University of Miami Facilities Department, for providing access to and facilitating collection of data from Richter Library chiller plant, utilized for the experimental investigation phase of this study. Resources, procedures and outcomes utilized and generated as part of this study, sets an example for positive benefits of interdisciplinary collaboration between Architectural Engineers, Facility Managers and Energy Managers. This has been demonstrated by direct interaction of the researcher associated with this study and the University of Miami Facilities Department, by having access to, and ability to collect data from an actual chilled water plant in use at the Coral Gables campus. The outcome of this collaboration has not only benefited the academic program offered by the Civil, Architectural and Environmental Engineering Department at the University of Miami, it has also provided new design approaches for Architectural Engineers and useful maintenance and energy management tools for the operations, maintenance and energy management teams at the University Facilities Department.

A special thanks to Professor Antonio Nanni, for not only serving as my committee member, but more importantly, for encouraging and providing me the opportunity to pursue this dream. He continually and persuasively conveyed a spirit of adventure in regard to my potential to achieve this goal at a late stage in my academic career. Without his vision and constant encouragement this dissertation would not have been possible.

TABLE OF CONTENTS

LIST OF FIGURES

LIST OF TABLES

# LIST OF PUBLICATIONS

1. **Andiroglu, E**. Wang, G., Song, L. Kiamehr, K. 2015. Development of a Virtual Pump Water Flow Meter Using Power Derived from Comprehensive Energy Loss Analysis. Science and Technology for the Built Environment section at ASHRAE (submitted on April 2015).
2. **Andiroglu, E**., Wang, G., Song, L. 2013. Development of a Virtual Water flow Meter using Pump Head and Motor Power. Zero Energy Mass Customization Housing (ZEMCH2013) International Conference, October 30-Nov 1, 2013, Miami, FL.
3. Wang, G., **Andiroglu, E**., Sprinkle, J. E. 2015. Experimental Investigation of Energy Performance of a Variable-Frequency Drive on a Drive-Motor-Pump System. Submitted for presentation at the ASHRAE Annual Conference in Atlanta. ASHRAE Transactions, Volume 121, Part 2.
4. Wang, G., Song, L., **Andiroglu, E**., Shim, G. 2014. Investigations on a virtual airflow meter using projected motor and fan efficiencies. HVAC&R Research. 20(2):1-10.

# LIST OF NOMENCLATURE

| | |
|---|---|
| d | = design |
| D | = impeller diameter |
| f | = VFD output frequency, Hz |
| H | = pump head, Pa |
| $H_m$ | = manufacturer pump head, Pa |
| $I_1$ | = stator input current, A |
| $I_2$ | = rotor or load current, A |
| k | = pump curve correction factor, kPa/(L/s)$^2$ |
| ℓ | = fan or pump curve factor |
| PF | = power factor |
| Q | = pump water flow rate, L/s or fan air flow rate, m$^3$/s |
| $R_1$ | = stator winding resistance, Ohm |
| $R_2$ | = rotor winding resistance, Ohm |
| $R_c$ | = core loss resistance, Ohm |
| s | = motor slip based on synchronous speed |
| V | = VFD output voltage, V |
| $V_1$ | = input voltage, V |
| $V_2$ | = rotor or load voltage, V |
| $V_m$ | = magnetizing or air gap voltage, V |
| W | = power, kW |

$W_F$ = motor power friction loss, kW

$W_{f/p}$ = fan or pump power, kW

$W_{F\&W}$ = motor power friction and windage losses, kW

$W_{input}$ = motor input power, kW

$W_{motor}$ = VFD output power, kW

$W_{motor,ideal}$ = ideal motor input power, kW

$W_{rotor}$ = motor rotor mechanical output power, kW

$W_R$ = reactive power, kW

$W_{shaft}$ = pump shaft power, kW

$W_{VFD}$ = VFD input power, kW

$W_W$ = motor power windage loss, kW

$W_{water}$ = mechanical work received by water, kW

$X_1$ = stator leakage reactance. Ohm

$X_2$ = rotor leakage reactance. Ohm

$X_m$ = magnetizing reactance, Ohm

$\eta$ = efficiency

$\eta_{f/p}$ = fan or pump efficiency

$\eta_{harm}$ = harmonic-degraded efficiency

$\eta_{motor}$ = motor efficiency

$\eta_{motor,ideal}$ = ideal motor efficiency based on purely sinusoidal power input

$\eta_{pump}$ = pump efficiency

$\eta_{VFD}$ = VFD efficiency

$\eta_{V\&H}$ = VFD-harmonic efficiency

$\eta_{raw}$ = motor raw efficiency

$\omega$ = relative pump speed based on the reference speed, rpm

$\omega_{syn}$ = relative speed, rpm

Subscripts:

d = design

i = sample

n = sample

r = reference speed

s = static

sine = sinusoidal

syn = synchronous

# CHAPTER 1

# INTRODUCTION

There has been no shortage of studies, discussions and debates surrounding the concept of energy efficiency over the past 40 years. In the early 1970s, when two international petroleum crises led to dramatic rises in the cost of energy, the major industrial countries were forced to consider a sobering possibility: that the world's supply of energy resources might be finite. The U.S. Energy Information Administration (EIA, 2010) reports that, in coming years, building sector energy consumption will grow faster than that of industry and transportation. Between 2012 and 2030, total building sector energy consumption will increase by 4.74 Quadrillion Btu (QBtu). Industry will grow by 3.33 QBtu and transportation is expected to decrease by 0.37 QBtu (EIA 2010). To put these projections into perspective, 1 QBtu is equal to the delivered energy of thirty-seven 1000-MW nuclear power plants, or 235 coal-fired power plants at 200-MW each (EIA, 2010). Effectively addressing the U.S. and world's energy needs in the near and long-term has important design implications for the building sector. This may be accomplished with help of building sector professionals by implementing incremental set of targets. Building sector professionals can dramatically reduce U.S. and global energy consumption and greenhouse gas emissions (GHG) over the next twenty years and beyond. Heating, ventilation and air-conditioning (HVAC) systems in commercial and residential buildings are responsible for more than 40 percent of total energy use (DOE 2008). Energy consumption by pumps and fan motors significantly contribute to total energy consumed by building HVAC systems. When water distribution in water sourced HVAC systems and air distribution in variable volume air handling systems do not have

an accurate dynamic response to varying building demand loads, overall system efficiencies, and consecutively overall energy consumption at a given building declines substantially (DOE 2010).

Today, a variety of flow meters with advanced capabilities are available for use by the HVAC industry to measure flow in hot or chilled water systems and provide the baseline and load profile information necessary to evaluate and ultimately improve the efficiency of a system. Certain flow meters demonstrating a very high rate of accuracy can also be commissioned as revenue-grade thermal energy meters, used to monitor a customer's energy usage for billing purposes and provide an accurate picture of their energy consumption behaviors. However, various issues ranging from reliable performance and accuracy, space limitations and device and installation costs often prohibit physical flow meter integration into system plants (Wang et al. 2005). Such challenges render the use of virtual flow meters as the most ideal choice.

The purpose of this study is to develop virtual fan air flow meters and virtual pump water flow meters using the fan / pump-motor system performance. Potential benefits of virtual flow meters were clearly identified during the experimental investigations carried out as part of this study. Virtual air / water flow meters can be integrated into system controls as real-time correction and calibration tools for optimal operation; they can be instrumental for balancing, commissioning and energy accounting of centralized chilled water plants serving multiple buildings, or central station air handling systems with varying demand loads. This thesis, outlines the development of a virtual air / water flow meters based on fan / pump head and motor power, with high level of accuracy for all operating conditions. An overview of significance of integration of flow metering

applications into building energy management systems (EMS), along with types of physical and virtual flow meters available in the industry, as well as recent developments in virtual metering technology are presented in Chapter 2. Air / water flow meter theory based on fan / pump laws coupled with effects of motor and variable frequency drive (VFD) efficiency are discussed in Chapter 3. An experimental investigation of a simplified virtual air flow meter development model with all fan / pump and motor losses covered by a pseudo fan / pump efficiency is detailed in Chapter 4, while a similar model is discussed based on a different experimental set up for virtual water flow meter model in Chapter 5. Energy losses associated with VFD along with impact of VFD induced harmonics on overall motor energy losses and motor efficiency are investigated in Chapter 6. A more detailed look at impact of motor harmonic losses and harmonic-degraded VFD and motor efficiencies on the power-head based virtual water flow meter model is presented in Chapter 7. Chapter 8 provides a comparison of various virtual flow meter model accuracies based on experimental study outcomes. Finally, overall conclusions are summarized in Chapter 9.

# CHAPTER 2

# VIRTUAL SENSING TECHNOLOGY LITERATURE REVIEW

## 2.1 Challenges in achieving optimum operating efficiency

While efforts to reduce energy usage may not be new, energy efficiency has risen to even greater prominence in recent years as energy costs and environmental concerns continue to increase exponentially. No one is more aware of this trend than the HVAC industry, which must contend with an ever-expanding list of regulations, guidelines and initiatives emphasizing the importance of energy-efficient HVAC in buildings, as summarized below:

**Energy Policy Act of 2005** (EPAct)

Passed by the US Congress and signed into law by former President George W. Bush, the Energy Policy Act of 2005 focuses on reducing energy consumption in a number of ways, including establishing tax incentives and loan guarantees for energy efficiency measures on new buildings and HVAC systems. The Act also requires that all federal buildings install advanced metering systems capable of measuring energy consumption on a daily basis (in effect since October 2012).

**Leadership in Energy and Environmental Design** (LEED)

Developed by the US Green Building Council in 2000, LEED is an internationally recognized green building certification system providing third-party verification / commissioning that a building or community meets strict environmental standards in

such categories as energy efficiency, greenhouse gas emissions and indoor air quality. Flow metering can be a valuable tool for verification and commissioning process of systems.

**Clinton Climate Initiative** (CCI)

In 2006, former President Bill Clinton and his charitable foundation established the Clinton Climate Initiative with the goal of cutting global greenhouse gas emissions (CCI). One of the major programs stemming from this initiative is the Energy Efficiency Building Retrofit Program, which operates in large cities worldwide to retrofit existing buildings with energy-saving products, technologies and systems.

Additional guidelines for energy-efficient HVAC systems are set forth by technical organizations such as the American Society of Heating, Refrigerating and Air-Conditioning Engineers (ASHRAE), which boasts an international membership of more than 50,000. ASHRAE regularly publishes updated building standards that are widely accepted by building engineers and HVAC professionals, including standards related to energy efficiency in HVAC system design and operation.

As facility managers are now being held more accountable for the overall energy consumption of the buildings they oversee, having access to highly accurate and reliable flow metering technology has become vital. Flow meters make it possible for facility managers to measure the performance of various HVAC systems and ultimately make the best possible decisions to optimize efficiency and manage energy consumption.

It is clear that energy efficiency is not a passing trend, but rather a sweeping influencer of worldwide social, political and economic thought. Accordingly, legislation related to the more efficient use of energy by buildings is likely to increase in both abundance and stringency in the coming years. This makes it crucial for facility managers to carefully monitor the performance of the various HVAC systems responsible for maintaining the environmental comfort of a building, whether it is a small residential apartment complex or an immense international airport.

Keeping HVAC systems running properly and at peak efficiency is the first step in managing facility energy use. In spite of years of studies, demonstration programs, and published stories to the contrary, most facility organizations today still operate in a reactive mode. Though facility executives know that is far better to schedule maintenance activities using planned and predictive maintenance tools, most continue to spend the bulk of their resources operating reactively. The most common reasons cited for this is the lack of sufficient resources (DOE 2010). This approach to maintenance with respect to HVAC systems is particularly troubling given the role that HVAC systems play in today's facilities. The importance of good HVAC system maintenance goes beyond just controlling energy use. Buildings today depend on properly operating systems for more than just people comfort. For example, most telecommunications systems have requirements for specific environmental conditions to operate properly. Temperatures and humidity levels that fall outside of this range can lead to interruption in services and even costly system failures. Sometimes the difference between keeping a business running and having to shut down is nothing more than proper HVAC system operation and maintenance. Contributing to this belief is the unfortunate fact that HVAC systems are

not the most noticeable components in a facility. Unlike highly visible items, such as carpet or lighting systems, most HVAC systems are out of sight and out of mind, until something goes wrong. And when something does go wrong, it is too late for maintenance to be performed efficiently. Maintenance at that point becomes reactive (DOE 2010).

Reactive maintenance is the most costly way to maintain building HVAC systems. Organizations that have implemented comprehensive planned and predictive maintenance programs show dramatic decreases in maintenance costs. And when factors are included, such as extended equipment life, reduced energy use, less frequent system downtime, and decreased interruptions to building operations, organizations that have implemented comprehensive maintenance programs find that their total costs can be as much as 50 percent (DOE 2010) lower than the costs for those organizations that continue maintain equipment reactively. One of the easiest benefits to document is how HVAC maintenance affects energy efficiency. Facilities in which proper HVAC maintenance is completed will use at least 15 to 20 percent (DOE 2010) less energy than those where systems are allowed to deteriorate. For example, consider the operation of a central building chiller. Building chillers typically are the single largest user of electricity in a facility. To keep them operating as efficiently as possible, maintenance tasks must be performed on a daily, weekly, monthly and annual basis. Letting such tasks lapse, the efficiency of the plant will decrease, increasing energy use. Start with the chiller operating log; work with the chiller manufacturer or a service company to translate the log data into an operating efficiency curve for the chiller; develop a similar curve for what the efficiency of the chiller would be if all maintenance were performed at the recommended intervals. The

difference between the two operating efficiencies can be translated into energy and cost savings. Due to the high energy use of the equipment, even small increases in efficiency will result in large savings.

While the energy savings estimates for chillers, boilers, and many other HVAC systems is straight forward, others savings estimates may not be. Consider VAV systems where use of a flow station for volumetric flow tracking is essential in order to correlate outside air damper position and space load response using variable speed fan drive signal. In such system applications, fan motor power consumption may be significantly impacted. Outside air dampers require regular maintenance to respond properly to the temperature control system's demand for ventilation air. If the damper linkage is out of adjustment, or if it sticks open, more ventilation air will be introduced than necessary, requiring the system to use more heating or cooling energy to condition that air. Regular inspection, testing and maintenance of the damper will keep it operating properly, minimizing energy use (DOE 2010). In general, EMS with reliable sensors is essential to achieve HVAC system optimal operation.

**2.2 Significance of sensors for EMS**

EMS are centralized, interlinked, networks of hardware and software, which monitor and control the environment in commercial, industrial, and institutional facilities. While managing various building systems, the automation system ensures the operational performance of the facility as well as the comfort and safety of building occupants. EMS are also one of the main resources for property owners and engineers for ensuring optimum operating efficiencies.

Most of the automation system is behind the scenes as hardware devices and sensors mounted to equipment or hidden under floor or in the ceiling. Important data providing insight towards real time performance characteristics of building systems need to be collected and analyzed in real time, in order to be able to dynamically address deficiencies in system performance and avoid energy waste. From a central management perspective, the EMS resides as software on an operator workstation (computer) or is available as a web page. Various types of "controllers" and "data loggers" manage equipment and portions of the network. "Sensors" provide input data to the controllers. Some of the most significant devices in utilized in HVAC system monitoring are:

- Thermometers and pressure gauges

  They are required on the suction and discharge side of all pumps, chillers, boilers, heat exchangers, cooling coils, heating coils, and cooling towers.

- Duct static pressure gauges

  They are provided for the central air-handling unit air supply fan discharge, branch take-offs of vertical supply risers and at all duct locations at which static pressure readings are being monitored to control the operation of a VAV system.

- Differential static pressure gauges

  They are placed across filters in air-handling units and to measure building pressure relative to the outdoors.

- Flow Measuring Devices.

Airflow measurements are required for all central air-handling units. Measurements are provided at the supply air duct, return air duct, and the outside air duct.

- Water flow or energy measuring devices

  These are required for each chilled water refrigeration machine, hot water boiler, pump, and connections to district energy plants, in order to calibrate and optimize system operating efficiencies. In addition, individual water flow or energy measuring devices are very useful for monitoring chilled water flow rates serving computer rooms and chilled water and hot water lines to out leased spaces. Flow measuring devices are capable of communicating with the central EMS. Data obtained from water flow and air flow measuring devices confirm or validate ASHRAE 90.1 requirements.

- Power Meters

  These devices offer comprehensive power and energy measurement data that is unique to each system component it is applied to. Such data is very useful to EMS engineers for early fault detection of large power consuming system components and result in significantly reduced day-to-day operating costs.

Temperature, pressure, power and flow data typically provide four rudimentary measurement values; however, collectively they enable the determination of exceptionally important thermal energy production and

utilization metrics for data centers using chilled water as a cooling medium (DOE 2010).

Wang et al. (2012), developed an optimal supply air temperature control, which correlates supply airflow rate, for air handling units (AHUs). Gao et al. (2011), pointed out that energy efficient pump control strategies should maintain the water flow rate in the secondary loop lower than the water flow rate in the primary loop in chilled water systems. Zhao et al. (2014), developed several effective fault detection and diagnostic methods for chillers, which heavily depend on the water flow rates of evaporators and condensers. Celenza et al. (2015), demonstrated that the accuracy of water flow measurements is critical for heat meters in buildings.

**2.3 Significance of flow metering applications**

In current HVAC industry practice, the control and performance monitoring of equipment and systems are often limited by the number of physical sensors installed. The costs of hardware and installation are usually cited as the reason for not installing more sensors. Virtual sensors or meters may provide a lower-cost alternative to physical meters. Water flow measurements in hydronic systems are critical for operation, control, and fault detection of water sourced HVAC systems. Faulty or inefficient operations can lead to energy consumption 15% to 30% greater than optimal operation (Friedman et al. 2007). Available water flow measurements in chilled and / or condenser water loops can enhance the operating efficieny of multiple system components, including chilled water pumps, condenser water pumps, modulating water valves, chillers and air handling units by detecting faults more easily and consequently operating more efficiently. Significance

of air / water flow measurements in building HVAC systems may be highlighted based on components outlined in Figure 2.1 below and can be summarized as :

- Staging of pumps, fans, chillers
- Testing / Balancing & Commissioning
- HVAC fault detection
- Energy management & metering
- Equipment safety

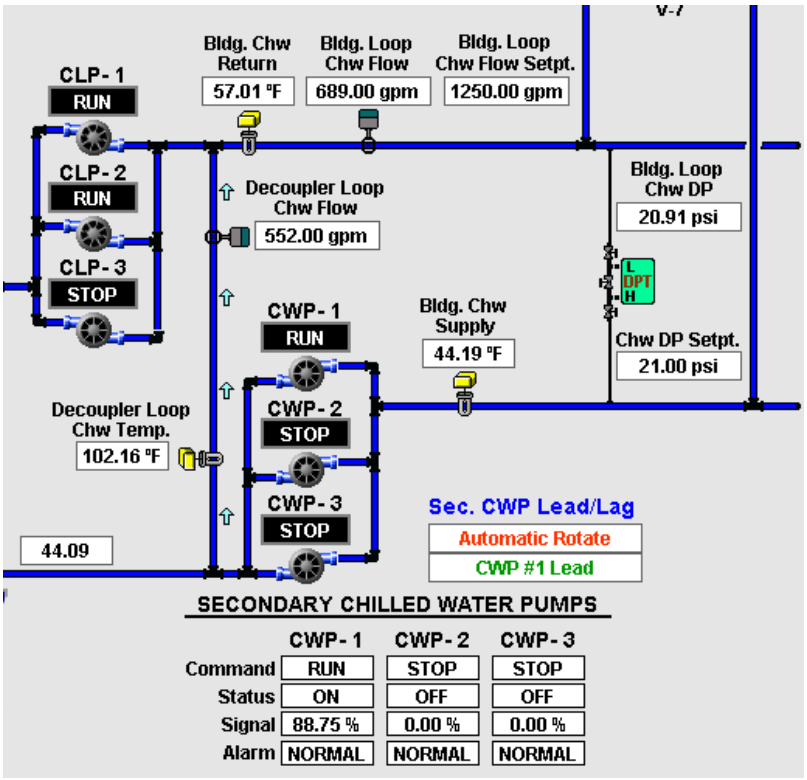


Figure 2.1: Building chilled water loop schematic example

Devices noted above are very important to a building engineer and provide essential data for maintaining optimum operating efficiency for systems, and ideal comfort levels for building occupants. Temperature and pressure sensors and gauges are relatively low cost devices and as a result, widely utilized in most buildings. While power meters may not be readily utilized in most building systems, power data is typically available at most HVAC system plants, as a byproduct of variable frequency drives installed for large motors. On the other hand, although essential, flow measuring devices are typically omitted in building HVAC plants due to their high cost.

While all HVAC system plants seem to have an adequate number of pairs of supply and return temperature sensors, flow measurement devices seem to be a little rarer; however simultaneously measuring flow and temperature provides an opportunity to gain a greater degree of control of a chiller plant,. Similarly, air flow measurements and control of VAV systems based on static pressure control is instrumental for minimizing supply fan energy for large central station type air handling units (Liu 2002). Electrical measurement describes “electricity”, which is (for all practical purposes) a “force”. Chilled water, on the other hand, is “thermal energy”, and has considerable mass, and can “give-up” or “absorb” heat while doing its work or when being processed through chillers, heat exchangers, or free cooling devices. With “two temperature sensors and a flow device”:

- the entire chilled water plant can be measured, and
- chilled water production of a chiller can be measured, and
- the chilled water consumption of various building zones can be measured, and

- in multi-use buildings, the consumption of each occupancy zone can be separated from the rest of the building (DOE 2010).

The units of measure are simple and whether you are partial to measuring chilled water production and consumption in "tons" or "kilowatts" of heat, the procedure can be done manually or (better yet) can be computed by a building automation system, and even updated and displayed in real time.

For example, the flow meter and temperature sensors may deliver their outputs to a building automation system in regionally appropriate (English or metric) units, and the EMS can continually calculate and display chilled water production or consumption. Typically, the chiller plants serve multiple departments within a building, with sets of these three tools installed, the opportunity to accurately apportion and "cost allocate" the thermal energy becomes easy.

Since flow is "time-based", in other words, expressed in cubic meters per second ($m^3/s$) or gallons per minute (GPM), the result of the calculation will also be "time-based", just like the kilowatthours of electricity (or any other input energy) used to produce the chilled water. These important, related time based measurements, chilled water produced and electricity used can be automatically compared, to assess the efficiency of the plant and the building(s) it serves. In summary, installation of sets of 2 temperature sensors and a flow device, can result in improved plant efficiency, as the information that it produces can be used to optimize pump and chiller performance, restore the originally intended delta-T to the chilled water system, and accurately allocate

chilled water use. In parallel with improved efficiency and comfort levels at the property, costs and cost allocation across the enterprise will likely improve.

**2.4 Types of flow meters in use and associated challenges** (ASHRAE 2009)

Today, a variety of flow meters with advanced capabilities are available for use by the HVAC industry to measure flow in hot or chilled water systems and provide the baseline and load profile information necessary to evaluate and ultimately improve the efficiency of a system (Yu, 2011). Certain flow meters demonstrating a very high rate of accuracy can also be commissioned as revenue-grade thermal energy meters, used to monitor a customer's energy usage for billing purposes and provide an accurate picture of their energy consumption behaviors.

Several different flow measurement technologies can adequately meet the needs of the HVAC industry. Below is a brief description of four types of flow metering technologies that are particularly well suited for HVAC flow measurement.

**Differential pressure**

The most traditional method for measuring the flow of liquids, gases and steam, differential pressure flow meters enjoy a longstanding reputation for reliability. This tried-and-tested technology has been utilized by the HVAC industry for many years to measure flow in a variety of applications, depending on which primary elements (pitot tubes, Venturi tubes, orifice plates, etc.) are paired with the meter (ASHRAE 2009). Appropriate applications include natural gas boilers, air ducts, combustion intakes, boiler stacks and chilled water.

**Electromagnetic**

Suitable for measuring the flow of almost all electrically conductive liquids, pastes and slurries, and an appropriate replacement for traditional mechanical flow meters when greater functionality is required, electromagnetic flow technology is the right choice for the vast majority of hot and chilled and water applications, including new installations and small line sizes below 12 in (30.5 cm).

**Vortex**

Vortex flow technology can provide accurate volumetric and mass flow measurements of steam, gas and liquid flow independent of conductivity, viscosity, temperature, density or pressure, and is not negatively impacted by high moisture content. This makes vortex flow meters ideal for measuring energy consumption in HVAC applications that experience fluctuating temperatures and/or pressures, including burners, boilers and compressed air systems.

**Clamp-on ultrasonic**

While other flow technologies often have difficulty coping with low load periods and low flow, clamp-on ultrasonic flow meters are capable of accurate flow measurement at any velocity. Clamp-on meters are particularly useful for retrofit projects in which the pipeline cannot be isolated, as well as for hot and chilled water sub-metering. Overall, clamp-on technology is optimal for measuring flow in a wide range of building management, power plant, university and district energy heating and cooling applications,

including condenser water, potable water, glycol, thermal storage, river and lake water, lake source cooling, chemical feed, and ammonia feed.

**2.5 Virtual flow meter**

Air / water flow rate is often determined by use of pressure based meters such as Pitot tube, Orifice plate or Venturi meter, (ASHRAE 2009). However, valves, bends and fittings close to the air / water flow measurement devices can cause errors. Long, straight duct / pipe sections should be installed upstream and downstream of the flow measurement devices to assure fully developed flows. These conditions are hard to be satisfied in actual systems. For existing systems, high retrofit cost may prohibit installing a new air or water flow meter. In addition, because flow measurement accuracy decreases as the flow rate decreases in variable volume systems, the accuracy of air or water flow measurements from traditional meters is not reliable at lower flow rates. The virtual air / water flow meters can be used along with other measurements to estimate fan / pump efficiency, cooling energy consumption and chiller efficiency in buildings, while serving as a valuable management tool for a building energy management and control system. Fans and pumps are always installed in HVAC sytems.

In fact, vitural sensing technology is not only applied in flow measurement but also is applied in other field. In this section, the general virtual sensing technology is first reviewed, then virtual flow sensors are reviewed.

**Virtual sensing / metering technology**

There has been steady development of virtual sensing technology over the past decade within a broad range of domains, including avionics, autonomous robots, telemedicine, traffic, automotive, nature and building monitoring and controls (Yu, 2011; Wang 2005).

A virtual sensor uses low-cost measurements and mathematical models to estimate a difficult to measure or expensive quantity. Virtual sensors have been successfully developed and applied in various fields within the past two decades. It is believed that widespread application of virtual sensors for buildings would enable a level of building optimization and improvement not previously considered to be economical. Embedded intelligence is a key to improving the performance of systems in terms of early fault detection, safety, calibration, energy efficiency, environmental impacts and cost. Building systems rarely provide feedback on energy efficiency or the need for service and generally do not provide optimized controls. Today, although significant gains have been achieved via use of EMS, often not enough improvements are noted in terms of overall operating efficiency in most buildings. Building systems can be very large and complex, often serving hundreds of zones with varying needs and controllers, requiring thousands of sensors to adequately monitor performance. With such large and complex systems, often cost becomes a prohibitive factor. Lowering the cost of sensing through the availability of virtual sensors helps in attacking this problem with potential for providing high level of performance monitoring information at significantly reduced cost. Virtual sensors have several other advantages in addition to lower cost. For example, virtual sensors could be more easily added as retrofits in existing buildings. In some cases, it is

very difficult to install physical sensors that can accurately measure a desired quantity. For example, it is very difficult to obtain accurate mixed air temperature measurements at the inlet of cooling coils or evaporators because the compactness of the mixing chamber creates highly non-uniform flow and temperature characteristics.

Steady, optimum performance in buildings require continuous commissioning of the building systems. Continuous commissioning can be further defined as continuous monitoring and automated fault detection and diagnostics of building systems. Within a building's life cycle, the majority of the human effort is placed on initial design and specification of the building HVAC systems, whereas the majority of the costs occur during long term operation and utilization of these systems. Problems that develop during operation are often ignored unless they directly or indirectly impact occupant comfort; unfortunately, the same problems often result in significant loss in operating efficiency (Cisco, 2005; Katipamula, 2005; Liu et al. 2004). Continuous commissioning is very costly in buildings, since it entails ongoing inspections, measurements, data collection and analysis; as result, even the very large buildings equipped with wide variety of EMS, perform such task only periodically. Although BAS managers intend to accomplish the same via remote monitoring of building systems, most systems lack embedded intelligence that could provide automated continuous commissioning with automated diagnoses and fault detection.

Virtual sensing techniques could facilitate the development of more cost-effective and robust diagnostic tools for optimal system operation. Some of the most recent developments in this area can be identified as follows:

**1. Vapor compression air conditioner application:**

- Virtual refrigerant charge sensor (Li & Braun, 2009)
- Virtual liquid line pressure sensor (Li & Braun, 2009)
- Virtual suction line pressure sensor (Li & Braun, 2009)
- Virtual evaporator pressure sensor (Li & Braun, 2009)
- Virtual condensing pressure sensor (Li & Braun, 2009)
- Virtual compressor discharge pressure sensor (Li & Braun, 2009)
- Virtual refrigerant flow rate sensor (Li & Braun, 2004, 2007)
- Virtual compressor power consumption sensor (Li & Braun, 2004, 2007)
- Virtual equipment energy ratio sensor (Li & Brain, 2004, 2007)
- Virtual compressor coefficient of performance sensor (Li & Braun, 2004, 2007).
- Virtual supply air humidity sensor (Li & Braun, 2004, 2007)

**2. Chiller**

- Virtual overall condenser heat loss coefficient (Wang and Cui, 2006; McIntosh, et al. 2000; Reddy 2007).
- Virtual overall evaporator heat loss (Wang and Cui, 2006; McIntosh, et al. 2000; Reddy 2007).
- Virtual reduced evaporator water flow (Wang and Cui, 2006; McIntosh, et al. 2000; Reddy 2007).
- Virtual reduced condenser water flow (Wang and Cui, 2006; McIntosh, et al. 2000; Reddy 2007).

**3. Heat pumps**

- Virtual check valve leakage for fixed orifice expansion device (Li & Braun, 2009).
- Virtual check valve leakage for thermal expansion valve (Li & Braun, 2009)
- Virtual reversing valve leakage indicator (Li & Braun, 2009).

**4. Air handling units**

- Virtual mixed air temperature sensor (Wichman & Braun, 2009)
- Virtual DX cooling coil capacity sensor (Yang & Li, 2010)
- Virtual DX cooling coil sensible heat ratio (Yang & Li, 2010)
- Virtual DX cooling coil cooling capacity (Yang & Li, 2010)
- Virtual filter efficiency sensor (Ward & Siegel, 2005)
- Virtual filter bypass low drop sensor (Ward & Siegel, 2005)

**5. Building envelope and zone systems**

- Virtual frequency of hot and cold complaints sensor (Federspiel, 2000)
- Virtual hot and cold complaints impact sensor (Federspiel, 2000)
- Virtual total solar radiation sensor (Seo, et al. 2008)
- Virtual direct solar radiation sensor (Seo, et al. 2008)
- Virtual diffuse solar radiation sensor (Seo, et al. 2008)

**Virtual flow meter**

Virtual flow metering is a method of calculating the flow rates through a system based on the existing instrumentation, knowledge of the facility and the properties of the fluid. This is made possible with the use of correlations that relate the flow rate to the

pressure drop through the system. Currently, although virtual flow metering can be considered as an alternative to physical metering, its accuracy in certain operating conditions is found to lack reliability.

Significance of use of flow meters in achieving and maintaining optimum efficiency in hydronic HVAC system applications has been summarized above. While a variety of different types of flow meters are available in the industry, their application and integration into building systems is not necessarily simple and easy. As pointed out above, various issues ranging from reliable performance and accuracy, space limitations and device and installation costs often prohibit physical flow meter integration into system plants. Such challenges renders the use of virtual flow meters as the most ideal choice.

Virtual meters provide a lower-cost alternative to physical meters. Li and Braun (2007) proposed two approaches to calculate the refrigerant flow rate through a compressor from measurable operating parameters. One approach utilizes suction and discharge pressure, suction and ambient temperature with empirical volumetric efficiency while another approach utilizes compressor power, discharge temperature and pressure, and suction temperature and pressure using energy balance. Yu et al. (2011) proposed a virtual supply air flow rate meter for rooftop units based on measuring outdoor air, return air and supply air temperature and outdoor air and zone air wet bulb temperature using empirical cooling capacity of the direct expansion (DX) coil. Zhao et al. (2012 and 2014) and Zhao (2015) estimated the chilled and condenser water mass flow rates through the evaporator and condenser of a chiller using the energy balance on the compressor, evaporator, and condenser. Measured refrigerant enthalpy at compressor outlet and inlet,

refrigerant enthalpy at condenser outlet, saturated liquid refrigerant enthalpy, condenser water outlet and inlet temperature, and evaporator water inlet and outlet temperature as well as estimated refrigerant mass flow rate are applied in the water flow calculation. Complex thermodynamic models and calibrations, and numerous direct measurements are required in these virtual flow meters.

Wang (2014) developed a simple method to determine the water flow rate through chillers by combining pipe resistance coefficients and pressure drop based on the Bernoulli's equation and the Darcy-Weisbach equation for pressure loss. This method only demands one measurement of the pressure drop and one calibration of the resistant factor. However, since the pressure drop is proportional to the flow squared, the accuracy within a low flow range may be significantly degraded. Swamy et al. (2012) estimated the water flow rate through a cooling coil using the similar fluid mechanic principle. To avoid the low pressure drop within a low flow range, differential pressure across both the coil and valve was applied. The valve installed characteristic curve needs to be calibration. Two measurements, the pressure drop and the control valve position, and one calibration are required in this virtual valve meter. Virtual meters developed for HVAC systems were summarized by Song et al. (2012, 2013).

The virtual meters that were discussed provide alternative methods to measure the supply airflow of DX rooftop units, the water flow in the condensing water and primary chilled water loops of chillers, and the chilled water through the cooling coil of AHUs. However, the return airflow of AHUs and the water flow in the secondary chilled water loop of chillers and in the primary and secondary hot water loops of boilers cannot be

measured using these virtual meters. In fact, motor-driven fans and pumps are essential components installed in HVAC systems and share the same governing laws. Variable frequency drives (VFDs) are widely used in HVAC systems to reduce fan and pump energy consumption by reducing the motor speed at partial flow rates. Since air or water flow rate, fan or pump head and power have correlations, which are determined by fan or pump performance, theoretically the flow rate can be virtually determined by either head, power, or both. The fan or pump head can be measured by a differential pressure transducer. On the other hand, the fan or pump shaft power is not measurable by a power meter, while the motor input power can be directly obtained from the connected VFD control panel and the VFD input power can be measured by a power meter. So the fan or pump shaft power can be calculated from either the motor input power with modifications using the motor efficiency or the VFD input power with modifications using both the motor and VFD efficiencies. The virtual fan and pump flow meters can measure both the supply and return airflow of AHUs and the water flow in the condensing water loop and primary and secondary chilled water loops of chillers as well as the primary and secondary hot water loops of boilers.

### 2.6 Virtual fan air /pump water flow meter

Air flow and water flow rates are also essential indices to detect faults of HVAC systems. Fault-free fan or pump power can be predicted based on measured flow rate and then compared with actual power to identify faults, such as faulty closed dampers or valves or an excessive pressure setpoint. The understanding of energy use distribution allows energy professionals to identify energy deficiencies and improve system performance. As a result, more and more thermal meters were installed at building levels.

For the buildings, which receive hot water and chilled water from a remote central plant, water flow rate has to be measured in order to obtain whole-building thermal energy uses. Virtual meters for HVAC systems have been referenced and summarized in this study under section 2.5 above.

Liu (2002) proposed a fan airflow meter that determines airflow rate using a measured fan head associated with an in-situ fan head curve. Figure 2.2 shows a fan head curve (a solid line) and a fan power curve (a dashed line) under a fixed fan speed. The approach of this fan-head-curve-based airflow meter is marked by (a) in Figure2.2. The accuracy of fan-head-curve-based airflow meters depends on the slope of the fan head-airflow curve. In other words, the errors of the fan head measurement can cause unacceptable errors with the airflow measurements if the fan head curve is flat, shown as the approach marked (b) in Figure 2.2. Unfortunately, the fan head curve always has a flat section under a certain airflow range. Therefore, the airflow measurement may have poor accuracy within a certain airflow range.

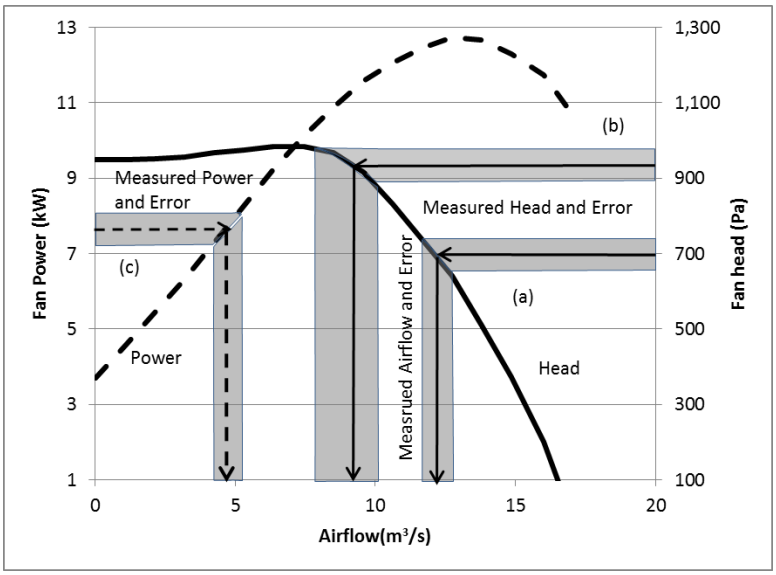


Figure 2.2: Fan head and fan power airflow meters.

To eliminate the error caused by the flat section of a fan head curve, a fan-power-curve-based fan airflow meter was developed by Wang and Liu (2007). The fan-power-curve-based fan airflow meter determines the fan airflow rate using fan power calculated from measured motor power with projected motor efficiency, shown as the approach marked (c) in Figure 2.2. In general, the fan power curve is steep in the airflow range where the fan head curve is flat, especially for backward centrifugal fans. Similar to fan-head-curve-based airflow meters, the accuracy of fan-power-curve-based fan airflow meters also significantly depends on the slope of the fan power-airflow curve.

To avoid dependence on the slope of either a fan head-airflow curve or a fan power-airflow curve, Wang and Liu (2005) developed a fan-power-head-based fan airflow meter. The fan airflow rate is determined based on both measured fan head and power as well as projected fan efficiency. Unlike the requirement of a steep fan head curve or power curve in both the fan-head-curve-based and fan-power-based airflow meters, a flat fan

efficiency curve is preferred in fan-power-head-based fan airflow meters for greater accuracy. It has been found that fan efficiency curves are flat most of the time, especially in a variable flow system with dynamic duct pressure reset controls (Wang and Liu 2005). Therefore, the fan-power-head-based fan airflow meters provide more accurate results in general. However, considering that VFDs are widely used in HVAC systems, significance of energy loses due to VFDs along with a clear understanding of harmonic motor loss impact on motor and fan efficiency is deemed essential.

Among electric motors, alternating current (AC) three-phase induction motors are widely used to operate pumps, fans, and compressors continuously in commercial buildings because of their effectiveness and low cost (DOE 2008). AC induction motors rotate at a nearly constant speed slightly deviated from their synchronous speed by a slip speed. The slip speed is approximately proportional to motor mechanical load while the synchronous speed is determined by the frequency of power supply and the number of electrical magnetic poles (Hughes, 2006). The typical synchronous speed is 3,600, 1,800, 1,200, or 900 rpm in the power systems with a rated frequency of 60 Hz.

The motor mechanical load is dynamic, especially for fans and pumps in HVAC systems. DOE (DOE 2008) presented that more than 40% of the motors in industrial applications operate at or below 40% of their rated load. Variable frequency drives (VFDs) can generate power output to motors with variable output frequency below the rated frequency and variable output voltage below the rated voltage. Since the shaft power to pumps or fans varies as the cube power of motor speed ratio, which is approximately proportional to the VFD output frequency, significant motor power reduction can be achieved by installing VFDs on pumps or fans. Energy savings of 50%

or more were observed when fixed speed systems are modified to allow the motor speed to match variable load requirements (DOE 2008). The energy savings have been the most appealing benefit to encourage wide applications of VFDs in HVAC industries.

In order to develop either a power-based or power-head-based virtual meter, motor efficiency has to be applied to calculate the pump and fan shaft power. The U.S. Department of Energy's (DOE) Industrial Technologies Program (ITP) developed the MotorMaster+ motor system management software, which can access motor performance data such as motor efficiency and power factor at 25%, 50%, 75% and 100% rated loads at the rated frequency for nearly 30,000 industrial electric motors (DOE 2008). Due to the lack of motor efficiency data at variable frequencies, DOE (2008) suggested that the motor efficiencies at variable frequencies be estimated based on the published efficiency at the rated frequency for National Electrical Manufacturers Association (NEMA) Design A and B motors. This simplified motor efficiency model was also adopted in the exploration of a power-based fan airflow meter (Wang and Liu 2007, Liu 2006), a power-head-based fan airflow meter (Wang and Liu 2005) and a power-head-based pump water flow meter (Wang et al. 2010). However, several experiments show that not only motor load, but also by power frequency, affects motor efficiency (Domijan et al. 1997, Gao et al. 2001, Burt et al. 2008).

Currently the most common VFD is the pulse width modulation (PWM) type. AC supply voltage is converted into direct current (DC) voltage by a rectifier, then the DC voltage is smoothed using filter capacitors in a DC link, and finally the smoothed DC voltage is converted back to AC voltage by an inverter. The DC voltage pulse is turned on and off at a switching frequency between 1 kHz and 20 kHz to result in an

approximately sinusoidal current, which contains harmonics, defined as the irregularities in the sinusoidal wave. The width of the pulse determines the resultant VFD output voltage while the changeover frequency between positive and negative pulses equals the VFD output frequency (DOE 2008, CEATI 2000).

Moreover, harmonics resulting from non-sinusoidal power created by VFDs can cause some disturbances in power systems. Harmonics not only interfere with sensitive electronics and communications systems, but also induce additional energy losses in the motors (Carrier 2005, G.E.D. Plessis, L. Lienbenberg, E.H. Mathews, 2013). The harmonic content is usually measured in terms of total harmonic distortion (THD). Electrical equipment is often rated to handle a certain amount of THD, typically 5% (DOE 2008). The energy losses of induction motors consist of stator copper loss, rotor copper loss, core or iron loss, stray load loss, and friction and windage losses (DOE 2008, A.Hughes 2006). Theoretically, the voltage harmonics cause additional core losses whereas the current harmonics cause additional copper losses in the stator and rotor windings (J.V. Gragger, A. Haumer, C. Kral, F. Pirker, 2008).

Manz and Morgan (Manz, L.B., R.B. Morgan, 1999) stated about another 5% to 10% thermal buildup in the motor caused by a VFD when it is running at the rated load. WEG (WEG, 2010) demonstrated that a frame 315 IEC motor fed by a PWM VFD at the rated frequency and load presents 15% additional motor power losses over the motor power losses without VFDs. Sousa et al. (Sousa, G.C.D., B.K. Bose, J. Cleland, R.J. Spiegel, and P.J. Chappell, 1992) and Gragger et al. (J.V. Gragger, A. Haumer, C. Kral, F. Pirker 2008) formulated the copper and core losses caused by harmonics. Boglietti et al. (A. Boglietti, A. Cavagnino, A.M. Knight, 2008) tested the impact of harmonics with PWM

power supply on core losses and the test results show that the core losses increase with the VFD output frequency and is not significantly affected by the PWM switching frequency. In fact, the motor efficiency degrade was not considered.

To date, head-power based virtual flow meter models developed have not considered motor efficiency in variable frequency conditions nor has the impact of VFD induced harmonics on motor efficiency.

As discussed previously, the fan or pump shaft power has to be derived using either the motor input power obtained from the connected VFD control panel or the VFD input power measured by a power meter. Even though the VFD control panel provides an economic approach to obtain the fan or pump shaft power without the use of a power meter, the accuracy of the VFD power reading is uncertain.On the other hand, the VFD efficiency is required using the power meter.

## 2.7 Objectives of the proposed study

The study detailed in this dissertation aims to develop a more accurate and reliable head-power based virtual air / water flow meter model for varying operating conditions and parameters with the following objectives:

1. Consider motor efficiency in variable frequency conditions
2. Verify VFD-induced harmonics impact on motor efficiency
3. Investige using two different power sources (VFD output reading vs power meter) comparatively, in an effort to evaluate the potential for elimantion of the power meter from the development model.

4. Verify and validate the developed meter models based on the three objectives identified by comparing the performance of the different meters.

Chapter briefs provided below, outline the approaches for achieving these objectives:

Chapter 3 of this study provides a theoretical understanding of the application of the affinity laws for pumps/fans used in hydraulics for HVAC systems while establishing the mathematical framework for expressing the relationship between variables involved in pump or fan performance such as head, volumetric flow rate, shaft speed and power. In addition theoretical model is developed for variable flow systems, investigating the performance characteristics of fan / pump motor as a result of installation of variable frequency drives (VFD). Ultimately, a comprehensive theoretical model is introduced for the development of virtual airflow and water flow meters.

Chapter 4 focuses on the development of head-power based virtual airflow meter, based on the theoretical foundation established in Chapter 3. In this chapter, motor efficiency model is developed based on data obtained from power meter as well as the VFD readings. However, a simplified approach is incorporated for the motor efficiency estimation, where motor losses are defined as stator losses, core losses and friction losses and the stray load losses as a result of the slip speed deviations in motor loads under varying frequency has not been detailed and simply combined into the stator rotor and core losses.

For the virtual air flow meter study, experiments were conducted on a fan-motor-VFD system in an AHU serving a portion of an institution building. The supply fan was equipped with a 3 hp (2.2 kW) motor and a VFD was installed for the motor. VFD frequency was modulated to maintain the supply air duct static pressure at its setpoint.

The fan head was measured using a pressure differential transducer, while the motor power was directly obtained through the VFD analog output or calculated from direct power meter measrements.

In parallel with Chapter 4, Chapter 5 outlines the procedures for the virtual water flow meter development. An experimental setup consisting of a pump, motor and VFD system was used. The pump head was measured using a pressure differential transducer while the motor power was again directly obtained through the VFD analog output. While the experimental study outlined in Chapter 4 was based on a small (3 HP) fan motor, a larger pump motor (20 HP) was utilized in this study, which provided an opportunity for validating the accuracy of power readings from VFD output.

While the developed virtual airflow and water flow meter models yielded fairly accurate results, their reliability over full operating frequency range were hindered, since a detailed breakdown of motor, and VFD power loses, including their impact on motor efficiency was not investigated in the mathematical model carried out in these studies.

Considering that VFDs are widely used in HVAC systems, Chapter 6 focuses on establishing the significance of energy loses due to VFDs along with a clear understanding of harmonic motor loss impact on motor efficiency. A new numerical method has been introduced accounting for the breakdown of the stray load losses as a result of the slip speed deviations in motor loads under varying frequency, separate from stator and core losses. In addition PF improvement, harmonic motor loss, and THD were investigated on a pump-motor-VFD system, consisting of a chilled water pump, an induction motor, and a VFD.

The focus of Chapter 7 is to improve accuracy of the developed head-power based virtual water flow meter by use of ideal motor input power model, calibrated based on VFD impact on motor efficiency, along with calibrated VFD efficiency. The motor power is either directly obtained through a VFD analog output or deriven from VFD input power measured by a power meter based on calculated VFD efficiency including harmonic motor losses. Then the pump efficiency model is projected through a calibration process. As a result, the uncertainties associated with the accuracy of motor power obtained from VFD and power meter discussed in chapters 4 and 5 are also clarified. With power distribution breakdown for the pump-motor-VFD system more clearly defined and analyzed, model has been developed to calculate shaft power more accurately. With shaft power known, the virtual water flow meter has been developed using measured pump head, calculated motor power, the projected VFD efficiency, the projected motor efficiency and the projected pump efficiency.

Chapter 8 provides a comparison of virtual air/water-flow meter models discussed in Chapters 4, 5 and 7 as well as comparison against head-based models previously developed by others. Based on the comparative analaysis of the developed data, this chapter successfully documents the improved reliability and accuracy provided by the virtual water flow meter developed in Chapter 7 compared to all other models.

Overall conclusions along with recommendations for future supporting studies are summarized in Chapter 9.

# CHAPTER 3

# FAN AIR / PUMP WATER FLOW METER THEORY

The affinity laws for pumps/fans are used in hydraulics for HVAC systems to express the relationship between variables involved in pump or fan performance such as head, volumetric flow rate, shaft speed and power. The affinity laws are useful as they allow prediction of the head discharge characteristic of a pump or fan from a known characteristic measured at a different speed. Since air or water flow rate, measurable fan or pump head and motor power determines fan or pump performance, theoretically the flow rate can be determined by either measureable fan or pump head, measured motor power, or both. Fan or pump performance is given by head curve, power curve and efficiency curve. The head curve and power curve under a speed other than design speed is obtained by affinity laws. On the other hand, the efficiency curve is a function of ratio of head to flow squared independent with speed. In this chapter, first the flow, head and power relation is discussed; then the virtual meter based on flow-head relation is outlined, followed by the virtual meter model based on the flow-power relation. Ultimately, the virtual flow meter based on the flow, head and power relation is developed. Finally, the pump/fan efficiency and motor efficiency modeling is discussed in details.

## 3.1 Head, power and flow relationship

Affinity laws are mathematical relationships that allow for the estimation of changes in fan or pump performance as a result of a change in one of the basic fan or pump variables. For fan or pump curves, the design speed can be regressed based on a set of

variables which are fan or pump head (H) and fan or pump flow rate (Q). This relationship can be expressed mathematically as

$$H = a_2 Q^2 + a_1 Q + a_0 \tag{3.1}$$

The total fan / pump head can be regressed as a function of the air / water flow rate using the design fan / pump performance curve.

$$H_d = \sum_{i=1}^{n} a_1 Q_d^i \tag{3.2}$$

where $a_i$ are constant and $i \geq 1$; equation (3.2) is a typical polynomial regression curve.

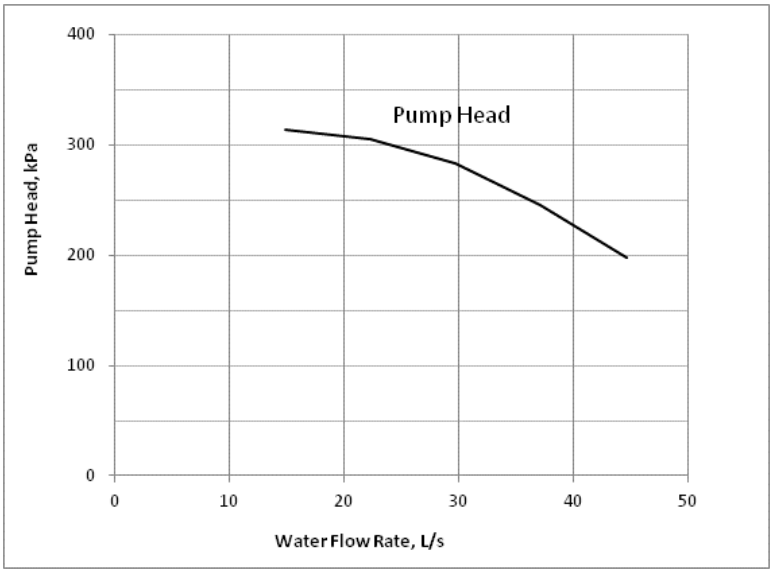


Figure 3.1: Typical Head - Flow rate curve at constant speed

The fan / pump power at the full speed is the function of the fan airflow / pump water flow, which can also be expressed in a polynomial format as

$$W_{\frac{f}{p},\ d} = \sum_{i=0}^{n} b_1 Q_d^i \tag{3.3}$$

where $b_i$ are constant and $i \geq 1$.

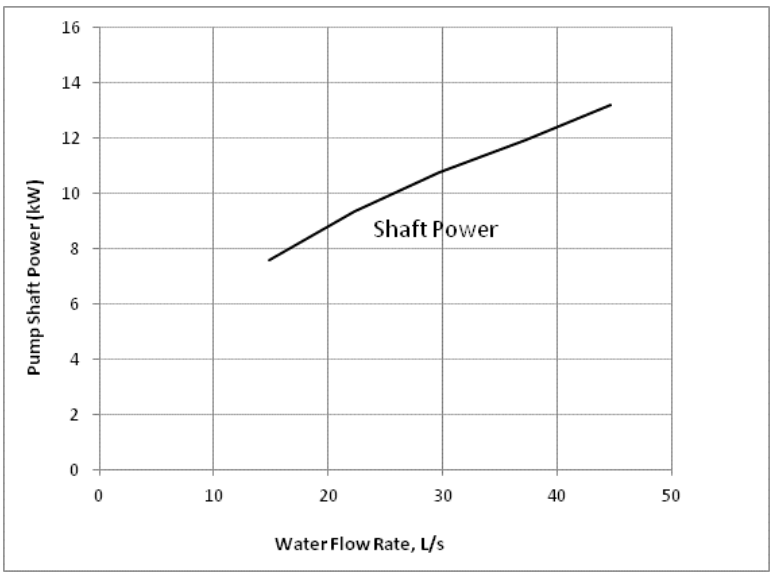


Figure 3.2: Typical Power - Flow rate curve at constant speed

**Affinity laws**

The general fan / pump laws defined in AMCA 99, Standards Handbook [2003], are summarized as follows:

$$Q_1 = Q_2 * \left(\frac{D_1}{D_2}\right)^3 \left(\frac{\omega_1}{\omega_2}\right) \tag{3.4}$$

$$H_1 = H_2 * \left(\frac{D_1}{D_2}\right)^2 \left(\frac{\omega_1}{\omega_2}\right)^2 \tag{3.5}$$

$$W_1 = W_2 * \left(\frac{D_1}{D_2}\right)^5 \left(\frac{\omega_1}{\omega_2}\right)^3 \tag{3.6}$$

Where subscript 1 denotes the variable for actual conditions for the fan / pump in consideration and subscript 2 denotes the variable for the test fan / pump when defining the affinity laws. Q is the volumetric flow rate, while D represents impeller diameter, H is the fan / pump total pressure, ω is the fan / pump speed and W is the useful power delivered to the air by a fan or to the water by a pump. When applying these laws to a given fan or a pump in variable flow conditions, $D_1/D_2=1$; thus the affinity laws are simplified as

$$Q_1 = Q_2 * \left(\frac{\omega_1}{\omega_2}\right) \tag{3.7}$$

$$H_1 = H_2 * \left(\frac{\omega_1}{\omega_2}\right)^2 \tag{3.8}$$

$$W_1 = W_2 * \left(\frac{\omega_1}{\omega_2}\right)^3 \tag{3.9}$$

However, the power in the fan / pump curve in the fan / pump power input to the fan / pump shaft. The fan / pump total efficiency ($\eta_{f/p}$) is the ratio of the power delivered to the air / water (W) to the mechanical power supplied to the fan / pump shaft ($W_{f/p}$).

$$\eta_{f/p} = W/W_{f/p} \tag{3.10}$$

Therefore the fan / pump power input at the correlated fan / pump power curve equation(3.2) must be adjusted using the fan / pump total efficiency equation (3.10). Because the fan / pump efficiency is not a constant value in the fan / pump performance chart, the fan / pump power output value is calculated using the fan / pump power curve point by point and a correlated fan / pump power output curve is derived:

$$W_{f/p,\ c} = \sum_{i=0}^{n} \ell_1 Q_d^i \tag{3.11}$$

where $\ell_i$ are constant and $i \geq 1$. $W_{f/p,\ c}$ is obtained by the fan / pump power curve and the efficiency curve is calculated using Eq. (3.10) at the design speed.

### 3.2 Head based flow meter model

In variable flow systems, variable frequency drive (VFD) is installed on a given fan or pump motor. The fan or pump head curve under partial speed can then be deduced using fan or pump law and based on Eq. (3.2) and (3.11) ; for a relative fan or pump speed ($\omega$), a ratio of actual fan or pump speed to the design fan or pump speed ($\omega_r$), the fan or pump curve can be expressed as

$$H(Q, \omega_r) = a_2 Q^2 + a_1 \omega_r Q + a_0 (\omega_r)^2 \quad (3.12)$$

Then an equation can be obtained by substituting the parameters in Eq. (3.2) using fan laws defined by Eq. (3.7) and (3.8) for fan / pump head at partial speed:

$$H = (\omega)^2 \sum_{i=0}^{n} a_1 (\frac{Q}{\omega})^i \quad (3.13)$$

When applying this to head based flow calculations (Liu 2006):

For i=1, it can be deduced that

$$H = a_1 \omega_r Q + a_0 (\omega_r)^2 \quad (3.14)$$

And therefore, the flow rate can be calculated using

$$Q = \frac{H - a_0 (\omega_r)^2}{a_1 \omega_r} \quad (3.15)$$

For i=2, based on Eq. (3.12),

$$H = a_0 (\omega_r)^2 + a_1 Q \omega_r + a_2 Q^2 \quad (3.16)$$

Then the flow rate can be calculated by solving Eq. (3.16) as :

$$Q = \frac{-a_1 \omega_r - \sqrt{a_1^2 * \omega_r^2 - 4 a_2 [a_0 \omega_r^2 - H]}}{2 * a_2} \quad (3.17)$$

Based on the above discussion, it can be summarized that Head based virtual air / water flow meters can be developed using fan / pump laws, based on measured fan / pump speed and fan / pump head and fan / pump curve data under a given speed (Liu 2006). Fan / pump head, H can be measured using a differential pressure transducer; fan / pump speed ratio, $\omega_r$ is the ratio of actual fan / pump speed divided by the design fan / pump speed, where design speed is defined as the full speed for a given fan / pump. When VFD is in use, this data can be obtained from the VFD panel as a function of a

control system command. Fan / pump curve coefficients constant ($a_i$) can be determined using manufacturer's curve data and based on developed in-situ fan / pump curve.

### 3.3 Power based flow meter model

For the fan / pump power at partial speed by substituting the parameters in Eq. (3.11) using fan law Eq. (3.7) and (3.9), the following equation can be expressed in a polynomial format:

$$W = (\omega)^3 \sum_{i=0}^{n} \ell_1 \left(\frac{Q}{\omega}\right)^i \tag{3.18}$$

When applying this to power based flow calculations (Liu 2006):

For i=1, it can be deduced that

$$W = b_0(\omega_r)^3 + b_1 Q(\omega_r)^2 \tag{3.19}$$

The flow rate can then be calculated using

$$Q = \frac{W - b_0(\omega_r)^3}{b_1 \omega^2} \tag{3.20}$$

For i = 2:

$$W = [b_0(\omega_r)^2 + b_1 Q \omega_r + b_2 Q^2] * \omega_r \tag{3.21}$$

Then the flow rate can be calculated by solving Eq. (3.21) for Q, as

$$Q = \frac{-b_1\omega_r - \sqrt{(b_1)^2(\omega_r)^2 - 4b_2[b_0(\omega_r)^2 - \frac{W}{\omega_r}]}}{2k_2} \tag{3.22}$$

Based on the above discussion, it can be summarized that Power based virtual air / water flow meters can be developed using Eq. (3.20) and (3.22) (Liu 2006); the air / water flow rates can be calculated using fan / pump power output, which is the shaft power delivered to the air / water and does not include any motor / drive losses. Typically,

it is very hard to measure the fan / pump power output without having flow measurement data available. However the fan / pump power output can be calculated using the fan / pump power input to the shaft and the fan / pump efficiency, which can be correlated from manufacturer's curve. The fan / pump power input can be calculated using measured motor input power and the drive losses. With this approach, flow rate is determined using the motor power, fan / pump speed and the in-situ power curve, which needs to be predetermined as part of a calibration process between fan / pump motor power consumption and the actual measured flow rate.

### 3.4 Head-power based flow meter model

Conventionally a fan or pump efficiency- flow curve is given under full or design speed by manufacturers. Since the fan or pump speed always varies in a variable flow system with a VFD, the affinity laws for fan or pump are applied to eliminate motor speed impact. Based on the affinity laws, a fan or pump working at points with the same ratio of the head to the flow square ($H/Q^2$) has constant efficiency no matter what the speed is, i.e., fan or pump efficiency is a unique function of the ratio of the head to the flow square ($H/Q^2$) and can be obtained based the head and power curve under the design speed, defined by Equations 3.2 and 3.3, or identified through a calibration.

$$\eta_{f/p} = \eta_{f/p}\left(\frac{H}{Q^2}\right) = \frac{Q \cdot H(Q)}{W_{f/p}(Q)} \qquad (3.23)$$

Then the flow rate can be obtained based on measured shaft power and head as well as identified or calibrated fan / pump efficinecy without the speed involved.

$$\mathrm{Q} = \frac{\mathrm{W_{f/p}} \cdot \eta_{\mathrm{pump}}(\frac{H}{Q^2})}{\mathrm{H}} \qquad (3.24)$$

In fact, fan and pump efficiency curves are flat at most of the operating conditions, especially in a variable flow system with dynamic differential pressure reset controls. Moreover, the fan or pump efficiency is independent with the fan or pump speed. Therefore, the power-head-based flow meters provide more accurate results in general. A more detailed approach is discused in the next section.

### 3.5 Head-power based flow meter development

VFDs are widely used in HVAC systems to adjust motor and fan / pump speed to match the variations of air/water flow demand. Under partial speed, the fan / pump power output ($W_{f/p}$) is correlated with both the flow rate and speed using Eq. (3.11). The fan / pump power output can be calculated using the fan / pump power input to the shaft and the fan / pump efficiency. Figure 3.3 shows an electrical configuration of a fan-motor-VFD system.

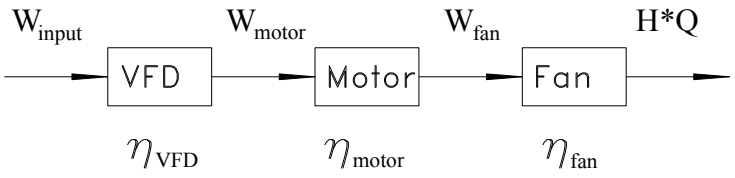


Figure 3.3: Electrical configuration of a fan-motor-VFD system

The VFD, motor and fan or pump sustain mechanical energy losses. The useful work (HQ) imparted into air or water can be determined by

1) the motor input power ($W_{motor}$) along with both motor and fan or pump efficiencies if the motor input power can be accurately obtained, or

2) the VFD input power ($W_{input}$) along with VFD, motor and fan or pump efficiencies if the motor input power is not available.

The motor input power ($W_{motor}$), input frequency and voltage are normally available in the VFD panel, which is an important by-product of VFDs. With reliable motor input power, the useful work can be expressed as

$$H \cdot Q = W_{motor} \cdot \eta_{motor} \cdot \eta_{pump} \tag{3.25}$$

Alternatively, motor input power ($W_{motor}$) can also be determined from measured VFD input power ($W_{input}$) along with VFD efficiency if a reliable power reading from the VFD is not available. The VFD input power is measured by a power meter upstream of the VFD under the rated power frequency. Because of variable power frequencies, the VFD output power or the motor input power is not measurable by a conventional power meter.

$$W_{motor} = W_{input} \cdot \eta_{VFD} \tag{3.26}$$

Since the pump head is easily measured using a differential pressure sensor, the pump water flow rate can be obtained using Equation (3.25) if the motor and pump efficiencies are known.

$$Q = \frac{W_{motor} \cdot \eta_{motor} \cdot \eta_{pump}}{H} \tag{3.27}$$

For a pump or fan without a VFD installed on its motor, a power meter has to be installed. In this case, the power meter can directly measure the motor input power under the rated power frequency without the VFD efficiency involved.

$$Q = \frac{W_{input} \cdot \eta_{VFD} \cdot \eta_{motor} \cdot \eta_{pump}}{H} \tag{3.28}$$

According to Equations (3.26), (3.27) and (3.28), besides the fan / punp efficiency, VFD, motor efficiencies need to be applied in the development of virtual air / water flow meters.

### 3.5.1 Motor efficiency

The U.S. Department of Energy's (DOE) Industrial Technologies Program (ITP) developed the MotorMaster+ motor system management software, which can access motor performance data such as motor efficiency and power factor at 25%, 50%, 75% and 100% rated loads at the rated frequency for nearly 30,000 industrial electric motors (DOE 2008). Due to the lack of motor efficiency data at variable frequencies, DOE (2008) suggested that the motor efficiencies at variable frequencies be estimated based on the published efficiency at the rated frequency for National Electrical Manufacturers Association (NEMA) Design A and B motors.

As outlined in various studies in the past, motor efficiency is impacted not only by motor power, but also by power frequency (Wang et al. 2005 / 2013, Burt et al. 2008, Gao et al. 2001, Domijan et al. 1997). According to motor theory, power frequency, voltage, and motor power impact motor efficiency. Motor efficiency is also related to motor power loss. For three-phase induction motors, motor losses include the resistance loss in copper rotor windings (or rotor loss) and copper stator windings (or stator loss), the magnetic energy dissipated in the motor's iron components (or core loss), the mechanical loss of moving parts (or friction loss) and the stray loss (IEEE 2004, Wang et al. 2013). Comprehensively, motor efficiency can be accurately estimated using the motor equivalent circuit theory if the parameters of the circuit are given. Wang et al.

(2013) has developed a method where motor equivalent circuit theory is applied to determine the equivalent circuit parameters based on the published motor efficiency and power factor at four power levels under the rated power frequency and voltage. A motor equivalent circuit is defined by six circuit parameters: stator winding resistance ($R_1$), rotor winding resistance ($R_2$), stator leakage reactance ($X_1$), rotor leakage reactance ($X_2$), magnetizing reactance ($X_m$), and core loss resistance ($R_c$). The loss of stator and rotor winding resistance corresponds to the copper losses and the loss of core loss resistance corresponds to the core or iron loss, while friction and windage losses are excluded from the rotor mechanical output power. The stray load loss is complicated and can be excluded from the rotor mechanical output power (IEEE4) or represented by a resistance (Kueck et al. 1996, Wang et al. 2013).

**Application of Equivalent Circuit Theory**

Figure 3.4 shows the schematics of an equivalent circuit with the six circuit parameters identified as stator winding resistance ($R_1$), rotor winding resistance ($R_2$), stator leakage reactance ($X_1$), rotor leakage reactance ($X_2$), magnetizing reactance ($X_m$), and core loss resistance ($R_c$). The relative power frequency (f), the ratio of actual frequency to the rated frequency, is applied to calculate the reactance under a frequency other than the rated frequency.

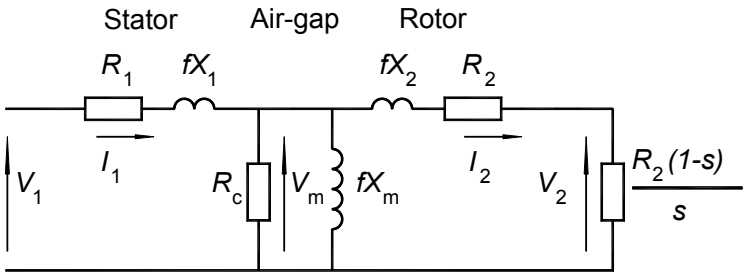


Figure 3.4 Equivalent circuit with the parameters referred to the primary side.

As outlined earlier ,there are five components of loss in an induction motor; these can be summarized as:

- Primary or stator copper loss
- Secondary or rotor copper loss
- Core or iron loss
- Stray loss
- Friction loss

The stray load loss resistance is combined into the stator, rotor and core loss resistances since all of them are unknown. The friction and windage losses are normally treated as a constant under the rated frequency. In this case, it can be accounted for by the core resistance (Wildi 2002) or estimated separately from the equivalent circuit calculations by exclusion from the rotor mechanical output power (Hughes 2006). However, when variable frequency applications are considered , the friction and windage losses are also variable. The stator loss, rotor loss and core loss can be easily calculated with constant stator winding resistance, rotor winding resistance and core resistance using the equivalent circuit theory.

According to the method developed by Wang et. al (2005), the stator or input current ($I_1$), the rotor or load current ($I_2$), the rotor or load voltage ($V_2$), and the magnetizing or air gap voltage ($V_m$) can be calculated based on the input voltage ($V_1$) and the six circuit parameters as well as the relative power frequency (f) and the slip (s).

The rotor mechanical output power ($W_{rotor}$) can be expressed as

$$W_{rotor} = 3(I_2)^2 R_2 \frac{1-s}{s} \tag{3.29}$$

The motor input power ($W_{motor}$) is balanced with the rotor mechanical output power ($W_{rotor}$) as well as the core loss ($R_c$), the rotor loss ($R_2$), and the stator loss ($R_1$).

$$W_{motor} = \frac{3(V_m)^2}{R_c} + 3(I_2)^2 R_2 + W_{rotor} \tag{3.30}$$

In fact, the rotor mechanical output power includes the motor mechanical output power to the shaft and the friction and windage mechanical losses;

$$W_{rotor} = W + W_{F\&W} \tag{3.31}$$

The mechanical losses need to be estimated in these conversions. The mechanical losses include friction loss ($W_F$) due to bearing friction, and windage loss ($W_W$) due to air resistance, which is primarily caused by the cooling fan. The estimated total mechanical loss is about 5% to 15% of the total loss under the rated power and frequency (DOE 2008, Corino 2008).

$$W_{F\&W,d} = W_{F,d} + W_{W,d} = (5\% - 15\%) \cdot (\frac{1}{\eta_d} - 1) \cdot W_d \tag{3.32}$$

Friction and windage losses under frequencies other than the rated frequency can be calculated from the rated friction and windage losses. Mademlis et al. (2004) suggested that the mechanical losses be proportional to the square of motor frequency. Sousa and Bose (1992) treated the mechanical losses proportional to the cube of motor frequency.

The most accurate model separates the friction loss and the windage loss. With this model, the friction loss is proportional to the motor frequency while the windage loss is proportional to the cube of the motor frequency (Dey et al. 2008, Gieras et al. 1997). In this study, the separate mechanical loss model is adopted.

$$W_{F\&W} = f \cdot W_{F,d} + f^3 \cdot W_{W,d} \tag{3.33}$$

The motor raw efficiency can be expressed as

$$\eta = W/W_{motor} \tag{3.34}$$

Therefore, motor efficiency can be expressed as a function of power voltage (V) and frequency (f) as well as motor input power ($W_{motor}$) for a given motor if these six circuit parameters are known.

$$\eta_{motor} = \eta_{motor}(f, V, W_{motor}) \tag{3.35}$$

The VFD usually has different settings to control the V/f ratio, even though the simple setting is to maintain a constant ratio, which is equal to the ratio of the rated voltage to the rated frequency. Figure 3.5 shows the motor efficiency-motor input power curves of a 3 hp motor under six different power frequencies with a constant V/f ratio based on the simulation conducted by Wang et al. (2013). Theoretically the motor efficiency is impacted by motor load as well as frequency and it is obvious that variable frequency has a significant impact on motor efficiency. For example, the motor efficiency increases from 64% under the rated frequency (60 Hz) to 78% under a frequency of 30 Hz under the same motor input power of 0.5 kW.

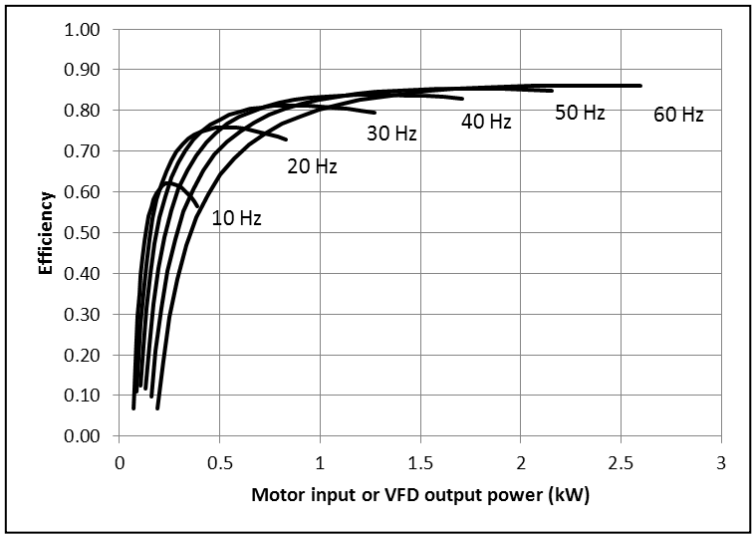


Figure 3.5: Motor efficiency under variable frequencies.

### 3.5.2 VFD efficiency

The VFD efficiency is needed to calculate the motor input power in Equation (3.26) if a reliable power reading from the VFD is not available and a power meter has to be installed to measure the VFD input power.

In spite of the energy savings and PF improvement, VFDs, as electrical devices, still consume energy by the semiconductor components residing in control circuits. There is no widely accepted test protocol that allows for efficiency comparisons between different VFD models or brands. DOE (DOE 2012) presented the efficiency data of PWM VFDs with rated load from 5 to 200 HP provided by one VFD manufacturer, which are listed in Table 3.1.

Table 3.1: Efficiencies of typical VFDs.

| Load (%) | 1.6 | 12.5 | 25 | 42 | 50 | 75 | 100 |
|---|---|---|---|---|---|---|---|
| VFD Rating (HP) | VFD Efficiency (%) | | | | | | |
| 5 | 35 | 80 | 88 | 91 | 92 | 94 | 95 |
| 10 | 41 | 83 | 90 | 93 | 94 | 95 | 96 |
| 20 | 47 | 86 | 93 | 94 | 95 | 96 | 97 |
| 30 | 50 | 88 | 93 | 95 | 95 | 96 | 97 |
| 50 | 46 | 86 | 92 | 95 | 95 | 96 | 97 |
| 60 | 51 | 87 | 92 | 95 | 95 | 96 | 97 |
| 75 | 47 | 86 | 93 | 95 | 96 | 97 | 97 |
| 100 | 55 | 89 | 94 | 95 | 96 | 97 | 97 |
| 200 | 61 | 81 | 95 | 96 | 96 | 97 | 97 |

According to these data in table 3.1, the VFD efficiency is very high under the full load, varying from 95% to 97%, and slightly decreases as the load decreases. Currently, VFD energy losses are considered minimal.

For a given VFD, the VFD efficiency varies with the VFD output or motor input power rather than measurable VFD input power, as shown in Table 3.1. However, it is straightforward to convert the VFD efficiency into a regressed function of VFD input power.

$$\eta_{VFD} = \eta_{VFD}(W_{input}) \tag{3.36}$$

As discussed previoiuly, the motor power input from VFDs is not purely sinusoidal power which contains harmonics impact, defined as the irregularities in the sinusoidal wave (DOE 2008, CEATI 2000). Harmonics induce additional energy losses in the motors (Carrier 2005, Gragger et al. 2008). Theoretical model discussed in this chapter has the harmonic motor loss lumped in the the pseudo fan/pump efficiency. A precise motor efficiency with consideration of harmonic motor loss is developed in Chapter 6 and is applied to develop a more accurate virtual flow meter in Chapter 7.

### 3.6 Summary

In this chapter, first the flow, head and power relation is discussed based on affinity laws; then the virtual meter model based on the flow-power relation is developed from either the VFD input power, measured by a power meter, or the motor input power, obtained from the VFD control panel, and measured fan/pump head, using the pump/fan efficiency, motor efficiency and VFD efficiency models.

# CHAPTER 4

# VIRTUAL AIR FLOW METER EXPERIMENTAL INVESTIGATION

This chapter focuses on the development of head-power based virtual airflow meter, based on the theoretical foundation established in Chapter 3. A virtual airflow meter is developed based on measured motor power and fan head with calibrated motor and fan efficiency model. In the developed model, the fan head is measured using a pressure differential transducer. The motor power can be directly obtained through a VFD or calculated using the measurement of a direct power meter. A simplified comprehensive motor efficiency model without impact of VFD induced harmonic losses is applied to estimate the motor efficiency from the motor power, voltage and frequency using the equivalent circuit. Then an in-situ fan efficiency curve is obtained through a calibration process in order to relate virtual flow rates to actual fan head measurements and finally the developed meter is validated by comparing calcualted and measured airflow rate . The detailed theory and implementation of a virtual airflow meter model is introduced in this chapter along with an experiment used for the development and validation of the virtual air flow meter.

## 4.1 Experimental setup and data collection

Experiments were conducted on a fan-motor-VFD system in an AHU serving a portion of an institution building.

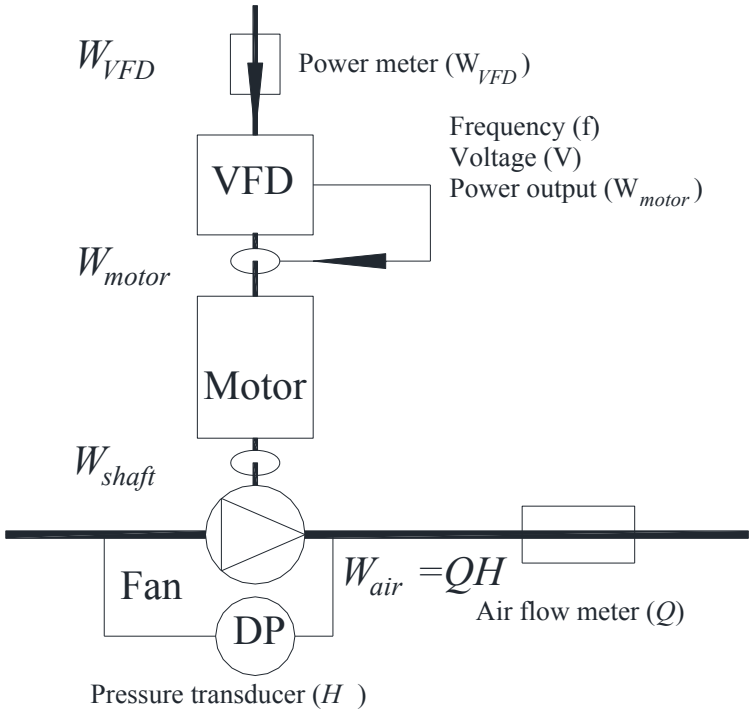


Figure 4.1. Schematic of a fan-motor-VFD system.

The supply fan was equipped with a 3 hp (2.2 kW) motor and a VFD was installed for the motor. VFD frequency was modulated to maintain the supply air duct static pressure at its setpoint. The fan head was measured using a pressure differential transducer, while the motor power was directly obtained through the VFD analog output or calculated from direct power meter measrements.

Shown in Figure 4.2 is the air handling unit (AHU) with a total capacity of 8 tons, serving seven thermal zones, including a lobby, faculty and graduate student offices, and two restrooms used in this study. The total conditioned space was about 2,300 square feet (214$m^2$).


Figure 4.2: Air Handling Unit used in the experimental test site

The supply fan had a forward curve blade and was equipped with a 3 hp (2.2 kW) motor. The motor information is introduced in Table 4.2 in a later section. Figure 4.3 shows the VFD installed on the 3 hp (2.2 kW) motor of the supply fan and the VFD frequency was modulated to maintain the supply air duct static pressure at its setpoint.


Figure 4.3: VFD installed on Fan Motor

A computer, serving as a server in a building EMS as shown in Figure 4.4, was connected to the experimental system through an universal control network for control, real-time monitoring, data collection and storage purposes.

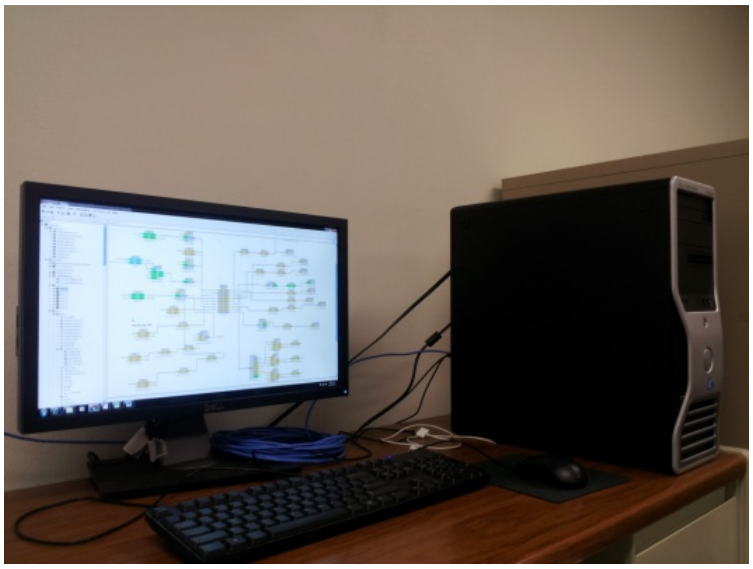

Figure 4.4: EMS server and universal control network

Figure 4.5: EMS Control Panel

Even though the initial design was to obtain the motor input power and frequency from two analog output channels by two data loggers and obtain the motor input frequency from one analog input channel, it was found that all VFD operation parameters could be obtained through EMS using MODBUS connection, a popular communication protocol; as results, the VFD operation feedback were sent to the EMS; picture of the EMS panel is shown in Figure 4.5. The operation feedbacks included VFD output voltage, current, power and actual frequency. This provided opportuneties to evaluate collected data quality through data loggers. In addition, a conventional airflow station (with accuracy within 2% of actual flow rate) was installed on the supply duct for the fan efficiency curve calibration and virtual flow measurement validation as shown in Figure 4.6 below.

Figure 4.6: Air Flow Station installed in duct

Figure 4.7 shows a power meter (±1% of rated current) installed on the upstream of the VFD to measure the VFD input power in order to validate the accuracy of the power reading from the VFD. It is important to note that as part of this study, no correlation was made with impact of harmonic losses induced by VFD when arriving at projected motor efficiency.

Figure 4.7: Power Meter installed upstream of VFD

Figure 4.8: Differential pressure meter installed on ductwork

Both the airflow and power meters were connected to the EMS. Besides variables that were obtained through the EMS and external data loggers, a portable differential pressure meter was also installed for fan head measurements; Figure 4.8 shows the picture of the differential pressure meter installed on ductwork at discharge side of air handling unit.

The supply fan operated under routine control sequences during the experiment. One duct static pressure reset test was also in experiments during the same period. Therefore, several sudden fan speed step changes were observed which allowed for consistantly validated data collection contributing to the robustness of the developed virtual flow meter.

In the given experimental set up, for all five required measured inputs as shown in Figure 4.9, the airflow rate and fan head were directly measured by installed physical sensors while other three motor related inputs could be obtained in different ways.

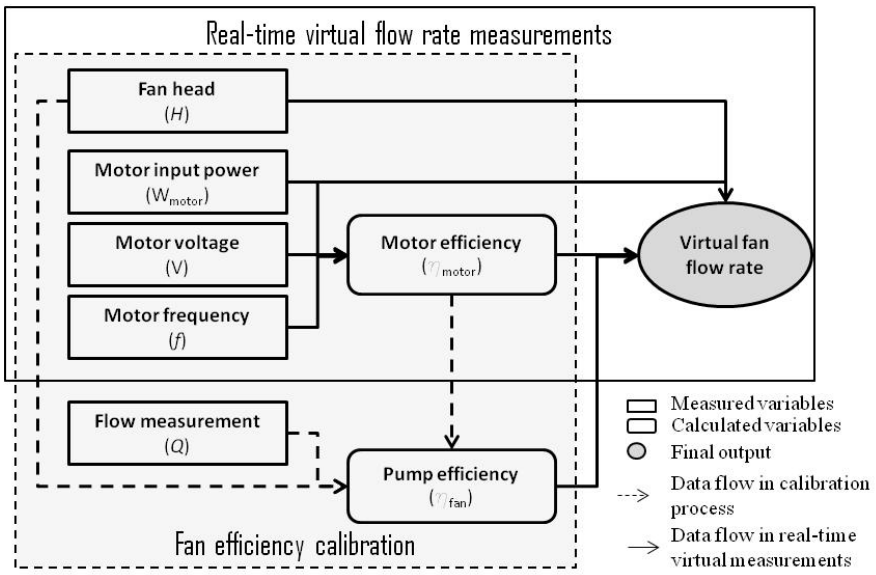


Figure 4.9 : Virtual air flow meter implementation flow chart.

- The motor frequency could be obtained from :
  1) one analog input or frequency command to the VFD and
  2) VFD speed feedbacks to the EMS.
- The motor voltage could be obtained through :
  1) calculated voltage by the predefined VFD voltage and frequency (V/f) ratio, which is usually required by VFD operations;
  2) from one analog output on the VFD panel by a data logger and
  3) from VFD output voltage feedbacks to the EMS.
- The motor power could be obtained through :
  1) from one analog output on the VFD panel by a data logger;
  2) from VFD output power feedbacks to the EMS, which may not be available for most VFDs; and
  3) by installed power meter upstream of the VFD. In the last case, the power meter readings need to be adjusted by VFD efficiencies, as shown in Equation (3.24).

The available measurement options are summarized in Table 4.1. The middle column in Table 4.1 shows the standard or lower cost options for a typical HVAC system while the options in the right column are considered more accurate yet higher cost options. In the experiments, a preliminary test was conducted first to compare the deviations between two colums for each measured input. And in the virtual airflow sensor implemetation, the accuracy of the virtual airflow meter was compared by using the measurements from the different options.

Table 4.1: Available measurement options

| Inputs | Standard option | Experiment add-ins |
|---|---|---|
| Motor frequency | VFD command | VFD feedbacks to EMS |
| Motor voltage | Calculated by V/f ratio | a) VFD feedbacks to EMS;<br>b) Analog output on the VFD panel using a data logger |
| Motor power<br>(with harmonic losses ignored) | VFD feedbacks to EMS | a) Analog output on the VFD panel using a data logger;<br>b) A power meter |

**4.2 Preliminary tests**

One set of preliminary tests was conducted from January 23 to January 24, 2013. The purpose were to

- compare the VFD frequency command and actual frequency from EMS feedback
- compare the calculated voltage based on the V/f ratio, voltage analog output and voltage recorded from EMS feedback;
- compare the power analog output, power from EMS feedback, and calculated power based on the VFD input power measured by a power meter.

Figure 4.10 compares the VFD frequency commands and actual frequency feedbacks for a two hour period. A consistent error pattern of actual frequency feedback over the frequency command is observed at about 1.1% during entire preliminary test.

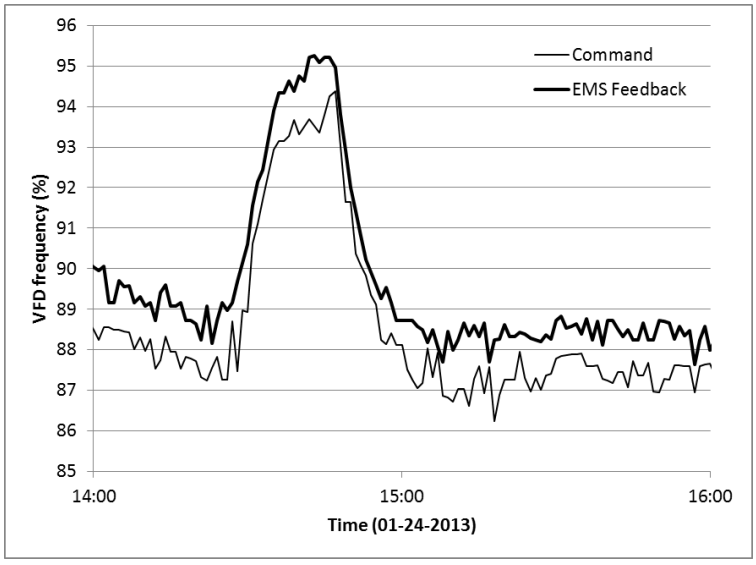


Figure 4.10: Comparison of VFD frequency command and actual frequency EMS feedbacks.

Figure 4.11 compares the voltage analog output, voltage EMS feedback, and calculated voltage based on the V/f ratio for a two hour period. A consistent error pattern of the voltage EMS feedback over both the voltage analog output and the calculated voltage by a constant V/f ratio were also observed. The average bias error of the voltage EMS feedback over the voltage analog output is 2.2V and the average bias error of the voltage EMS feedback over the calculated voltage was 0.7V.

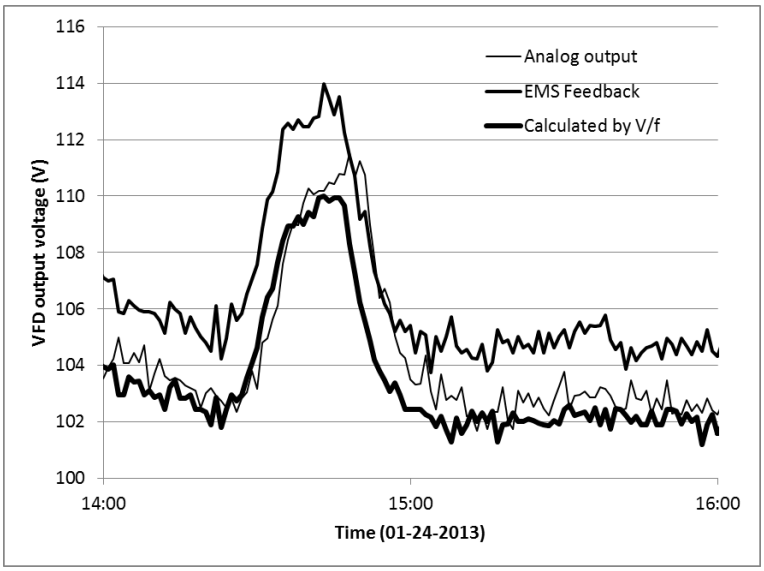


Figure 4.11: Comparison of the voltage analog output, voltage EMS feedback, and calculated voltage.

Figure 4.12 compares the power analog output, power EMS feedback reading, and calculated power based on the VFD input power measured by a power meter for a two hour period. Since the power EMS feadback only has one decimal place for the fraction part, the actual power feadback readings are limited to range from 0.4 to 1.1kW with an average power around 0.6 kW. Moveover, the power feedback fluctuates with variation of up to 33%. Therefore, the power from EMS reading for the small horsepower motors may not be considered reliable for use in the virtual airflow meter development. It was also observed that the power analog output by a data logger actually followed the EMS power reading pattern with unacceptable variations and cannot be used either. Only available power is the VFD input power measured by a power meter. As a result, according to Equation (3.24), the VFD efficiency has to be applied to convert the VFD input power to the VFD output power or the motor input in the virtual airflow meter

development. However, it is important to note that motor harmonic loses are ignored when carrying out this method.

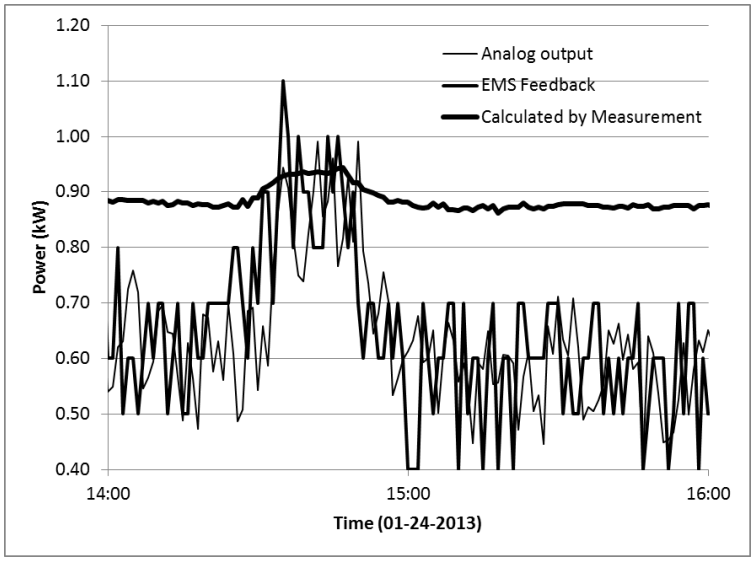


Figure 4.12: Comparison of the power analog output, power EMS feedback, and calculated power.

### 4.3 Fan efficiency calibration

Two separate experiments were conducted from January 25 to January 31 and February 7 to February 10, 2013. One was used to calibrate the fan efficiency and another was used to validate the virtual airflow meter. The calibration of the fan efficiency needs a wide range of the ratio of the head to the flow square. The later section of the experiments obviously has a wider range of the ratio, so it was selected for the fan efficiency calibration. As discussed earlier in section 3.4 of Chapter 3, fan or pump efficiency is a unique function of the ratio of the head to the flow squared, as represented by equation 4.1 below.

$$\eta_{f/p} = \eta_{f/p}\left(\frac{H}{Q^2}\right) = \frac{QH}{W_{f/p}} = \frac{QH}{W_{motor} \cdot \eta_{motor}} \quad (4.1)$$

As shown by the dashed lines in Figure 4.9, inputs needed to obtain an in-situ fan efficiency curve are the motor efficiency, motor input power, fan head and fan airflow rate. Motor input power ($W_{motor}$) is determined from measured VFD input power ($W_{input}$) along with VFD efficiency

$$W_{motor} = W_{input} \cdot \eta_{VFD} \quad (4.2)$$

The motor efficiency is an indirectly calculated input from motor frequency, motor voltage and motor input power. In this test, the actual frequency feedbaks, voltage EMS feedbacks and calculated motor input power from the power meter are used to calculate motor efficiency for the best results.

Therefore, with motor power, motor efficiency defined, head and flow rates measured, fan efficiency can be regressed as a polynomial function of the ratio of the head to the flow square ( $H/Q^2$ ) through the calibration.

$$\eta_{f/p} = \eta_{f/p}\left(\frac{H}{Q^2}\right) \quad (4.3)$$

The experimental motor was discussed by Wang et al (2013), where more details can be found. The published motor data are listed in Table 4.2 and the estimated circuit parameters are listed in Table 4.3.

Table 4.2. Published motor performance data as well as converted data

| Manufacturer | AO-Smith | | | |
|---|---|---|---|---|
| Model | EPACT | | | |
| Motor type | NEMA Design B | | | |
| Size (HP) | 3 | | | |
| Speed (RPM) | 1800 | | | |
| Full load speed | 1765 | | | |
| Voltage (V) | 200 | | | |
| Load (%) | 100% | 75% | 50% | 25% |
| Efficiency (%) | 86.5 | 85.7 | 83.0 | 75.3 |
| Power factor (%) | 75.5 | 68.5 | 57.9 | 38.4 |

Table 4.3. Calculated equivalent circuit parameters

| Parameter (ohm) | Value |
|---|---|
| Stator winding resistance | 0.6957 |
| Stator leakage reactance | 2.010 |
| Magnetizing reactance | 410.9 |
| Core loss resistance | 19.21 |
| Rotor winding resistance | 0.2348 |
| Rotor leakage reactance | 1.347 |

The actual frequency feedbacks and voltage EMS feedbacks are show in Figure 4.13.

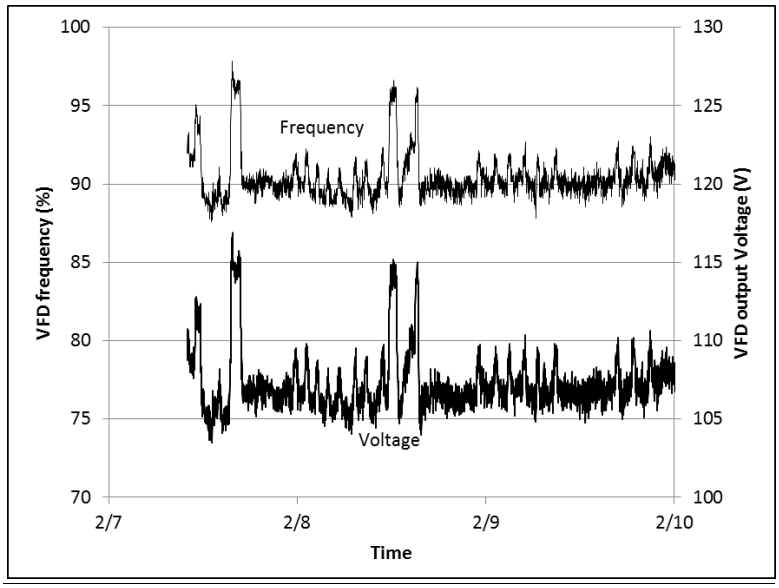


Figure 4.13 : Measured VFD actual frequency and output voltage.

Due to the lack of the VFD efficiency for the 3 hp motor, the efficiency data for the 5 hp motor in Table 3.1 is used to determine the VFD efficiency. With projected VFD efficiency, the motor input power can be obtained from the measured VFD input power using Equation (3.26). Figure 4.14 shows the measured VFD input power and projected VFD output power.

Finally the motor efficiency can be projected based on estimated VFD power output in Figure 4.14 and actual frequency and voltage feedbacks in Figure 4.13. The motor efficiency is also demonstrated in Figure 4.14.

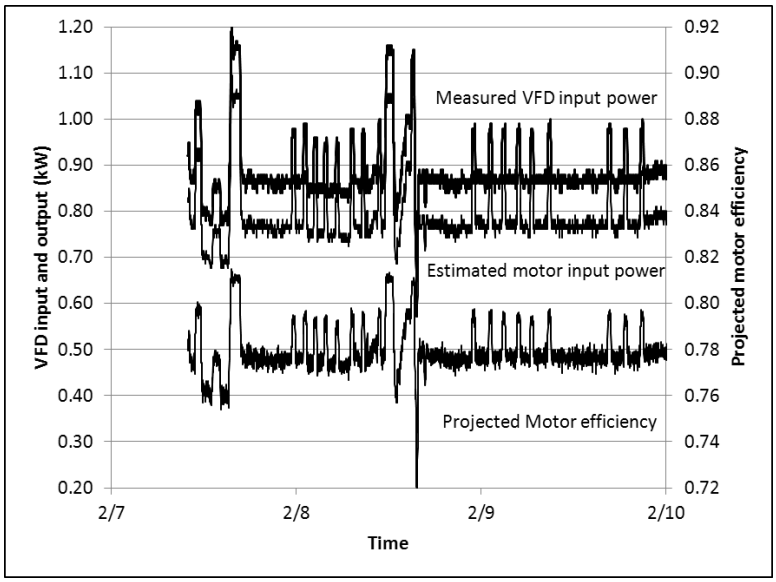


Figure 4.14: Projected motor efficiency based on VFD frequency, output voltage and power.

Both fan airflow rate and fan head measurements are required to calculate the fan efficiency and the ratio of the head to the airflow square. Figure 4.15 shows the measured fan airflow rate and head during the calibration.

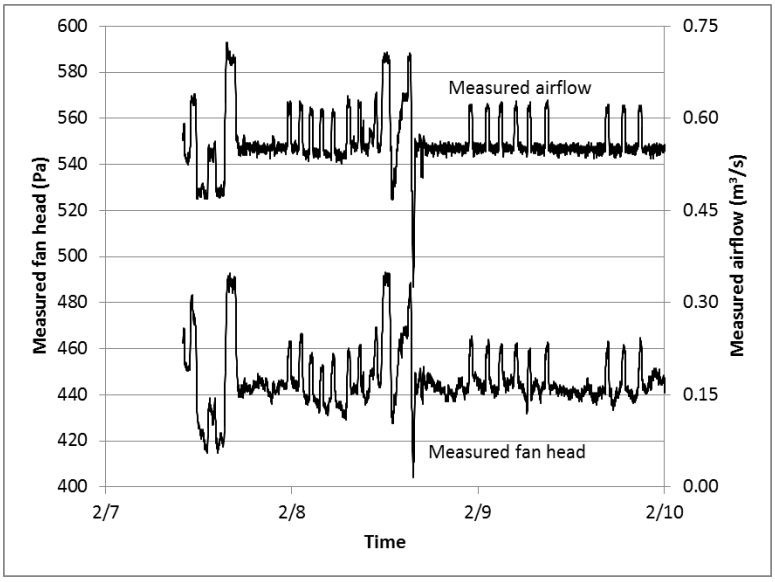


Figure 4.15: Measured fan airflow and head.

Then the fan efficiency can be derived from the measured fan head and airflow rate in Figure 4.15 and projected motor power and estimated motor efficiency in Figure 4.14 by Equation (4.4). Figure 4.16 shows the fan efficiency vs. the ratio of the fan head to the fan airflow square.

The fan efficiency curve in Figure 4.16 can be regressed as a second order polynomial expression of the ratio of the fan head (in Pa ) to the fan water flow (in $m^3/s$) square.

$$\eta_{fan} = -(9.59985E-08)\left(\frac{H}{Q^2}\right)^2 + (2.45167E-04)\left(\frac{H}{Q^2}\right) \pm 0.255485 \quad (4.4)$$

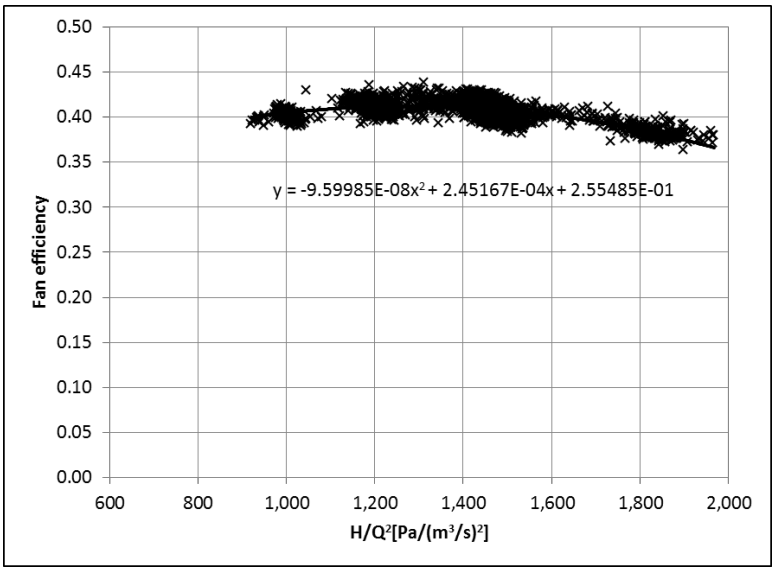


Figure 4.16: Projected fan efficiency vs. ratio of fan head to fan airflow square.

### 4.4 Virtual airflow meter calculation and validation

Now the virtual fan air flow meter has been developed using Equations (3.26) and (3.27) as well as the calibrated VFD efficiency by Equation (3.36), the calibrated motor efficiency by Equation (3.35), and the calibrated fan efficiency by Equation (4.4). The

basic equation is an implicit expression of the airflow rate due to the flow-related fan efficiency. Therefore, the trial and error method has to be applied for the flow rate calculation. Since the fan head is easily measured using a differential pressure sensor, and motor and fan efficiencies have been determined, the fan air flow rate is obtained using the following equation:

$$Q = \frac{W_{input} \cdot \eta_{VFD} \cdot \eta_{motor}(W_{motor} V, f) \cdot \eta_{f/p}\left(\frac{H}{Q^2}\right)}{H} \tag{4.5}$$

Figure 4.17 displays the airflow rate measured by the existing physical airflow meter and the developed virtual airflow meter in a one-week period. A close-up figure by reducing the airflow range from 0-0.8 $m^3/s$ to 0.45-0.70 $m^3/s$ and the time period from a week to 12 hours is also shown in Figure 4.17.

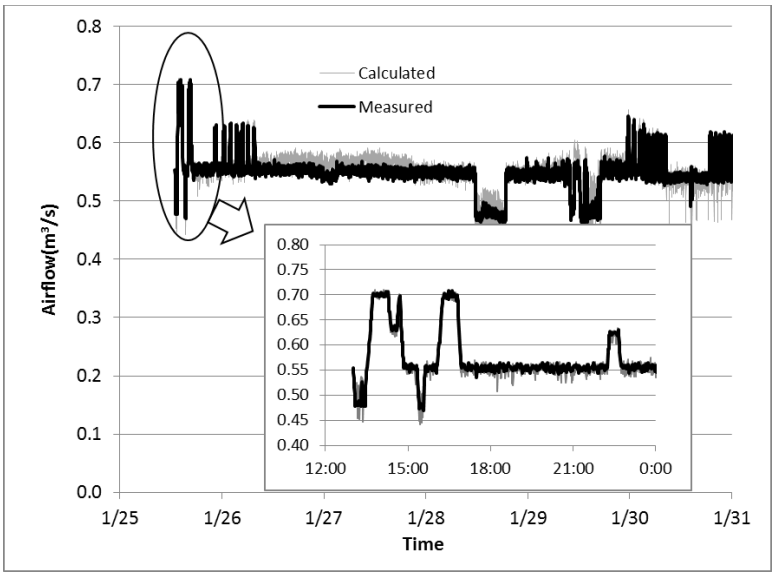


Figure 4.17: Comparison of measured airflow and calculated airflow.

The airflow is obtained by the virtual airflow meter with the new calibrated fan efficiency curve and compared with a physical airflow meter. The coefficient of determination is 0.716 for instant readings and 0.812 for five minute moving average. The results show that accuracy of the virtual flow meter is robust among different motor related input measurement options, although 1.1% power frequency bias and 0.7V voltage bias exist in the standard measurement options.

## 4.5 Summary

The theory of virtual airflow flow meters with a simplified comprehensive motor efficiency model is demonstrated. The airflow rate can be virtually determined using the motor power, voltage and frequency and the fan head as well as the calibrated motor and fan efficiency. The virtual airflow meter was also experimentally tested and developed on an air handling unit. The experiment results showed strong support for the developed meter model.

# CHAPTER 5

## VIRTUAL WATER FLOW METER EXPERIMENTAL INVESTIGATION

Following the experimental investigation of a simplified virtual air flow meter development model with all fan and motor losses covered by a pseudo fan efficiency (Wang et al. 2014), as detailed in Chapter 4, a new experimental study was conducted using a pump-motor-VFD system in order to demonstrate the development of the virtual water flow meter with a similar method. This chapter explores a theoretical model of virtual water flow meter in order to identify the relationship of pump water flow rate with measurable pump head, motor power, and power frequency and voltage; then demonstrates a procedure to implement a virtual water flow meter and validate the virtual pump water flow meter through an experiment. Again, in this study, a simplified motor efficiency model was implemented, where all motor losses were combined and covered by a pseudo pump efficiency. Figure 5.1 shows the schematic flow diagram for the pump-motor-VFD system implemented for the development of the proposed virtual water flow meter.

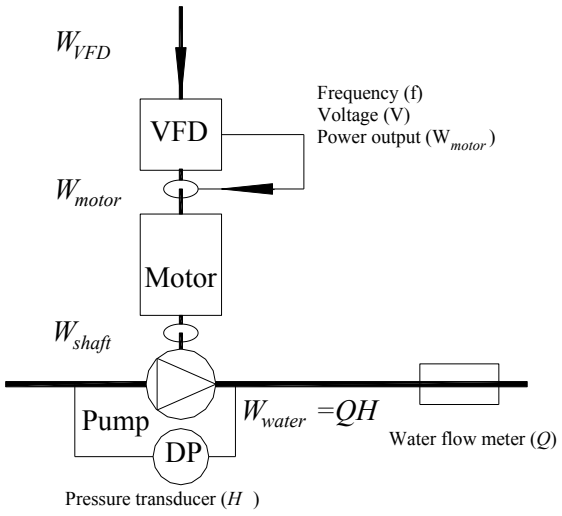


Figure 5.1. Schematic of a pump-motor-VFD system.

## 5.1 Virtual water flow meter implementation

According to Equation (3.25), motor input power, pump head, and motor and pump efficiencies are needed for the virtual water flow meter. Motor input power and pump head are directly measureable inputs, but motor efficiency and pump efficiency are indirectly calculated. Motor efficiency can be calculated in real time based on measured motor input power, power frequency and voltage once the six circuit parameters are determined by the given motor manufacturer's information. The preferred pump efficiency applied in Equation (3.25) is in-situ pump efficiency, which corresponds to actual head measurements and needs to be obtained through a calibration process, rather than pump efficiency obtained from manufacturer's pump curves. Therefore, the pump efficiency calibration requires a temporary water flow measurement device such as an ultrasonic water flow meter.

The entire implementation process is illustrated in the flow chart in Figure 5.2.

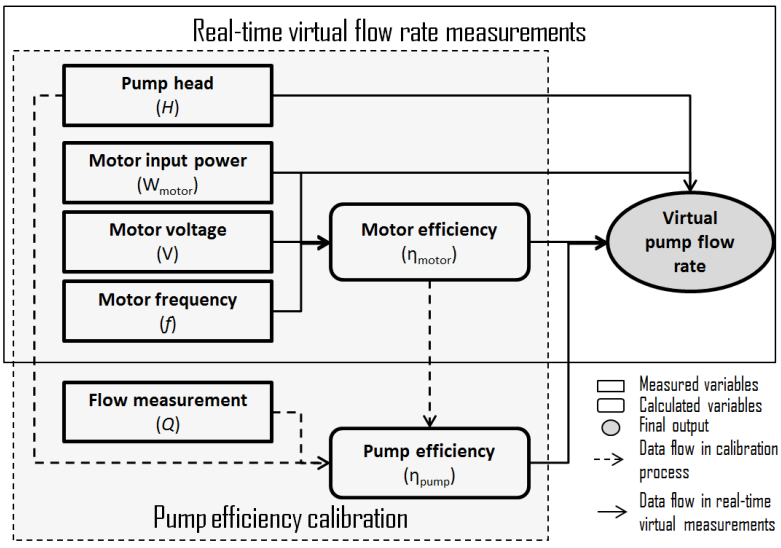


Figure 5.2 : Virtual water flow meter implementation flow chart.

Overall, four permanent measured inputs, including pump head, motor input power from the VFD, motor frequency and motor voltage, and one temporary input, i.e., water flow measurements, are needed. Since the power frequency is always an input signal to the VFD, and most VFDs have a capacity to provide the motor input power and voltage signals through analog output channels, ideally only one permanent physical sensor for pump head measurement is needed for the virtual water flow meter implementation.

## 5.2 Virtual water flow meter experimental setup

The experimental set up consisted of all relevant components and parameters based on measured motor power and pump head along with projected motor and pump efficiency models. The essential compononets for the experimental study were:

- Chilled water pump and manufacturer's pump power, head and efficiency curves
- Pump head measurement using a pressure differential transducer
- VFD for frequency, voltage and motor input power measurements
- Power meter for VFD input power measurement
- Flow meter for pump calibration and calculated flow rate validation.
- Data loggers for validating VFD output readings

The experiments were conducted on a pump-motor-VFD system in a chilled water booster plant located at the Richter Library Building at University of Miami Coral Gables Campus. Figure 5.3 shows the experimental test site and pump used.

Figure 5.3: Chilled water pumps at the experiment site.

The chilled water booster loop utilized is a 200 mm diameter nominal main pipe fed by two pumps with alternating duty cycles. During the experiment, the system was set to operate continuously using one pump only without duty cycling. The pump in use is rated with a flow rate of 0.0379 $m^3/s$ at 240 kPa of head. The motor in use is rated at 24.3 kW (20 hp). The motor information is introduced in Table 5.1 in a later section. Data was collected from the VFD installed on the 24.3 kW (20 hp) motor of the chilled water pump as the VFD frequency was modulated by the plant controls parameters.

Real-time monitoring and data collection was established at the experiment site from April 23rd 2013 to May 31st 2013, in order to obtain the five essential input measurements (water flow rate, pump head, motor frequency, motor voltage & motor power) necessary for the modeling study, as follows:

1. The motor input power and frequency from two analog output channels, as well as the motor input frequency from one analog input channel at the VFD were recorded by two data loggers. The operation feedback included VFD output voltage, current, power, and actual frequency. This provided opportunities to evaluate collected data quality by

data loggers. As in the case of air flow meter study, harmonic loses were ignored when arriving at motor input power and efficiency.


Figure 5.4: Motor input power and frequency measurements from VFD output panel

2. A conventional externally installed ultrasonic water flow station (with accuracy within 2% of actual flow rate) was installed on the chilled water pipe for the pump efficiency curve calibration and virtual flow measurement validation.

Figure 5.5a: Ultrasonic water flow meter by Siemens


Figure 5.5b: Ultrasonic water flow meter by Siemens

3. A power meter (±1% of rated current) was installed upstream of the VFD to measure the VFD input power in order to validate the accuracy of the power reading from

the VFD. However, data obtained from VFD analog output was used as the source for motor input power in this study.

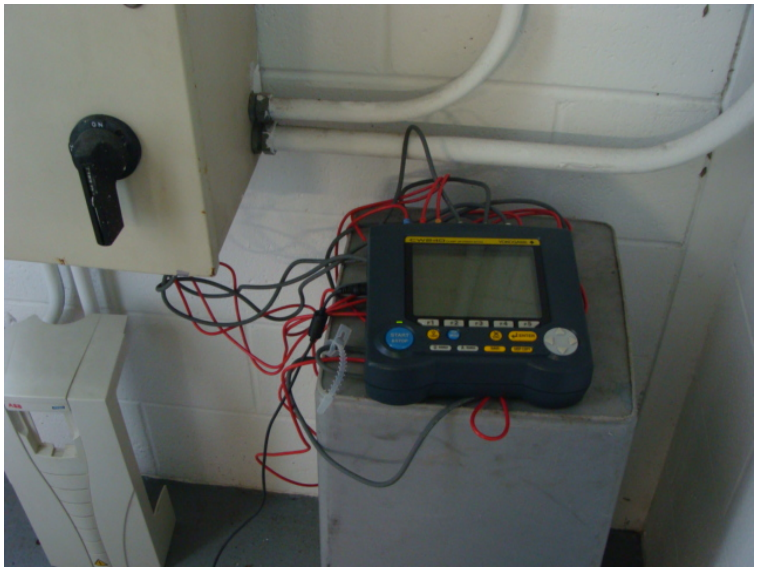

Figure 5.6: Power meter installed ahead of VFD .

4. A differential pressure transducer was installed at pump discharge for pump head measurements. Data gathered from the water flow meter, power meter, the differential pressure transducer and VFD analog output channels were stored and downloaded.


Figure 5.7: Differential pressure transducer for head measurement at pump discharge.

### 5.3 Pump efficiency calibration

Two separate experiments were conducted from April 24th to May 2nd and May 3rd to May 17th 2013. The first experiment is used to calibrate the pump efficiency model shown in Equation (3.6), and the second experiment is used to validate the virtual water flow meter. The calibration on the pump efficiency model needed a wide range of the ratio of the head to the flow squared, which should cover all possible ratios of the head to the flow squared for the validation.

As shown by the dashed lines in Figure 5.2, the inputs needed to obtain an in-situ pump efficiency curve are motor efficiency, motor input power, pump head and water flow rate. Motor efficiency is an indirectly calculated input from motor frequency, motor voltage and motor input power.

As discussed earlier in section 3.4 of Chapter 3, fan or pump efficiency is a unique function of the ratio of the head to the flow squared, as represented by equation 5.1 below.

$$\eta_{f/p} = \eta_{f/p}\left(\frac{H}{Q^2}\right) = \frac{QH}{W_{f/p}} = \frac{QH}{W_{motor} \cdot \eta_{motor}} \quad (5.1)$$

The published motor data are listed in Table 5.1 and the estimated circuit parameters are listed in Table 5.2. Then the motor efficiency can be projected based on actual motor freqeuncy, motor voltage and motor input power with a method devleoped in this study. VFD analog output data was used as the source for motor input power. It is important to point out that harmonic motor loses were ignored when developing the model outlined with this study.

Table 5.1.Published motor performance data as well as converted data.

| | | | | | | | | |
|---|---|---|---|---|---|---|---|---|
| Manufacturer | AO-Smith | | | | | | | |
| Model | BHD4J01I | | | | | | | |
| Motor type | NEMA Design B | | | | | | | |
| Size (HP) | 20 | | | | | | | |
| Speed (RPM) | 1800 | | | | | | | |
| Full load speed | 1766 | | | | | | | |
| Voltage (V) | 460 | | | | | | | |
| Load (%) | 25 | 51 | 75 | 88 | 100 | 115 | 124 | 148 |
| Efficiency (%) | 43 | 66 | 76 | 79 | 80 | 81 | 82 | 82 |
| Power factor (%) | 89 | 93 | 93 | 93 | 93 | 93 | 92 | 91 |

Table 5.2.Calculated equivalent circuit parameters.

| Parameter (ohm) | Value |
|---|---|
| Stator winding resistance | 0.27623 |
| Stator leakage reactance | 1.56348 |
| Magnetizing reactance | 21.93410 |
| Core loss resistance | 721.59211 |
| Rotor winding resistance | 0.20668 |
| Rotor leakage reactance | 1.04753 |

Figure 5.8 shows the actual frequency and voltage from the VFD and Figure 5.9 shows the actual VFD output power and projected motor effiiciency.

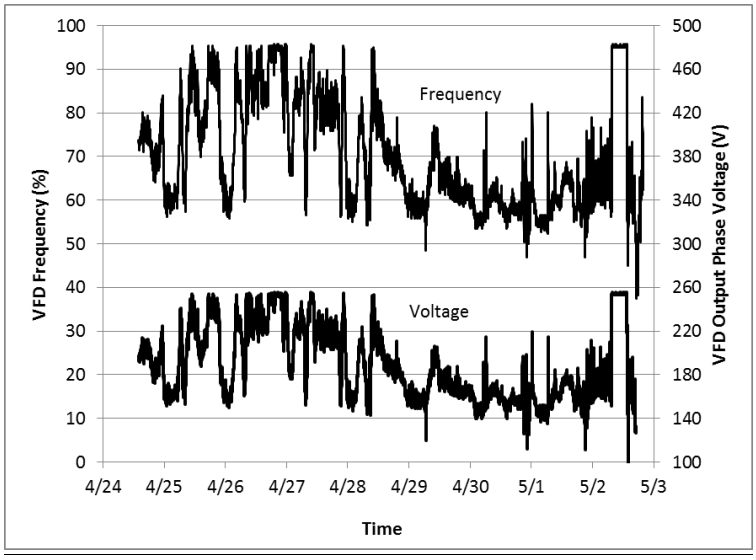


Figure 5.8: Measured VFD actual frequency and output voltage.

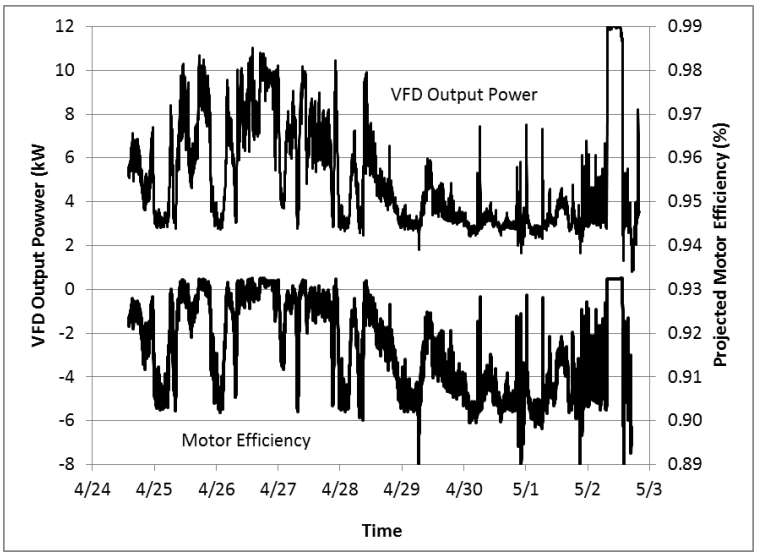


Figure 5.9: Projected motor efficiency based on VFD frequency, output voltage and power.

Both pump water flow rate and pump head measurements are required to calculate the pump efficiency and the ratio of the head to the water flow squared. Figure 5.10 shows the measured pump water flow rate and head during the calibration.

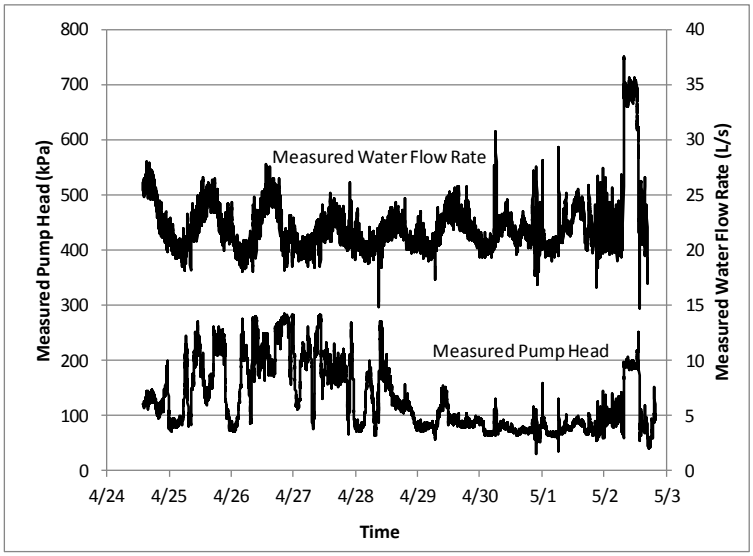


Figure5.10: Measured pump water flow and head.

Then the pump efficiency can be derived from the measured pump head and water flow rate in Figure 5.10 and measured motor power and projected motor efficiency in Figure 5.9 by Equation (3.39). Figure 5.11 shows the pump efficiency versus the ratio of the pump head to the pump water flow squared.

The pump efficiency curves in Figure 5.11 can be regressed as a second order polynomial expression of the ratio of the pump head (in Pa) to the pump water flow (in L/s) squared in two different ratio ranges for accurate results

$$\eta_{\text{pump}} = \begin{cases} -4\times10^{-6}\cdot(\text{H/Q}^2)^2 + 0.0021\cdot(\text{H/Q}^2) + 0.3364 & H/Q^2 < 360 \\ -9\times10^{-8}\cdot(\text{H/Q}^2)^2 + 2\times10^{-5}\cdot(\text{H/Q}^2) + 0.6525 & H/Q^2 \geq 360 \end{cases} \tag{5.2}$$

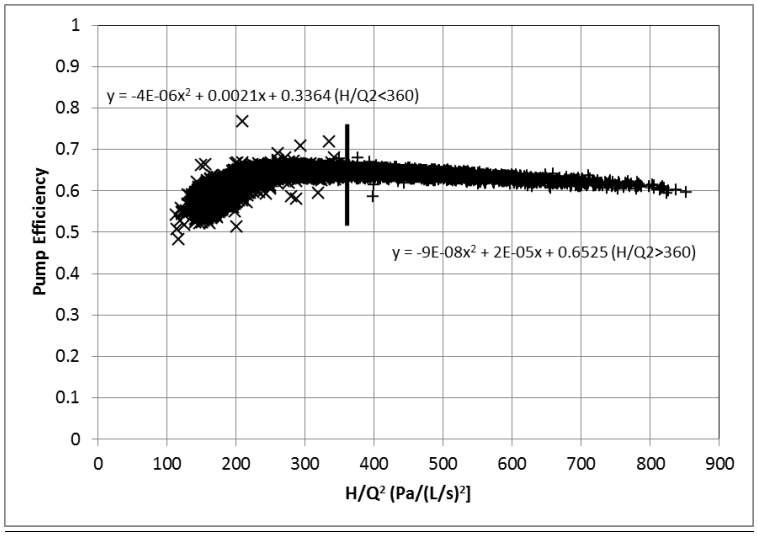


Figure 5.11: Projected pump efficiency versus ratio of pump head to pump water flow squared.

### 5.4 Virtual water flow rate calculation and meter validation

Now the virtual pump water flow meter has been developed using Equations (3.26) and (3.27) as well as the calibrated motor efficiency by Equation (3.35), and the calibrated pump efficiency by Equation (5.2) following the same procedure previously developed in air flow meter study. Significance of harmonics induced by VFDs on overall motor energy losses were not detailed when arriving at motor efficiency. As in the case of air flow meter study, the basic equation is an implicit expression of the water flow rate due to the flow-related pump efficiency. Therefore, the trial and error method has to be applied in the flow rate calculation. With pump head measured using a differential pressure sensor, and motor and pump efficiencies determined, the pump water flow rate is obtained using the following equation:

$$Q = \frac{W_{motor} \cdot \eta_{motor}(W_{motor}V, f) \cdot \eta_{f/p}\left(\frac{H}{Q^2}\right)}{H} \tag{5.3}$$

Figure 5.12 compares the water flow rate measured by the ultrasonic water flow meter installed at the experiment site and the developed virtual water flow meter in a two-week period. A close-up figure by reducing the time period from two week to 12 hours is also shown with Figure 5.12.

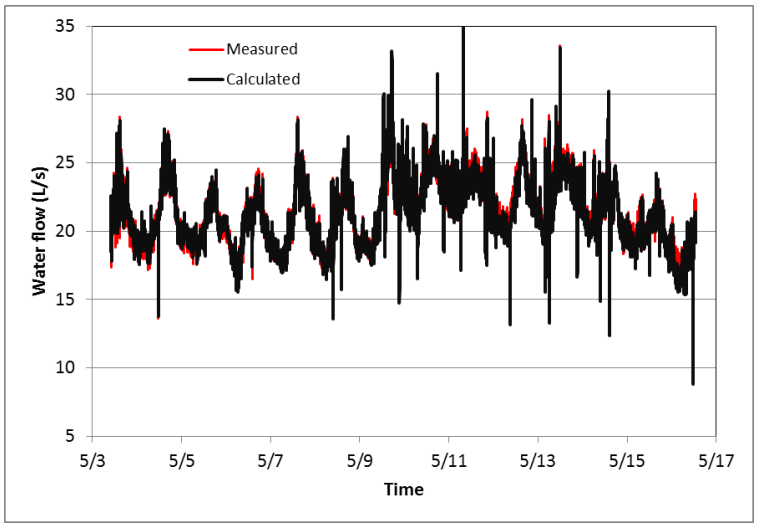


Figure 5.12: Comparison of measured water flow and calculated water flow.

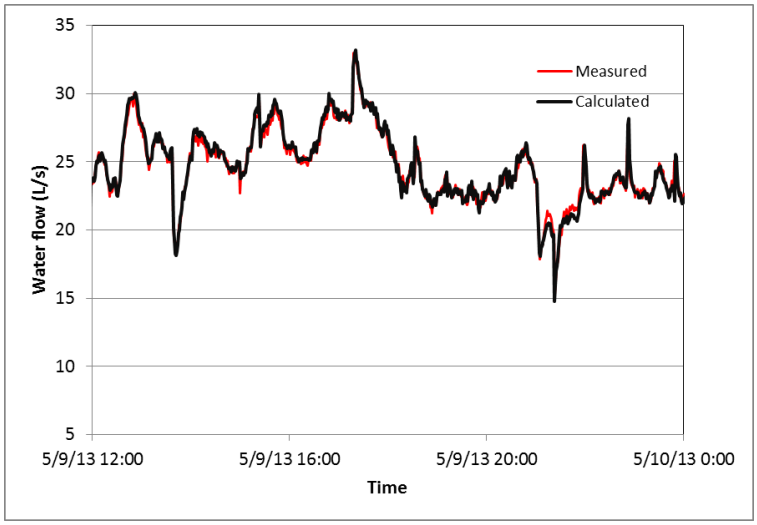


Figure 5.13: Close-up comparison of measured water flow and calculated water flow over 12 hour period.

## 5.5 Summary

The theory of virtual water flow meter with a simplified comprehensive motor efficiency and pump efficiency model is demonstrated. As previously demonstrated in Chapter 4 for virtual air flow meter study, the water flow rate can be virtually determined

based on measured motor power, voltage and frequency, and pump head as well as the projected motor and pump efficiency models. In order to further validate the referenced model, the concept was also experimentally tested on a chilled water pump. The water flow determined by the developed virtual water flow meter agrees well with the ultrasonic water flow meter measurement as indicated by the R-square of 0.88 for instant measurement. It is also important to point out that as discussed previously, the pump power has to be calculated using either the motor input power obtained from the VFD control panel or the VFD input power measured by a power meter. Even though the VFD control panel provides an economic approach to obtain the fan or pump power without the use of a power meter, the accuracy of the VFD power reading is uncertain. As documented in Chapter 4 of this study, a virtual airflow meter of a fan with a 2.2 kW or 3 hp motor installed using both approaches has been investigated (Wang et. al 2014). The virtual airflow meter using the VFD input power produced consistently more accurate results. On the other hand, the motor input power from VFD control panel did not yield as accurate results since the power data from the VFD in use was limited to increments of 0.1 kW and the motor in use was small. In this chapter, with a larger (20 HP) pump motor used in the experimental development model for the virtual water flow meter, motor efficiency calculations have been carried out based on VFD output power only. Considering that the water flow determined by the developed virtual water flow meter agrees well with the ultrasonic water flow meter measurement as indicated by the R-square of 0.88 for instant measurement, it can be suggested that in applications with larger motors, the approach based on use of VFD output data can be considered reliable.

# CHAPTER 6

# IMPACT OF ENERGY LOSSES BY VFDS

As noted in the experimental studies carried out for the development of virtual air and water flow meter models in Chapters 4 and 5, motor harmonic loses were ignored when deriving motor efficiencies based on measured and calculated motor power and power data gathered from VFD analog outputs. Considering that VFDs are widely used in HVAC systems, significance of energy loses due to VFDs along with a clear understanding of harmonic motor loss impact on motor efficiency is deemed essential for improved accuracy of the proposed virtual flow meter models.

To date, motor efficiency models developed in previous virtual air flow and water flow meter studies have been based on motor losses consisting of stator losses, core losses and the friction losses. The stray load losses as a result of the slip speed deviations in motor loads under varying frequency has not been investigated in detail and simply combined into the stator rotor and core losses.

As part of this study, in an effort to address this deficiency, and in order to quantify and arrive at a better understanding of the energy performance of VFDs along with their impact on motor efficiency models, a new numerical method has been introduced. In addition, PF improvement, harmonic motor loss, and THD were investigated on a pump-motor-VFD system, consisting of a chilled water pump, an induction motor, and a VFD.

Directly measured data gathered from the experimental design site was used to demonstrate system power reduction, PF improvement and THD impact. Next a power distribution energy analysis was conducted to identify VFD power loss and harmonic

motor loss using the motor equivalent circuit theory, and conclusions were drawn to summarize the energy performance of the VFD.

### 6.1 Experimental investigation

Figure 6.1 shows a schematic of the test system. The VFD receives sinusoidal power supply at the rated frequency and voltage from a power system and then outputs PWM power at variable output frequencies and voltage to the motor. The pump receives shaft work from the motor and imparts mechanical power to chilled water.

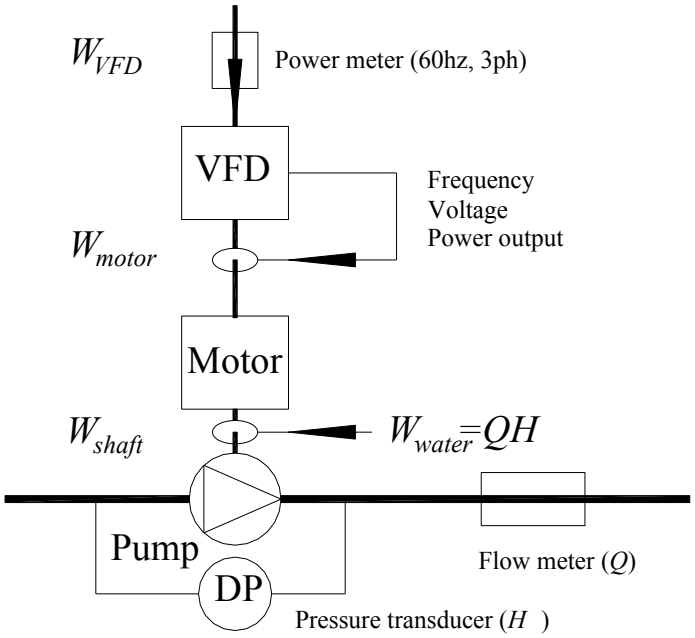


Figure 6.1. Schematic of a pump-motor-VFD system.

The pump is a 3x4x11pump with impeller diameter of 0.2619 m, suction diameter of 0.10 m and discharge diameter of 0.08 m. The design flow is $37.9 \times 10^{-3}$ $m^3/s$, the design head is 239 kPa and the design shaft power is 12.1 kW at a reference speed of 1,750 rpm relative to a synchronous speed of 1,800 rpm. The pump head and power curves at 1,750 rpm were obtained from the pump manufacturer catalog, shown in Figure 6.2.

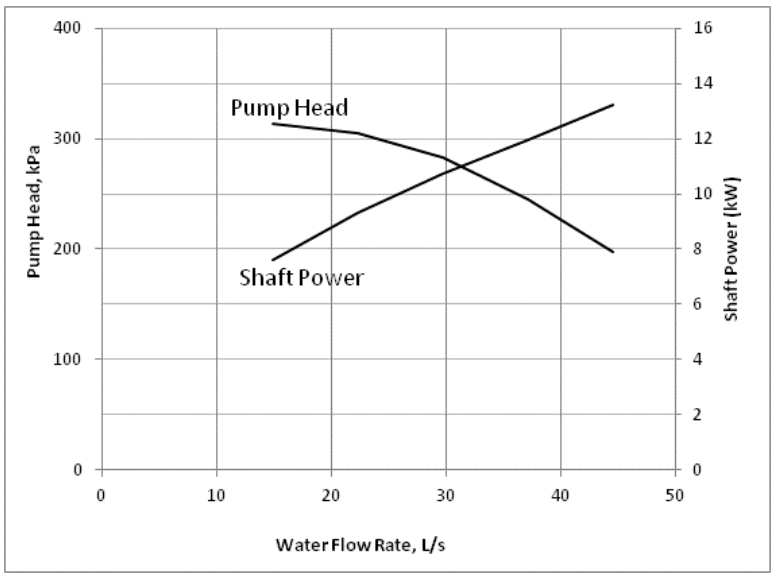


Figure 6.2 Pump head and power curves at 1800 rpm.

A 15 kW (or 20 HP) 460 V three-phase induction motor provides power to the pump. The motor nameplate and performance data, including efficiency and PF under eight different load levels, were provided by the motor manufacturer and are listed in Table 5.1 included in the previous chapter. The motor speed is 1,766 rpm under the rated load (15 kW or 20HP), power frequency (60 Hz) and voltage (460 volt).

An ACH550 380-480V 15kW (or 20HP) three-phase VFD was installed on the motor. The design output current is 31 Amps. The ACH550 VFD is a highly efficient and dependable PWM drive designed specifically for the HVAC industry. The VFD receives a 0-10 V output frequency command from a building automation system and had two 4-20 mA analog outputs from its control panel, which could be assigned to VFD output current, voltage, frequency, power and torque to the motor.

A conventional power meter was installed on the power supply upstream of the VFD to measure the VFD input (active) power ($W_{VFD}$), as shown in Figure 6.1. Besides the

active power, the power meter was also used to measure other power variables on the power supply, such as phase voltage, current, reactive power, PF as well as harmonic content and THD of voltage and current. Such data provided sufficient evidences to present system power reduction, PF improvement, and harmonic level impact in this study.

Two VFD analog outputs were assigned to output voltage and motor input power. A data logger with multiple channels was used to record relative output frequency (f), power voltage (V) and motor input power ($W_{motor}$) by connecting the output frequency analog input and two analog outputs of the VFD.

A conventional ultrasonic water flow meter was installed on the chilled water pipe to measure the pump water flow rate, while a differential pressure transducer was installed between the discharge and suction of the pump to measure pump static head. The measured water flow rate and pump static head are used to calculate the mechanical power received by the water and to project the pump shaft power with the pump efficiency curve. The meter installations are also shown in Figure 6.1.

**6.2 Test and data collection**

The same experimental setup detailed in the previous chapter was used and data was gathered from April 24th to May 17th 2013. All data, including the VFD (or system) input power, the VFD output power, frequency and voltage, the pump water flow rate, and the pump static head, were recorded at a one-minute interval. The system was operated under routine control sequences during the experiment.

The VFD relative output frequency varied from 40% to 96% during the experiment. Figure 6.3 demonstrates the measured system power input within different relative output frequency groups versus the water flow rate. It is obvious that the system power input significantly decreases as the output frequency decreases through the VFD. The system power input dropped from 14 kW to 2 kW when the output frequency dropped from 96% to 50%.

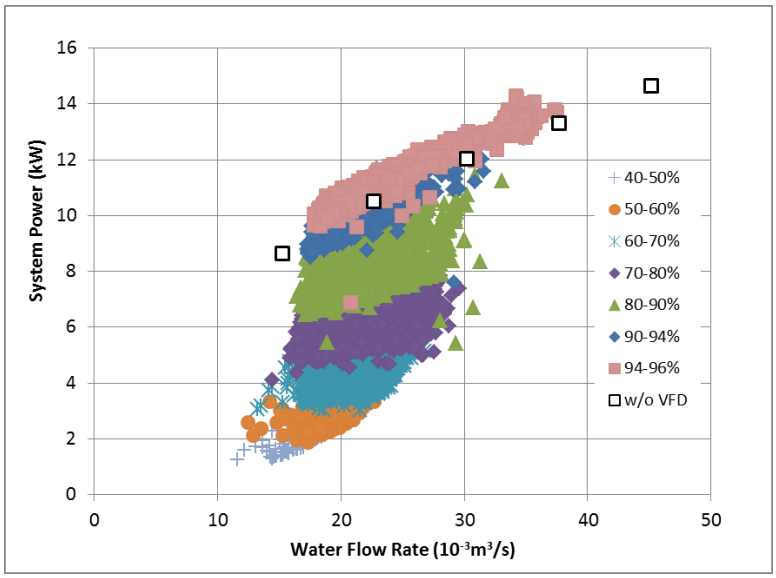


Figure 6.3. Impact of VFD on system power input.

Since the VFD in the system does not have a bypass function, the system input power without a VFD could not be measured by the power meter when the system is in service. However, the system input power without a VFD can be estimated at any water flow rate by combining the shaft power versus water flow rate curve in Figure 6.2 and the motor efficiency versus shaft power relation in Table 5.1. The estimated system power inputs without a VFD are also presented in Figure 6.3 with square markers. An interesting finding is that the pump-motor-VFD system with the relative output frequency above 94% will use more power than directly fed system by the sinusoidal power without a VFD.

Since the system input power through the VFD will keep moving upward in Figure 6.3 if the output frequency rises from 96% to 100%, the power difference at the rated frequency between the two systems with and without the VFD is obvious. The power difference presents the power losses due to the VFD installation at the rated frequency. The detail VFD related power losses will be discussed later.

It is important to point out that the system input power was still significantly reduced by about 50% at the relative output frequency between 70% and 80%, even though the VFD related power losses were considered.

### 6.3 Power factor improvement

Figure 6.4 demonstrates the measured PF upstream of the VFD within different relative output frequency groups versus the water flow rate. Similar to the estimated system input power, the PF without a VFD is estimated at any water flow rate by combining the shaft power versus water flow rate curve in Figure 6.2 and the PF versus shaft power relation in Table 5.1. The PFs without the VFD were also shown in Figure 6.4 with square markers. It is obvious that the VFD significantly improves the PF in the power system. The PF varied from 0.75 to 0.95 with the relative output frequency between 0.4 and 0.96, compared with the PF between 0.65 and 0.75 without a VFD.

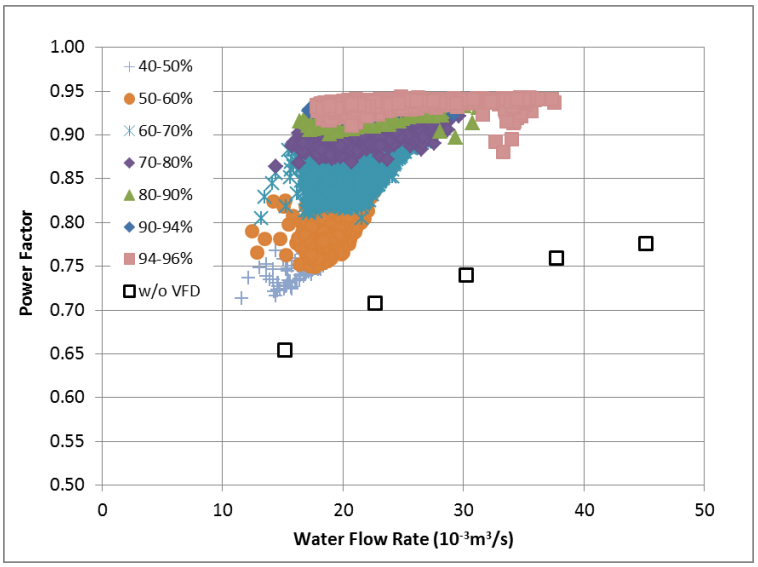


Fig. 6.4. Impact of VFD on system PF.

## 6.4 Harmonics by the VFD

The THD for the voltage and current upstream of the VFD was also measured by the power meter. Figure 6.5 shows the measured THD of voltage and current. The voltage has a minimal harmonic impact with the THD less than 1% but the current has a significant harmonic impact with the THD from 35% to 90% when the relative output frequency varies from 0.96 to 0.40. According to DOE (DOE 2008), electrical equipment typically can handle 5% THD, therefore, existence of serious interference of harmonics with sensitive electronics and communications equipment is anticipated in the same power distribution environment.

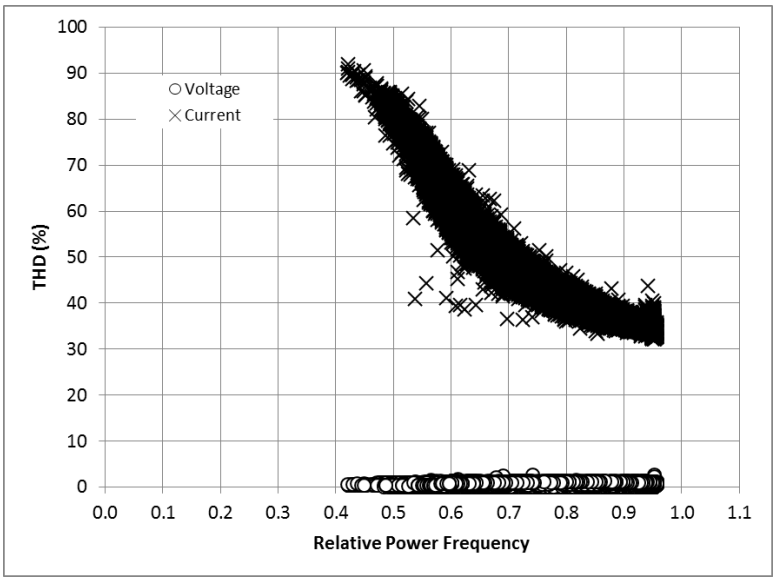


Figure 6.5. Harmonic impact on the power system.

## 6.5 VFD power loss and harmonic motor loss analysis

Since the VFD input power ($W_{VFD}$) is easily measured by the conventional power meter while the motor input power ($W_{motor}$) is directly obtained from the VFD panel without using a power meter, it is easy to identify the VFD power loss as the difference between the VFD input power and motor input power.

In order to identify harmonic motor loss caused by the VFD distortions, it is essential to measure the ideal motor input power fed by pure sinusoidal power at the VFD output frequency. Unfortunately the direct measurement is not practical because the pure sinusoidal power supply at a frequency below the rated frequency is not available and the power at a frequency below the rated frequency is not measurable by a conventional power meter. Therefore, the motor equivalent circuit method has to be employed to estimate the ideal motor input power from the pump shaft power.

In this section, first the motor equivalent circuit method introduced earlier is applied, then the method to obtain the pump shaft power is identified, and finally the power distribution is investigated to identify the harmonic motor power and VFD power loss.

Since the circuit parameters of an induction motor are usually not published by motor manufacturers, they have to be determined from test data, published data or statistical data. Wang, et al. (G. Wang, L. Song, S. Park, 2013) proposed and validated a method to estimate these parameters using published motor nameplate data as well as published motor efficiencies and PFs at different load levels at the rated frequency. Therefore, motor equivalent circuit method was applied as discussed in previous chapters and the six circuit parameters, including stator winding resistance ($R_1$), rotor winding resistance ($R_2$), stator leakage reactance ($X_1$), rotor leakage reactance ($X_2$), magnetizing reactance ($X_m$), and core loss resistance ($R_c$), were estimated based on motor performance data shown in Table 5.1. The six estimated circuit parameters were documented in Table 5.2 in the previous chapter.

With these six known circuit parameters, motor efficiency ($\eta_{motor}$) and motor slip (s) fed by purely sinusoidal power can be expressed as a function of power voltage (V) and relative output frequency (f) as well as motor output power or pump shaft power ($W_{shaft}$) (G. Wang, L. Song, S. Park, 2013) . Among three impacts, the motor efficiency is more sensitive to the pump shaft power and less sensitive to the power voltage and frequency. Generally the motor input power ($W_{motor,sine}$) fed by pure sinusoidal power can be estimated using motor efficiency and pump shaft power.

$$W_{motor,\ sine} = \frac{W_{shaft}}{\eta_{motor}(V,f,W_{shaft})} \tag{6.1}$$

In Eq. (6.1), the power voltage (V) and relative output frequency (f) can be obtained from the VFD control panel, like the motor input power. However, the pump shaft power is not measurable and a method should be developed to obtain the pump shaft power from other measureable variables.

### 6.6 Pump shaft power

Theoretically, the pump shaft power can be calculated from the following two methods:

1. Calculated by measured water flow rate and pump speed with the pump shaft power curve in Figure 6.2 or
2. Calculated by measured water flow rate and pump head with a pump efficiency curve, which is created from both the pump head and shaft power curves Figure 6.2.

For Method 1, a pump and its connected motor rotate at a same speed, therefore, it always operates at a speed below the motor synchronous speed deviated by a slip speed. Normally the pump head and power curves are provided by the pump manufacturer at a reference speed, typically 1,750 rpm relative to a motor synchronous speed of 1,800 rpm at a rated frequency of 60 Hz. According to ISO (ISO 2012), pump performance data can be obtained at any speed, however, all test data at the speed in deviation from the reference speed shall be translated to the basis of the reference speed using the affinity laws. Therefore, the manufacturer pump curve is just a reference curve at the reference speed, rather than the actual operating curve driven by a motor fed by the rated frequency power.

Based on the pump shaft power curve, $W_{shaft,r}(Q)$, at the reference speed, the shaft power ($W_{shaft}$) is a function of the water flow rate (Q) and relative pump speed (ω).

$$W_{shaft} = \omega^3 \cdot W_{shaft,r}\left(\frac{Q}{\omega}\right) \tag{6.2}$$

The relative pump speed is defined as the ratio of actual pump speed to the reference speed and is determined by the relative output frequency (f), relative synchronous speed ($\omega_{syn}$), and motor slip (s). The relative synchronous speed is the ratio of the synchronous speed (such as 1,800rpm) to the reference speed (such as 1,750 rpm) while the motor slip (s) is the ratio of the slip speed to the synchronous speed. Similar to the motor efficiency, based on the motor equivalent circuit method, the motor slip is a function of the relative output frequency (f) and voltage (V) and pump shaft power ($W_{shaft}$) (Andiroglu, E., Wang, G., Song, L. 2013). So the relative pump speed can be expressed as

$$\omega = f \cdot \omega_{syn}\left[1 - s\left(V, f, W_{shaft}\right)\right] \tag{6.3}$$

A numerical method has to be employed to obtain the motor slip (s), relative pump speed (ω), and pump shaft power ($W_{shaft}$) from given or measured water flow rate (Q), relative output frequency (f), and output voltage (V) by integrating Eqs. (6.2) and (6.3).

For Method 2, based on the affinity laws, the pump efficiency is a function of the ratio of the pump head to the water flow squared independent of the pump speed. Figure 6.6 presents the pump efficiency curve derived from the manufacturer pump head and shaft power curves under the reference speed, defined in Figure 6.2.

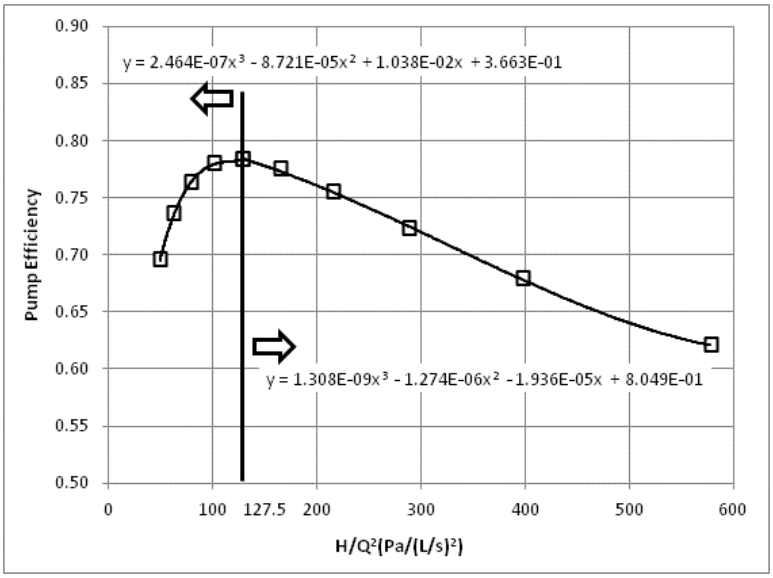


**Figure 6.6 Pump efficiency curve.**

With the efficiency curve, $\eta(H/Q^2)$, the pump shaft power ($W_{shaft}$) is easily obtained from the mechanical power ($W_{water}$) received [by] the water, which is the product of the water flow rate (Q) and pump head (H).

$$W_{shaft} = \frac{W_{water}}{\eta_{pump}\left(\frac{H}{Q^2}\right)} = \frac{HQ}{\eta_{pump}\left(\frac{H}{Q^2}\right)} \tag{6.4}$$

Both methods for the pump shaft power calculations depend on an indirectly measured input, either the relative pump speed or pump head measurements. The relative pump speed is projected from the relative output frequency using Eq. (6.3) while the pump head has to be converted from pump static head, which is actually measured by differential pressure transducer. In this study, both methods are tested through the quality checks of the pump speed and head measurements in order to determine an appropriate method to obtain the pump shaft power.

**Qualification of pump speed measurement**

The pump static head curve at the synchronous speed of 1,800 rpm can be developed from measured water flow rate and pump static head at actual relative pump speed using the affinity laws. The curve at the synchronous speed was developed using Eqs. (6.5).

$$Q_{syn} = \frac{\omega_{syn}}{\omega} \cdot Q \tag{6.5a}$$

$$H_{s,syn} = \frac{(\omega_{syn})^2}{\omega^2} \cdot H_s \tag{6.5b}$$

Figure 6.7 shows the developed pump static head curve at the synchronous speed with different relative output frequency groups. The projected pump static head curve at the synchronous speed would be a consistent curve if the projected relative pump speed is accurate. Unfortunately, Figure 6.7 demonstrates that a consistent curve is only obtained for the relative output frequency above 70%. The upward-spreading pump static head – water flow data for the relative output frequency below 70% reveal that the projected speed was lower than the actual speed. The relative pump speed projection had unacceptable errors at low output frequency below 70%. As a result, the shaft work cannot be calculated accurately with the relative pump speed at all output frequencies using Equations (6.2) and (6.3).

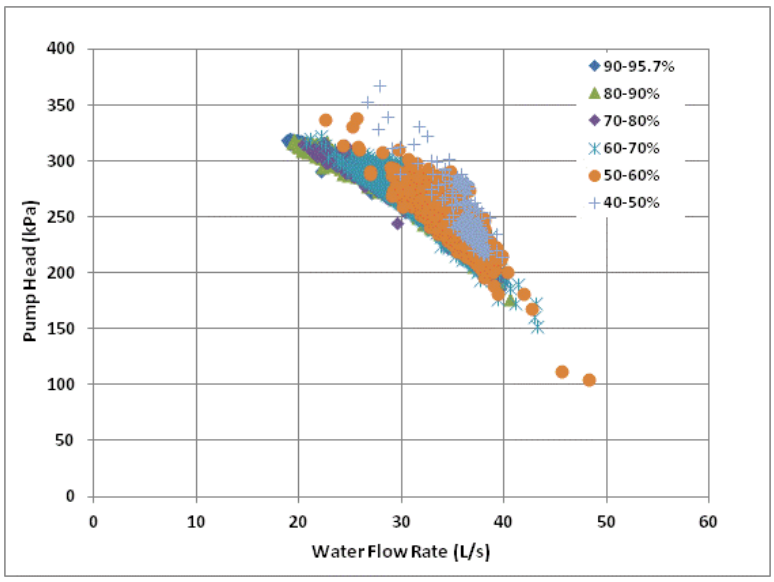


Fig. 6.7 Projected pump head curves at 1800 rpm.

**Qualification of pump head measurement**

The velocity pressure difference due to different pipe sizes between pump suction and discharge and the additional pressure loss of pipe and fittings between two points connected by the pressure transducer have to be considered when the measured pump static head is converted to the pump head, specified by manufacturer's pump performance data. According to the fluid flow basics, the difference between the measured pump static head and the manufacturer pump head is also proportional to the water flow rate squared.

$$H = H_s + k \cdot Q^2 \tag{6.6}$$

Then the correction factor (k) is determined by converting and comparing the manufacturer pump head curve and the measured pump static head curve both at the same

synchronous speed using the least squared method. Since the relative pump speed projections are accurate for the relative output frequency higher than 70%, as shown in Figure 6.7, the pump static head and water flow measurements with the relative output frequency above 90% were used in order to obtain the more accurate correction factor. The correction factor was regressed as $3.33 \times 10^4$ kPa/$(m^3/s)^2$.

Figure 6.8 compares the corrected pump head curve with the manufacturer curve at the synchronous speed. The curve with diamond markers is the measured pump static head; the curve with cross markers is the corrected pump head using Equation (6.6), and the curve with square markers is the manufacturer pump curve defined in Figure 6.3. The corrected pump head curve matches the manufacturer pump head curve very well with the standard deviation of 2.6 kPa.

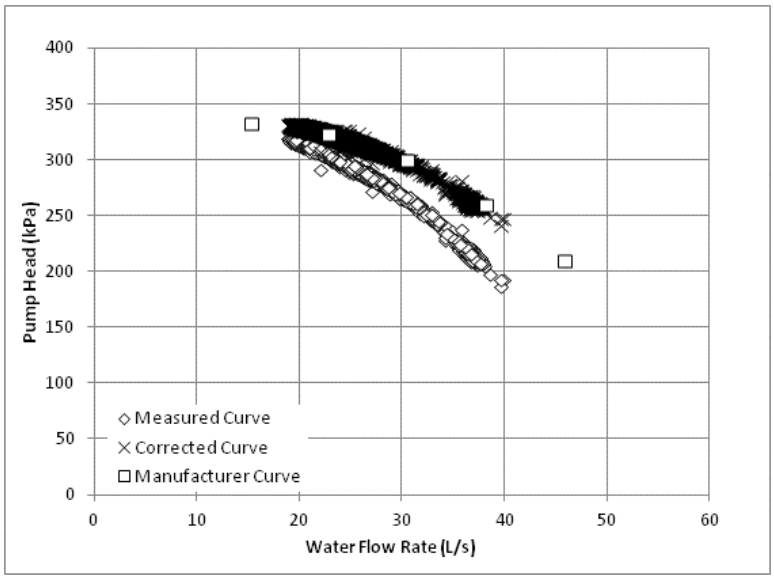


Figure 6.8 Corrected pump head from measured static pump head.

In summary, the pump shaft power will be calculated from the measured pump water flow rate and pump static head using Equations (6.4) and (6.6) in the investigation.

## 6.7 Power distribution in the Pump-Motor-VFD System

Now the power distribution in the pump-motor-VFD system is developed by

- Mechanical power received by the water; the product of water flow rate and pump head, determined by Equation (6.6)
- Pump shaft power, determined by Equation (6.4)
- Ideal motor input power fed by sinusoidal power, determined by Equation (6.1)
- Actual motor input power fed by the existing VFD, read from the VFD control panel
- VFD input power, measured by the power meter

Consequently, the power losses can be identified by

- VFD power loss, the difference between the VFD input power and actual motor input power
- Harmonic motor loss, the difference between the actual motor input power and ideal motor input power
- Conventional motor power loss without the VFD distortion, the difference between the ideal motor input power and pump shaft power
- Pump power loss, the difference between the pump shaft power and water mechanical power.

Figure 6.9(a) compares the power distribution in the pump-motor-VFD system for a 12-hour period with absolute value in (a) and relative value based on the motor power

input fed by sinusoidal power in (b). The relative output frequency is also shown in the same figure. The average power percentages in the pump-motor-VFD system during this period are listed within parentheses in Figure 6.9(b). The results show that actual system input energy has a 21% increase caused by the VFD, including 14% additional energy consumed by the VFD and 7% additional motor energy losses caused by harmonics, compared with the system fed by pure sinusoidal power. Over the actual system energy input, 11.6% was consumed by the VFD and 5.8% was consumed by motor due to the harmonics.

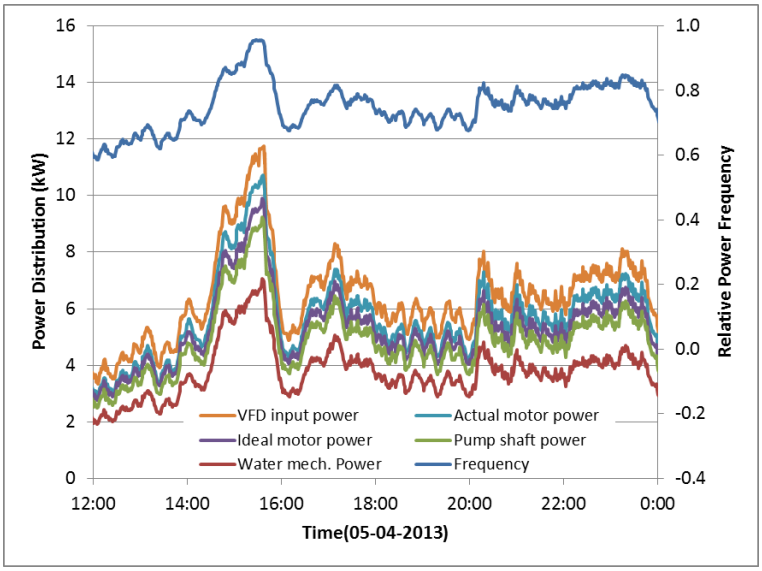


Figure 6.9a. Power distribution in a pump-motor-VFD system.

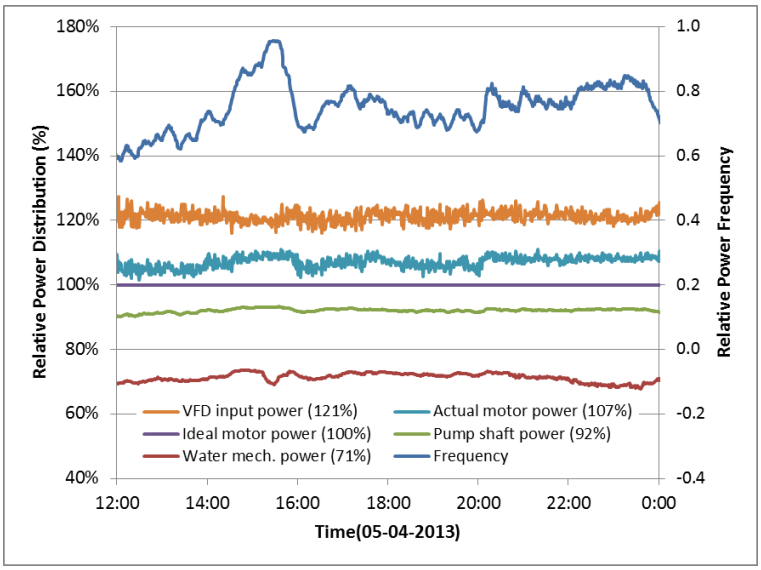


Figure 6.9b. Power distribution in a pump-motor-VFD system.

The measured VFD energy loss, 11.6%, in the studied system is significantly higher than previously published data. According to DOE (DOE 2012), the published VFD energy loss is only in the 3% to 7% range when the output load varies from 100% to 25% of the rated load for a 15 kW (or 20 HP) VFD system. Further experimental studies with different motors are needed to verify the actual VFD energy loss. Based on the measured results, serious attention should be given to the conclusion that the additional energy losses, especially when VFDs operate at high output frequency, will place an additional thermal strain on the motor's rotor and stator windings and consequently will cause insulation breakdown resulting in damage and reduced life of motors. This outcome further validates previous concerns and recommendations referenced in DOE (DOE 2012, Energy Tips). Figure 6.10 presents the VFD-related power losses, which include VFD power loss and harmonic motor power loss versus the system power input with different

relative output frequency groups. The absolute power losses are shown in (a) and relative power losses based on the system input power a.re shown in (b). The absolute power losses in Figure 6.10(a) reveals that the absolute power losses increase linearly as the system input power increases as well as the output frequency increase. The relative power losses in Figure 6.10 (b) reveals that the percentage of the VFD related power losses is about 17.4 % of the system power input on average, regardless of the system input power and output frequency in the tested system. Moreover, the relative power losses have a wide band at low power frequencies and a narrow band at high power frequencies.

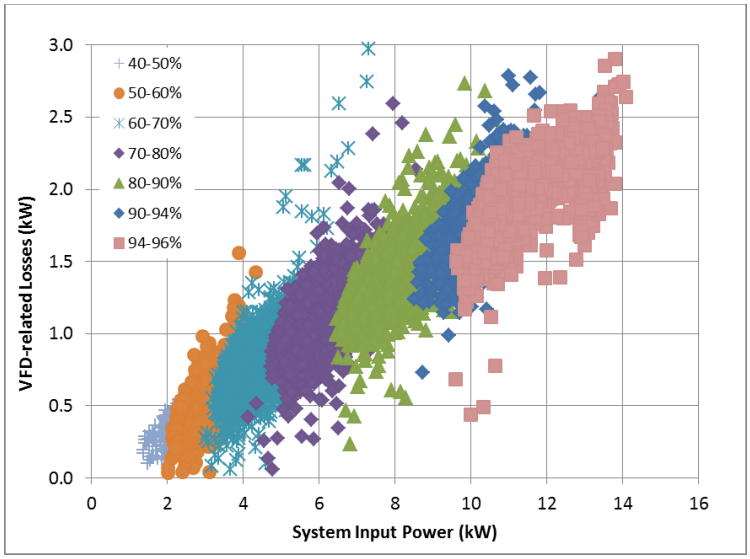


Figure 6.10a. VFD-related power losses.

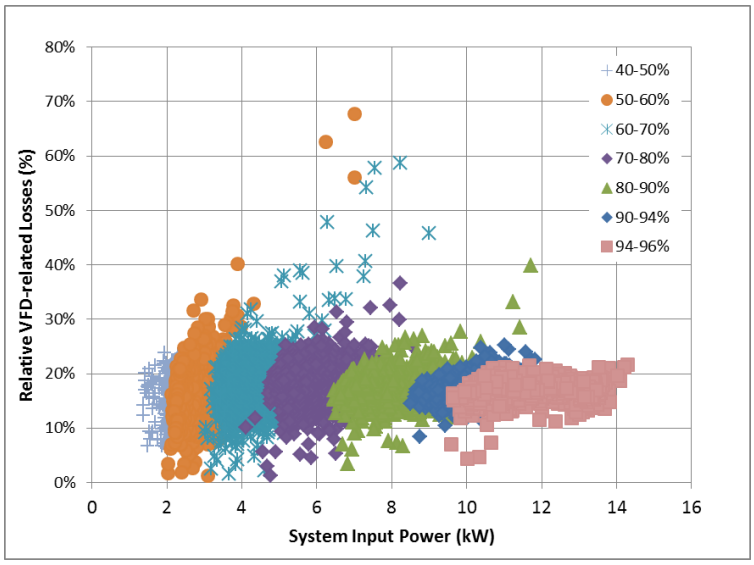


Figure 6.10b. VFD-related power losses.

Figure 6.11 presents the VFD related power losses versus the relative output frequency of the VFD. It reveals the same result as Figure 6.10(a) that the VFD related power losses decreases as the VFD output frequency decrease. It can also be seen that the VFD related power losses quickly decrease to zero when the relative output frequency drops below 40%.

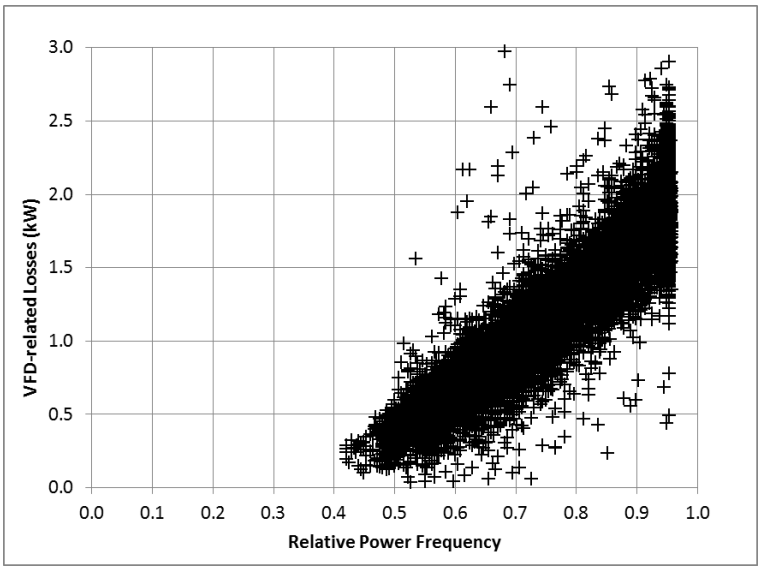


Figure 6.11 Impact of power frequency on VFD-related energy losses.

## 6.8 Summary

In order to quantify the energy performance of VFDs, an experiment was conducted on a pump-motor-VFD system. During the investigation, the VFD input power was measured by a power meter, the actual motor input power was obtained from the VFD control panel, the ideal motor input power without VFD distortion was estimated using the equivalent circuit theory, and the pump input power was calculated from the measured water flow rate and pump head. The power meter also measured power factor (PF) and total harmonic distortion (THD). The experiment results show that the VFD itself consumed 11.6% of the system input power and the harmonics caused 5.8% additional motor power losses even though the VFD can significantly reduce the system input power at partial frequencies. Moreover, while the PFs were significantly improved, the VFD created serious current harmonics with the THD between 35% and 90%

observed on the power supply to the system. Based on these findings, it is warranted that impact of VFD losses and harmonics-degraded VFD efficiency needs to be further detailed and investigated when arriving at motor efficiency as part of the power-head based virtual flow meter models discussed in Chapters 4 and 5.

# CHAPTER 7

## IMPACT OF MOTOR EFFICIENCY ON POWER-HEAD BASED MODEL

In this chapter, with power distribution breakdown for the pump-motor-VFD system more clearly defined and analyzed, model has been developed to calculate shaft power more accurately using two different approaches. With shaft power known, similar to method followed in Chapter 5, the virtual water flow meter has been developed using Equation (3.28) as well as the projected VFD efficiency by Equation (3.36), the projected motor efficiency by Equation (3.35), and the projected pump efficiency by Equation (3.23).

The focus of this chapter is to improve accuracy of the developed head-power based virtual water flow meter as a result of clear definition and impact of harmonic losses on comprehensive motor efficiency. The pump head is measured using a differential pressure transducer. The comprehensive motor efficiency model is applied to project the motor efficiency from measured motor power, voltage and frequency using the motor equivalent circuit theory. The motor power is either directly obtained through a VFD analog output or deriven from VFD input power measured by a power meter based on calculated VFD efficiency including harmonic motor losses. Then the pump efficiency model is projected through a calibration process. The detailed theory and implementation of the proposed virtual water flow meter model is introduced in this chapter along with the experimental study carried out for the development and validation of the virtual pump water flow meter model described above. For improved accuracy, the virtual water flow meter model is developed based on two different approaches; one with motor power obtained through VFD analog output while the other with motor power driven

from VFD input power provided by power meter. Outcome of each approach is then validated based on actual flow readings provided by a physical flow meter at the experiment site. In the event that the model developed based on use of motor power through VFD analog output yields reliable and accurate result, the need to use a power meter in the development of the virtual flow meter may be eliminated, further simplifying the proposed model while also reducing associated implementation costs.

### 7.1 Theory

As discussed previously, the fan or pump power has to be calculated using either the motor input power obtained from the VFD control panel or the VFD input power measured by a power meter. Even though the VFD control panel provides an economic approach to obtain the fan or pump power without the use of a power meter, the accuracy of the VFD power reading is uncertain. As documented in Chapter 4 of this study, a virtual airflow meter of a fan with a 2.2 kW or 3 hp motor installed using both approaches has been investigated (Wang et. al 2014). The virtual airflow meter using the VFD input power produced consistently more accurate results. On the other hand, the motor input power from VFD control panel did not yield as accurate results since the power data from the VFD in use was limited to increments of 0.1 kW and the motor in use was small.

No matter which approach is selected, motor efficiency has to be applied to calculate the pump or fan power in order to develop either a power-based or power-head based virtual flow meter. The U.S. Department of Energy's (DOE, 2008) Industrial Technologies Program (ITP) developed the MotorMaster+ motor system management software, which can access motor performance data such as motor efficiency and power

factor at 25%, 50%, 75% and 100% rated loads at the rated frequency for nearly 30,000 industrial electric motors (DOE 2008). Due to the lack of motor efficiency data at variable frequencies, DOE (2008) suggested that the motor efficiencies at variable frequencies be estimated based on the published efficiency at the rated frequency for National Electrical Manufacturers Association (NEMA) Design A and B motors. This simplified motor efficiency model was also adopted in the exploration of a power-based fan airflow station (Wang and Liu 2007), a power-head-based fan airflow station (Wang and Liu 2005) and a power-head-based pump water flow station as detailed in Chapter 5 of this study (Wang et al. 2010). Several experiments have been conducted on the motor efficiency at variable frequencies (Domijan et al. 1997, Gao et al. 2001, Burt et al. 2008). The results show that the motor efficiency is actually impacted not only by motor load, but also by power frequency. Theoretically, motor efficiency with pure sinusoidal power can be accurately estimated using the motor equivalent circuit theory if the parameters of the circuit are given. Wang et al. (2013) successfully developed a method to determine the equivalent circuit parameters based on the published motor efficiency and power factor at the rated power frequency and voltage. In Chapters 4 and 5 of this study, this method has been applied to estimate the motor efficiency in the development of a power-head based fan airflow meter and a power-head based pump water flow meter respectively. A pseudo fan/pump efficiency was applied to cover all other energy losses through the motor and fan/pump and was regressed through a calibration process.

In fact, the motor power input from VFDs is not purely sinusoidal power. The motor energy loss includes an ideal motor energy loss associated with purely sinusoidal power and a harmonic motor energy loss associated the non-sinusoidal power provided by the

VFD. As detailed in Chapter 6 of this study, a method has been developed to identify actual additional motor harmonic loss in a VFD-motor-pump system (Wang et al. 2015).

Even though the harmonic loss is embedded in the motor efficiency, the previous studies conducted by Wang et al. (2014) and Andiroglu et al. (2013) as documented in Chapters 4 and 5 of this study had it coupled with the pseudo fan / pump efficiency (Andiroglu et al 2015). Therefore, one of the primary focus of emphasis on this chapter is to develop virtual pump water flow meters using the comprehensive motor efficiency, broken down as harmonic-degraded efficiency and ideal motor efficiency. The same studies (Wang et al. 2014) also failed to use the motor input power to develop a virtual fan airflow meter due to the unreliable power reading from the VFD installed on the small motor in use. Therefore, the second purpose of the proposed model in this chapter is to validate virtual pump water flow meters using the motor input power obtained from the VFD and the VFD input power measured by a power meter comparatively. First the water flow correlation with the measured pump head and available power input as well as pump, motor, and VFD efficiency functions is developed. The motor efficiency includes the harmonic-degraded efficiency, which covers the additional motor harmonic loss. Then the calibration procedure is designed to identify the pump, motor, and VFD efficiencies. Finally, the experiment is conducted to develop, calibrate and validate a virtual pump water flow meter on a VFD-motor-pump system.

**7.2 Virtual pump water flow meter model**

Figure 7.1 shows a configuration of a pump-motor-VFD system. The VFD receives the power at the rated frequency and voltage, and transforms it into the power at variable frequency and voltage. The motor receives the variable frequency power and drives the

pump at the variable speed. Since the motor input power received from the VFD is not purely sinusoidal power, additional harmonic energy losses are introduced into the motor. The pump receives the shaft power from the motor to create the water pressure increase or the pump head and generate the water flow.

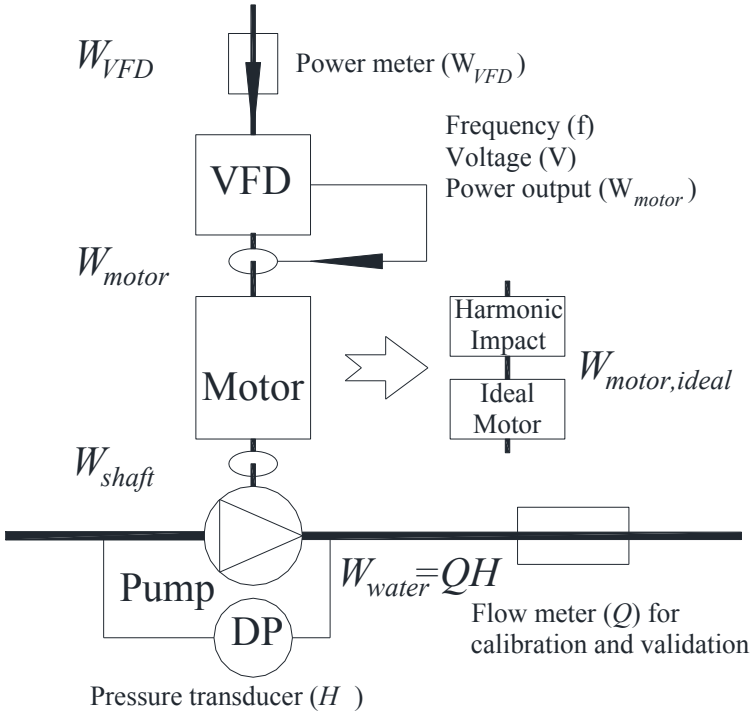


Figure 7.1: VFD-motor-pump system with available measurements.

Unlike costly and unreliable water flow ($Q$) measurements by physical flow meters, the pump head ($H$) can be easily and accurately measured by a differential pressure transducer (DP). Meanwhile, the VFD input power ($W_{\text{VFD}}$), can be measured by a power meter and the motor input power ($W_{\text{motor}}$) can be obtained from the VFD control panel. Besides the motor input power, the VFD control panel can also provide the VFD output frequency ($f$) and voltage ($V$). The correlation of the pump water flow with the

measurable pump head and either the VFD input power or VFD output power as motor input power will be explored to develop a virtual pump water flow meter.

**Basic correlation of water flow**

Since the VFD, motor and pump sustain energy losses, the VFD, motor and pump efficiencies are introduced to cover these energy losses through the VFD-motor-pump system. The mechanical work ($W_{water}$) imparted into water, which is the product of the pump head ($H$) and water flow rate ($Q$), can be determined by the pump input (shaft) power ($W_{\text{shaft}}$) along with pump efficiency ($\eta_{\text{pump}}$).

$$W_{water} = H \cdot Q = W_{shaft} \cdot \eta_{pump} \tag{7.1}$$

The pump shaft power can be determined by the motor input power ($W_{\text{motor}}$) along with the motor efficiency ($\eta_{\text{VFD}}$).

$$W_{shaft} = W_{motor} \cdot \eta_{motor} \tag{7.2}$$

Therefore, the pump water flow rate can be obtained from the measurable pump head and motor input power with identified pump and motor efficiencies, if the motor input power can be accurately read from the VFD control panel.

$$Q = \frac{W_{motor} \cdot \eta_{motor} \cdot \eta_{pump}}{H} \tag{7.3}$$

On the other hand, if the VFD panel reading is not reliable, the motor input power has to be calculated from the VFD input power ($W_{\text{VFD}}$), which can be measured by a power meter, along with the VFD efficiency ($\eta_{\text{VFD}}$).

$$W_{motor} = W_{VFD} \cdot \eta_{VFD} \tag{7.4}$$

Therefore, the pump water flow rate can be obtained from the measurable pump head and VFD input power with identified pump, motor and VFD efficiencies.

$$Q = \frac{W_{VFD} \cdot \eta_{VFD} \cdot \eta_{motor} \cdot \eta_{pump}}{H} \tag{7.5}$$

Equations (7.3) and (7.5) provide a basic formula for virtual pump water flow meters (Andiroglu et al. 2015). Since the pump head and VFD input power or motor input power can always be obtained through a differential pressure transducer, a power meter or the VFD control panel, the application of the formulas defined by Equations (7.3) and (7.5) relies on the identification of pump, motor and VFD efficiencies. In addition, since a calibration process is needed, a portable ultrasonic water flow meter is installed in the system, as shown in Figure 7.1.

## 7.3 Breakdown of system efficiency

### Pump efficiency

Based on the affinity laws, the pump efficiency can be expressed as a unique function of the ratio of the pump head to the water flow rate squared for a given pump.

$$\eta_{pump} = \frac{HQ}{W_{shaft}} = \eta_{pump}\left(\frac{H}{Q^2}\right) \tag{7.6}$$

### Motor efficiency

The motor energy loss includes an ideal motor energy loss associated with purely sinusoidal power and a harmonic motor energy loss associated the non-sinusoidal power provided by the VFD. In order to properly represent these two losses, the motor power distribution is split into two parts; a harmonic component and an ideal motor, as shown in

Figure 7.1. The ideal motor energy loss is considered by the ideal motor efficiency ($\eta_{motor,ideal}$), which is defined as the ratio of the pump shaft power ($W_{\text{shaft}}$) to the ideal motor input power ($W_{motor,ideal}$). The ideal motor efficiency fed by purely sinusoidal power is determined based on VFD output voltage ($V$), frequency ($f$) and ideal motor input power (Wang et al. 2013).

$$\eta_{motor,ideal} = \frac{W_{shaft}}{W_{motor,\ ideal}} = \eta_{motor,\ ideal}(V, f, W_{motor,ideal}) \qquad (7.7)$$

The harmonic motor energy loss is considered by the harmonic-degraded efficiency ($\eta_{harm}$), which is defined as the ratio of the ideal motor input power ($W_{motor,ideal}$) to the motor input power ($W_{\text{motor}}$). The harmonic-degraded efficiency is expressed as a function of motor input power ($W_{\text{motor}}$).

$$\eta_{harm} = \frac{W_{motor,\ ideal}}{W_{motor}} = \eta_{harm}(W_{motor}) \qquad (7.8)$$

Therefore, the overall motor efficiency can be expressed as

$$\eta_{motor} = \frac{W_{shaft}}{W_{motor}} = \eta_{harm}(W_{motor}) \cdot \eta_{motor,ideal}[V, f, W_{motor}\eta_{harm}(W_{motor})] \qquad (7.9)$$

**VFD efficiency**

According to Equation (7.5), the VFD efficiency has to be applied to determine the pump water flow if the VFD input power rather than the motor input power is available. As presented by DOE (2012), the VFD efficiency, defined as the ratio of the motor input power ($W_{\text{motor}}$) to the VFD input power ($W_{\text{VFD}}$), can be expressed as a function of the VFD input power.

$$\eta_{VFD} = \frac{W_{motor}}{W_{VFD}} = \eta_{VFD}(W_{VFD}) \quad (7.10)$$

As shown in Figure 7.1, the pump head is easily measured using a differential pressure transducer, the motor input power is obtained from the VFD control panel, which also provides the VFD output frequency (*f*) and voltage (*V*), and the VFD input power is measured by a power meter. With pump, motor and VFD efficiencies identified in Equations (7.6), (7.9) and (7.10) , the pump water flow rate ($Q$) is correlated with the motor input power ($W_{\text{motor}}$) or VFD input power ($W_{\text{VFD}}$) and pump head ($H$), as well as the VFD output frequency (*f*) and voltage (*V*). The basic equation of a virtual pump water flow meter using motor input power can then be expressed as (Andiroglu et al. 2015)

$$Q = \frac{W_{motor} \cdot \eta_{harm}(W_{motor}) \cdot \eta_{motor,ideal}[V, f, W_{motor}\eta_{harm}(W_{motor})] \cdot \eta_{pump}\left(\frac{H}{Q^2}\right)}{H} \quad (7.11)$$

The ideal motor input power can also be calculated based on the VFD input power along with the VFD efficiency and harmonic-degraded efficiency.

$$W_{motor,ideal} = W_{VFD} \cdot \eta_{VFD}(W_{VFD}) \cdot \eta_{harm}[W_{VFD} \cdot \eta_{VFD}(W_{VFD})] \quad (7.12)$$

To simplify the calibration process, the VFD efficiency and the harmonic-degraded efficiency are com

power meter.

$$\eta_{V\&H} = \frac{W_{motor,ideal}}{W_{VFD}} = \eta_{VFD}(W_{VFD}) \cdot \eta_{harm}[W_{VFD} \cdot \eta_{VFD}(W_{VFD})] = \eta_{V\&H}(W_{VFD}) \quad (7.13)$$

With the VFD-harmonic efficiency, the basic equation of the virtual water flow meter using the VFD input power can be expressed as: (Andiroglu et al. 2015)

$$Q = \frac{W_{VFD} \cdot \eta_{V\&H}(W_{VFD}) \cdot \eta_{motor,ideal}[V, f, W_{VFD}\eta_{V\&H}(W_{VFD})] \cdot \eta_{pump}\left(\frac{H}{Q^2}\right)}{H} \quad (7.14)$$

## 7.4 Efficiency identification and calibration

Equations (7.11) and (7.14) provide a basic formula for a virtual pump water flow meter development. Wang et al. (2013) proposed an approach to estimate the ideal motor performance based on the motor input power data, including ideal motor input power, frequency and voltage. On the other hand, the pump efficiency, harmonic-degraded efficiency and the VFD-harmonic efficiency have to be calibrated through an experiment. In this section, first, the ideal motor performance estimation is briefly reviewed, then the pump efficiency calibration procedure is developed by integrating manufacturer pump curves with pump head and water flow measurements, and finally the calibration expressions of the harmonic-degraded efficiency and the VFD-harmonic efficiency are derived.

### Ideal motor efficiency and slip estimation

An induction motor is characterized by an equivalent circuit with six circuit parameters, including stator winding resistance, rotor winding resistance, stator leakage reactance, rotor leakage reactance, magnetizing reactance, and core loss resistance (Hughes 2006, Wildi 2002, IEEE. 2004). The motor equivalent circuit provides a method to evaluate the induction motor performance.

Since the circuit parameters of an induction motor are usually not published by motor manufacturers, they have to be determined from test data, published data or statistical data. Wang et al. (2013) proposed and validated a method to estimate these parameters using published motor nameplate data as well as published motor efficiencies and power factors at different load levels at the rated frequency.

With these six identified circuit parameters, ideal motor efficiency ($\eta_{\text{motor,ideal}}$) and motor slip ($s$), fed by purely sinusoidal power, can be expressed as a function of VFD output voltage ($V$), frequency ($f$) and either ideal motor input power or pump shaft power using the equivalent circuit method .

**Calibration of pump efficiency associated with measured pump head**

Conventionally, pump performance curves, such as pump head and shaft power curves, are given as a function of the pump water flow rate at a design pump speed by pump manufacturers.

$$H = H_{m,d}(Q) \tag{7.15}$$

$$W_{shaft} = W_{shaft,d}(Q) \tag{7.16}$$

The pump efficiency associated with the manufacturer pump head ($H_m$) can be easily obtained from these two given pump performance curves. However, the measured pump head ($H$) by a differential pressure transducer actually is the static pressure difference between two connection points of the transducer rather than the manufacturer pump head. First, the velocity pressure between two connection points is different due to different pipe sizes between pump suction and discharge. Secondly, the additional pressure loss of pipe and fittings exist between two connection points. Therefore, the measured pump head has to be converted to the manufacturer pump head in order to apply given pump performance curves to obtain the pump efficiency. According to the fluid flow basics, the difference between the measured pump head and the manufacturer' pump head is proportional to the water flow rate squared.

$$H = H_m - kQ^2 \tag{7.17}$$

Based on the affinity laws, the pump efficiency can be expressed as a unique function of the ratio of the pump head to the water flow rate squared. The pump efficiency associated with the measured pump head ($H$) can be regressed as a function of the ratio of the measured pump head to the water flow rate squared ($H/Q^2$) with a given correction factor ($k$) along with the manufacturer pump curves at the design speed defined by Equations (7.15) and (7.16).

$$\eta_{pump} = \frac{HQ}{W_{shaft}} = \frac{[H_{m,d}(Q) - kQ^2]Q}{W_{shaft,d}(Q)} = \eta_{pump}\left(\frac{H}{Q^2}\right) \tag{7.18}$$

The correction factor is a key variable to identify the pump efficiency using Equations (7.18) and is calibrated using measured operating data, including the pump water flow rate ($Q$) and measured pump head ($H$), and VFD output voltage ($V$) and frequency ($f$).

Based on the pump shaft power curve, $W_{\text{shaft,d}}(Q)$, at the design speed defined by Equation (7.16), actual pump shaft power ($W_{\text{shaft}}$) at actual water flow rate ($Q$) and relative pump speed ($\omega$) is determined using the affinity laws.

$$W_{shaft} = \omega^3 \cdot W_{shaft,d}\left(\frac{Q}{\omega}\right) \tag{7.19}$$

The relative pump speed is defined as the ratio of actual pump speed to the design speed and is determined by the VFD output frequency ($f$), relative motor synchronous speed ($\omega_{\text{syn}}$), and motor slip ($s$). The relative motor synchronous speed is the ratio of the motor synchronous speed (such as 1,800rpm) to the pump design speed (such as 1,750 rpm) while the motor slip (s) is the ratio of the slip speed to the synchronous speed. The motor slip ($s$) for a given motor can be calculated from the VFD output voltage (V), frequency ($f$) and pump shaft power ($W_{\text{shaft}}$) (Wang et al. 2013). Therefore, the relative pump speed can be expressed as

$$\omega = \frac{f}{60} \cdot \omega_{syn} \cdot [1 - s(V, f, W_{shaft})] \quad (7.20)$$

A numerical method is employed to calculate the relative pump speed (ω) by integrating Equations (7.19) and (7.20). The calculated relative pump speed is then applied to convert measured pump head at measured water flow to equivalent values at the design pump speed using the affinity laws.

$$Q_e = \frac{Q}{\omega} \quad (7.21a)$$

$$H_e = \frac{H}{\omega^2} \quad (7.21b)$$

The pump head and water flow calculated by Equations (7.21) form an equivalent measured pump head curve at the design pump speed, which is applied to determine the correction factor by comparing the manufacturer pump head curve at the design pump speed, defined by Equation (7.15). The sum of the squares of the residuals between the right and left sides of Equation (7.17) for all measured pump head, water flow rate, and calculated pump speed can be expressed as

$$S = \sum_{i=1}^{n} \left[H_{e,i} + k(Q_{e,i})^2 - H_{m,d}(Q_{e,i})\right]^2 = \sum_{i=1}^{n} \left[\frac{H_i}{(\omega_i)^2} + k\left(\frac{Q_i}{\omega_i}\right)^2 - H_{m,d}\left(\frac{Q_i}{\omega_i}\right)\right]^2 \quad (7.22)$$

Then the correction factor (k) is determined using the least squared method. With the identified correction factor, the pump efficiency function associated with the measured pump head can be regressed using equation (7.18).

**Calibration of harmonic-degraded efficiency and VFD-harmonic efficiency**

The ideal motor input power can be obtained from the pump shaft power and the ideal motor efficiency. The pump shaft power is calculated from the measured water flow rate ($Q$) and pump head ($H$) as well as regressed pump efficiency while the ideal motor efficiency is calculated from the VFD output voltage (V), frequency (f) and the pump shaft power using the motor equivalent circuit method (Wang et al. 2013).

$$W_{motor,ideal} = \frac{W_{shaft}}{\eta_{motor,ideal}(V,f,W_{shaft})} = \frac{HQ/\eta_{pump}\left(\frac{H}{Q^2}\right)}{\eta_{motor,ideal}[V,f,HQ/\eta_{pump}\left(\frac{H}{Q^2}\right)]} \quad (7.23)$$

Therefore, the harmonic-degraded efficiency can be calibrated from the motor input power obtained from the VFD control panel and the ideal motor input power calculated by Equations (7.23)

$$\eta_{harm} = \frac{W_{motor,ideal}}{W_{motor}} = \frac{HQ/\eta_{pump}\left(\frac{H}{Q^2}\right)}{W_{motor}\cdot\eta_{motor,ideal}[V,f,HQ/\eta_{pump}\left(\frac{H}{Q^2}\right)]} \quad (7.24)$$

Meanwhile, the VFD-harmonic efficiency can be calibrated using the VFD input power measured by a power meter replacing the motor input power

$$\mu_{V\&H} = \frac{W_{motor,ideal}}{W_{VFD}} = \frac{HQ/\eta_{pump}\left(\frac{H}{Q^2}\right)}{W_{VFD}\cdot\eta_{motor,ideal}[V,f,HQ/\eta_{pump}\left(\frac{H}{Q^2}\right)]} \quad (7.25)$$

Figure 7.2 summarizes the calibration and development process of a virtual pump water flow meter. The pump efficiency calibration associated with the measured pump head is not shown in this figure.

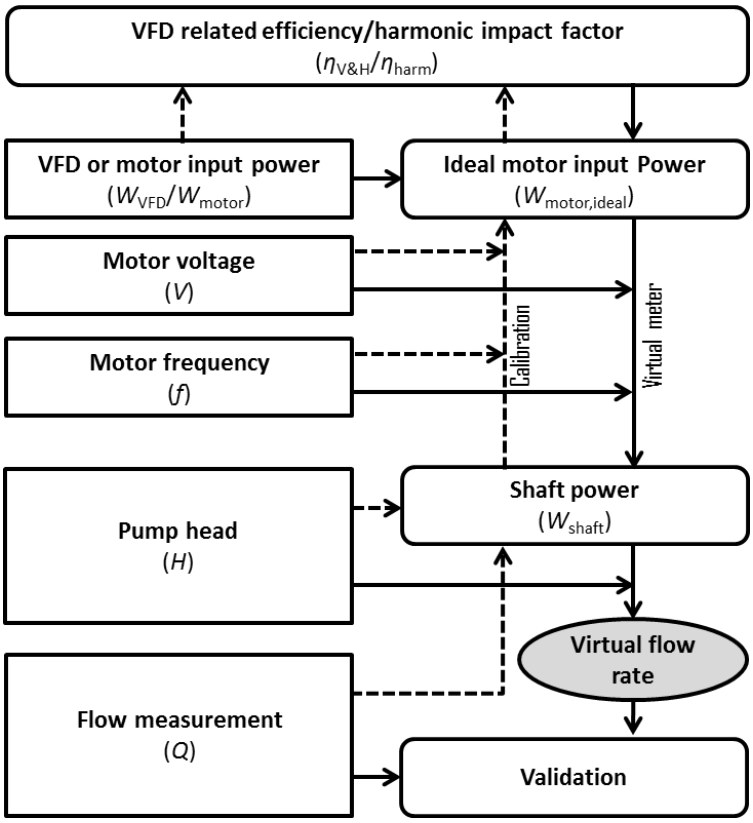


Figure 7.2: Calibration and virtual meter development.

## 7.5 Experiments

The experiments were conducted on a pump-motor-VFD system in a chilled water booster plant located at a library. The studied chilled water booster loop is a 200 mm nominal diameter main pipe fed by two pumps with alternating duty cycles and the VFD is modulated to maintain a building chilled water loop differential pressure setpoint. During the experiment, the system was set to operate continuously using one pump only without duty cycling.

Real-time monitoring and data acquisition were established at the experiment site as follows. The intended design was to obtain the motor input power and voltage from two

VFD analog output channels by two data loggers and obtain the motor input frequency from one VFD analog input channel by one data logger. A conventional externally installed ultrasonic water flow station was mounted on the chilled water pipe for the efficiency calibrations and virtual flow measurement validation. In addition to the noted variables and external data loggers, a differential pressure transducer was installed between the pump discharge and suction for pump head measurements.

Two separate experiments were conducted from April 24$^{th}$ to May 2$^{nd}$ and May 3$^{rd}$ to May 17$^{th}$ 2013 with a sample interval of one minute. The data collected from the first experiment was used to calibrate the pump, harmonic-degrade and VFD-harmonic efficiencies and develop a virtual pump water flow meter, while the data from the second experiment was used to validate the developed virtual water flow meter.

**Ideal motor efficiency**

A 15 kW (or 20 HP) 460 V three-phase induction motor provides power to the pump. The motor speed is 1,766 rpm at the rated load (15 kW or 20HP), power frequency (60 Hz) and voltage (460 volt). The motor nameplate and performance data, including efficiency and power factor at eight different load levels, were provided by the motor manufacturer and are listed in Table 7.1. The circuit parameters are then estimated using the method proposed by Wang et al. (2013) and listed in Table 7.2. With these six estimated circuit parameters, ideal motor efficiency ($\eta_{motor}$) and motor slip ($s$) fed by purely sinusoidal power is determined by VFD output voltage ($V$) and frequency ($f$) as well as either the ideal motor input power or the pump shaft power using the motor equivalent circuit method.

Table 7.1.Published motor performance data as well as converted data.

| Manufacturer | AO-Smith | | | | | | | |
|---|---|---|---|---|---|---|---|---|
| Model | BHD4J01I | | | | | | | |
| Motor type | NEMA Design B | | | | | | | |
| Size (HP) | 20 | | | | | | | |
| Synchronous speed (RPM) | 1800 | | | | | | | |
| Full load speed (RPM) | 1766 | | | | | | | |
| Voltage (V) | 460 | | | | | | | |
| Load (%) | 25 | 51 | 75 | 88 | 100 | 115 | 124 | 148 |
| Efficiency (%) | 43 | 66 | 76 | 79 | 80 | 81 | 82 | 82 |
| Power factor (%) | 89 | 93 | 93 | 93 | 93 | 93 | 92 | 91 |

Table 7.2.Calculated equivalent circuit parameters.

| Parameter (ohm) | Value |
|---|---|
| Stator winding resistance | 0.27623 |
| Stator leakage reactance | 1.56348 |
| Magnetizing reactance | 21.93410 |
| Core loss resistance | 721.59211 |
| Rotor winding resistance | 0.20668 |
| Rotor leakage reactance | 1.04753 |

**Pump efficiency associated with measured pump head**

The pump is a 3x4x11pump with impeller diameter of 0.2619 m, suction diameter of 100 mm and discharge diameter of 80 mm. The design flow is 37.9 L/s, the design head is 239 kPa and the design shaft power is 12.1 kW (or 16.2 hp) at a design speed of 1,750 rpm relative to a motor synchronous speed of 1,800 rpm. The pump head and shaft power curves at the design speed (1,750 rpm) were obtained from the pump manufacturer catalog, shown in Figure 3.

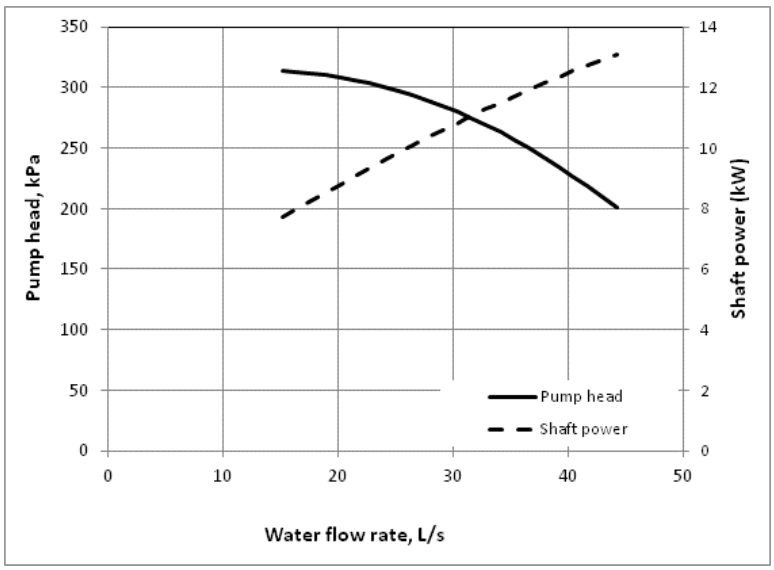


Figure 7.3: Pump head and shaft power curves at 1750 rpm.

The VFD output frequency is a key variable to calibrate the correction factor using Equations (7.19), (7.20) and (7.22). To guarantee the accuracy of the correction factor, only the measured data with the relative VFD output frequency above 70% are used. First, Equations (7.19) and (7.20) are applied to calculate the relative pump speed based on the measure water flow and VFD output frequency and voltage as well as the pump shaft power curve defined in Figure 7.3. Then the equivalent measured pump head curve at the design pump speed is created based on the calculated relative pump speed using Equations (7.21). Finally, the equivalent measured pump head is compared with the manufacturer pump head curve to determine the correction factor by minimizing the sum of the residuals in Equation (7.22) using the least squares method.

Figure 7.4 compares the calculated relative pump speed and measured relative VFD output frequency. It is clear that the relative pump speed is not equal to the relative VFD output frequency even though it is common to treat the relative pump speed as the same

as the relative VFD output frequency ideally. The ideal relationship is also drawn in the same figure. The reason for this offset is that the design pump speed is 1750rpm and the motor speed at the rated frequency is 1766 rpm. As a result, the relative pump speed is about 1% above the relative VFD output frequency.

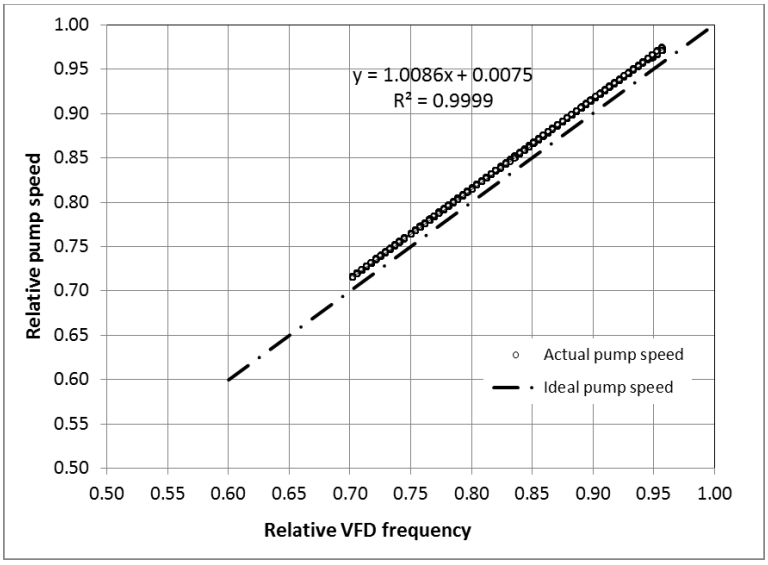


Figure 7.4: Pump speed verses VFD frequency.

Figure 7.5 compares the equivalent measured pump head curve marked by crosses with the manufacturer pump head curve marked with diamonds both at the design pump speed. The correction factor was regressed as 0.0374 kPa/(L/s)$^2$. The curve with circle markers represents the corrected pump head curve obtained from the manufacturer pump curve using Equation (7.17). The corrected pump head curve matches the measured pump head curve very well with the standard deviation of 2.21 kPa.

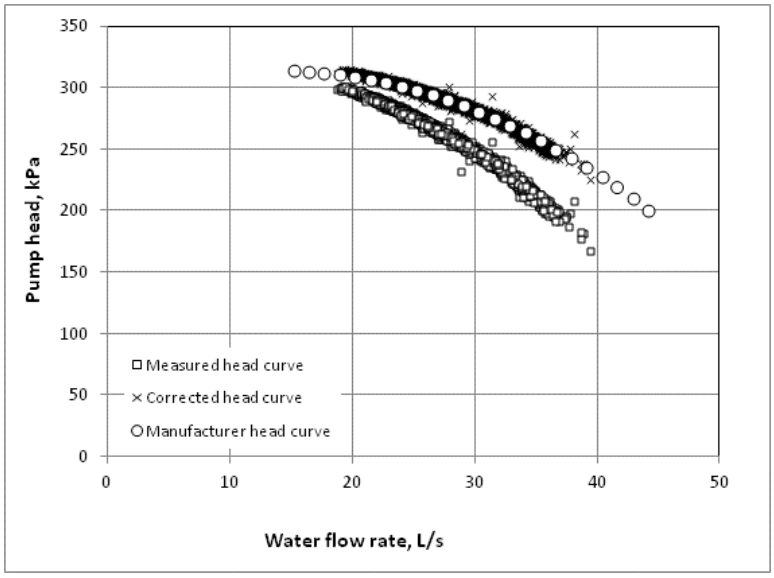


Figure 7.5: Measured, corrected and manufacturer pump head curves.

With the correction factor established, the pump efficiency associated with the measured pump head is obtained using Equation (7.18). Figure7.6 represents the pump efficiency curve with square markers versus the ratio of the measured pump head to the water flow squared. The manufacturer pump efficiency curve associated with the manufacturer pump head is also shown in Figure 7.6 with circle markers versus the ratio of the manufacturer pump head to the water flow squared.

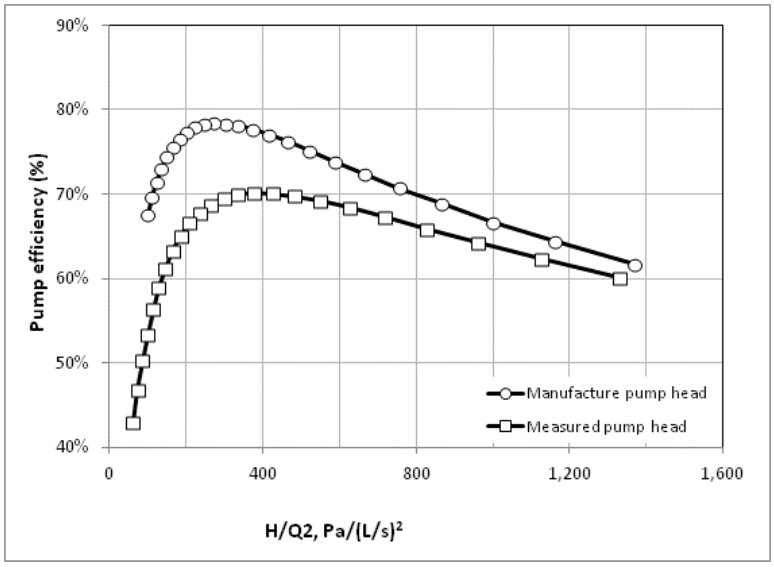


Figure 7.6: Pump efficiency curves associated with both measured and manufacturer pump head.

The pump efficiency curve associated with the measured pump head in Figure 7.6 is regressed with two, third order polynomials, each in different ratio range to improve the accuracy of the pump efficiency calculation.

$$\eta_{pump} = \begin{cases} 7.7635\times10^{-9}\left(\frac{H}{Q^2}\right)^3 - 9.3875\times10^{-6}\left(\frac{H}{Q^2}\right)^2 \\ +\,3.6386\times10^{-3}\left(\frac{H}{Q^2}\right) + 0.2458 \end{cases} \quad if\ \frac{H}{Q^2} \le 38 Pa/(L/s)^2$$

$$\eta_{pump} = \begin{cases} 1.5796\times10^{-10}\left(\frac{H}{Q^2}\right)^3 - 4.3120\times10^{-7}\left(\frac{H}{Q^2}\right)^2 \\ +\,2.5387\times10^{-4}\left(\frac{H}{Q^2}\right) + 0.6564 \end{cases} \quad if\ \frac{H}{Q^2} > 38 Pa/(L/s)^2 \qquad (7.26)$$

**Harmonic-degraded and VFD-harmonic efficiencies calibration**

With the calibrated pump efficiency curve associated with the measured pump head, the harmonic-degraded efficiency and VFD-harmonic efficiency are calibrated using

Equations (7.24) and (7.25) respectively. Figure 7.7 shows the harmonic-degraded efficiency versus the motor input power curve and the VFD-harmonic efficiency versus the VFD input power curve. Based on the data shown in Figure 7.7, the VFD-harmonic efficiency slightly decreases as the VFD input power decreases over the entire testing power range from 14 kW to 2 kW. On the other hand, the harmonic-degraded efficiency slightly increases as the motor input power decrease over the most testing power range from 12.5 kW to 3.5 kW but has a sudden drop and a sudden jump in a test power range between 3.5 kW and 1.5 kW. It is interesting that the VFD-harmonic efficiency that covers the harmonic-degraded efficiency does not show the sudden variation in the same power range; this may be an indication that the power reading from the VFD control panel is inaccurate when operating in the low power range. Figure 7.7 also shows that both the harmonic-degraded efficiency and VFD-harmonic efficiency curves have a wide band. This may result from the dynamic system operation. In general, more power is needed with a relatively low efficiency when the motor is accelerated and vice versa.

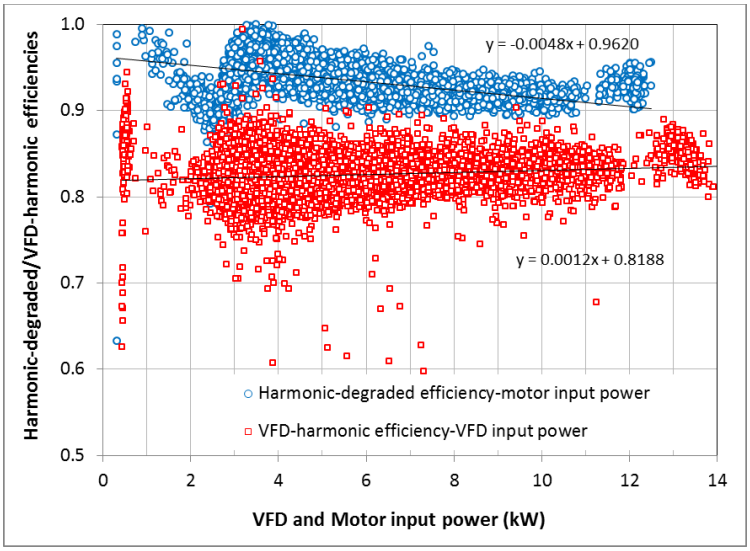


Figure 7.7: Harmonic-degraded and VFD-harmonic efficiencies.

As demonstrated by Figure 7.7 above, since the VFD-harmonic and harmonic-degraded efficiencies are approximately constant, the virtual flow meter model developed with harmonic effect embedded into the pseudo pump efficiency as detailed in Chapter 5 of this study, (Andiroglu et al. 2013) also achieves results with acceptable level of accuracy. However, the procedure developed in this Chapter provides a more accurate and reliable approach for the developed virtual water flow meter with a VFD-motor-pump system.

Even though the harmonic-degraded efficiency within the low power range has a sudden variation, the variation is still less than 10%. Meanwhile, the water flow rate within this power range is also small. Therefore, a linear regression is applied to project both the harmonic-degraded efficiency and VFD-harmonic efficiency. Based on the data in Figure 7.7, the harmonic-degraded efficiency and the VFD-harmonic efficiency are regressed as

$$\eta_{harm} = -0.0048W_{motor} + 0.962 \quad (7.27)$$

$$\eta_{V\&H} = 0.0012W_{VFD} + 0.8188 \quad (7.28)$$

## 7.6 Virtual water flow rate calculation and meter validation

With identified pump efficiency, Equaiton (7.26), harmonic-degraded efficinecy, Equation (7.27), and VFD-harmonic efficinecy, Equaiton (7.28) as well as the ideal motor efficinecy determined by the motor equivalent circuit method, the water flow rate can be calculated from the measured pump head, VFD output freqeuncy and voltage and either the motor input power or the VFD input power using Equation (7.11) or (7.14).

Since Equations (7.11) and 7.14) are implicit expression of the water flow rate, a numerical method, such as bisection method, has to be applied.

The data during the validation period included 19,500 samples with a one-minute sample interval, and were used for validating both approaches. Figure 7.8 compares the water flow rate measured by the ultrasonic water flow meter installed at the experiment site and the developed virtual water flow meter using the VFD input power and the motor input power respectively in a 6 hours period. Virtual water flow measurements obtained using either approach matched well with the measurements provided by the physical meter.

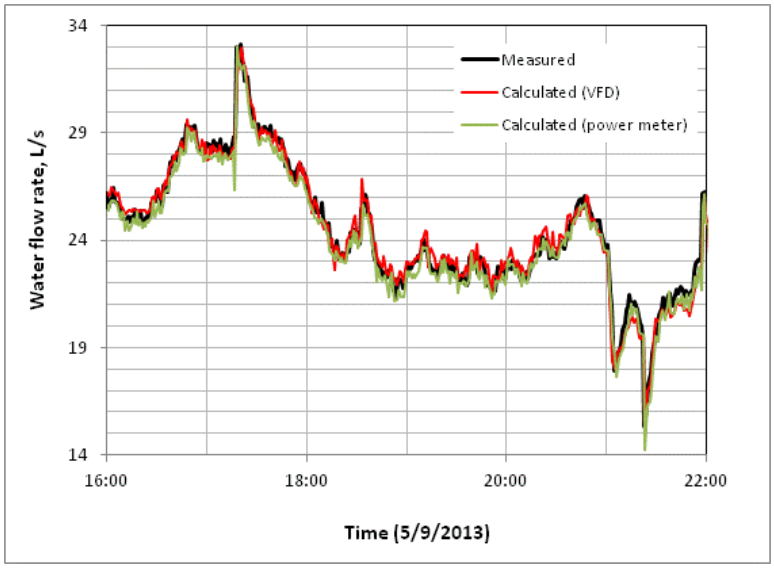


Figure 7.8: Comparison of measured water flow and calculated water flow over 6-hour period.

Figures 7.9 and 7.10 demonstrate the virtual water flow measurement error of two types of virtual pump flow meters, using the VFD input power measured by a power meter and the motor input power read from the VFD contorl panel respectively.

The coefficient of determination or R-square for the entire validation period is 0.97 using the VFD input power and 0.91 using the motor input power. The standard deviation for the entire validation period is 0.60 L/s for both of the virtual pump flow meters.

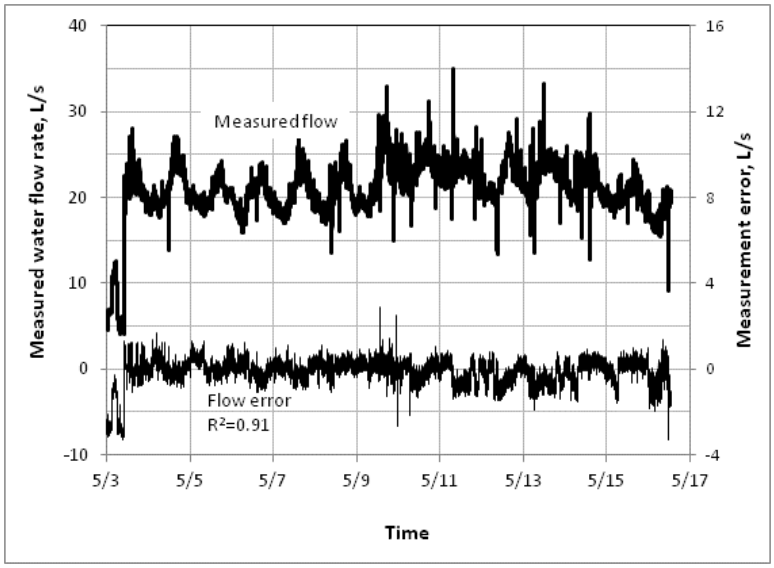


Figure 7.9: Measurement error over entire validation period using the motor input power

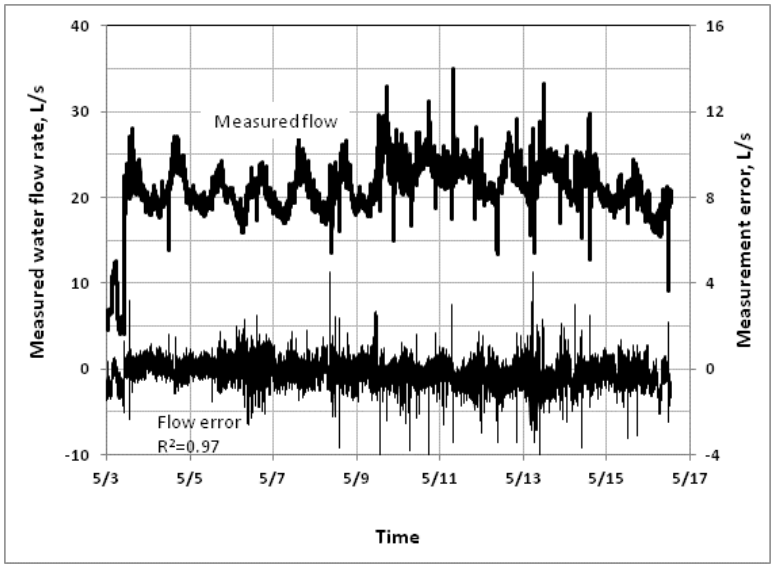


Figure 7.10: Measurement error over entire validation period with the VFD input power.

Figure 7.11 represents the level of agreement between actual measured water flow rate and calculated water flow rates using the devleoped virtual water flow meters. The experimental results show that the water flow rate determined by either of the virtual flow meters agrees well with the result from the installed ultrasonic water flow meter.

However, since the harmonic degraded efficiency obtained through application of linear regression cannot accurately represent the efficiency when operating in low power range, the virtual flow rate obtained using the motor input power from the VFD control panel shows more errors in this range.

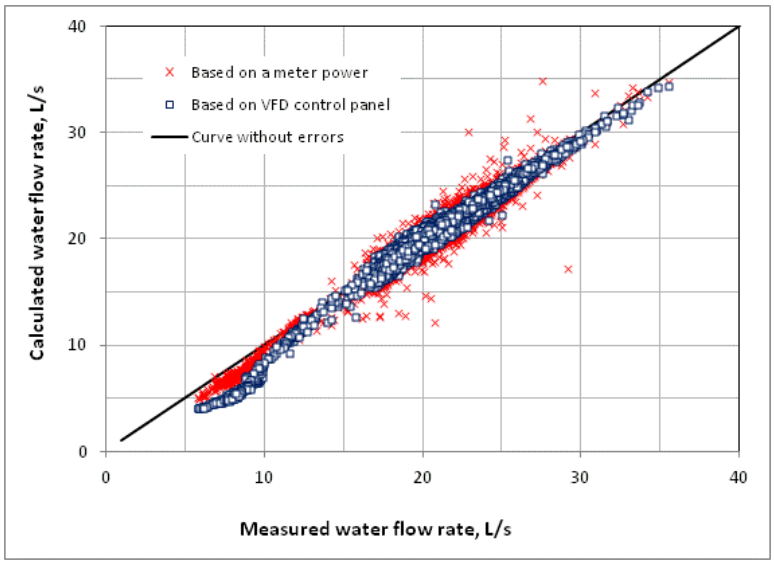


Figure 7.11: Virtual water flow rate versus measured water flow rate.

## 7.7 Summary

The water flow correlation with the pump head and VFD output frequency and voltage and either the VFD output power or the motor input was developed in association with pump, motor, and VFD efficiencies. The comprehensive pump, motor and VFD efficiency calibration procedures were designed with consideration of additional motor

harmonic loss. An experiment was conducted to develop, calibrate and validate a virtual pump water flow meter on a VFD-motor-pump system, which virtually determines the pump water flow rate based on the pump head measured by a water differential pressure transducer, VFD output frequency and voltage obtained from the VFD control panel and either the VFD input power measured by a power meter or the motor input power obtained from the VFD control panel. The water flow rates determined by the proposed virtual water flow meters agreed well with the actual water flow meter measurement for the full range of operating frequencies.

# CHAPTER 8

# COMPARISON OF DIFFERENT APPROACHES

In this chapter, outcome of multiple models and approaches for the development of virtual water flow meter are compared and analyzed in order to formulate a virtual water flow meter with the greatest accuracy and further rectify the significance of the proposed head-power based virtual flow meter in comparison to head-based model developed. Data collected from the experiment site was used for comparitive analysis of different approaches. In addition to the head-based model which is briefly outlined in this chapter based on the theoretical approach detailed in Chapter 3 earlier, the head-power based approaches implemented were the following:

- Harmonic loss coupled with pseudo pump efficiency for the development of Virtual Water Flow Meter.
- Using motor input power obtained from VFD output when detailing comprehensive motor efficiency broken down as harmonic-degraded efficiency and ideal motor efficiency for the development of Virtual Water Flow Meter.
- Using VFD input power measured by a power meter when detailing comprehensive motor efficiency broken down as harmonic-degraded efficiency and ideal motor efficiency for the development of Virtual Water Flow Meter.

The outcome from each case is then compared with actual flow rate measurements. The results are summarized in the following sections.

## 8.1 Head-based virtual water flow meter model and its outcome

The affinity laws is applied to convert measured pump head and water flow rate under actual pump speed to the head versus flow rate under the full speed. Figure 8.1 shows the converted pump head curve under the full speed.

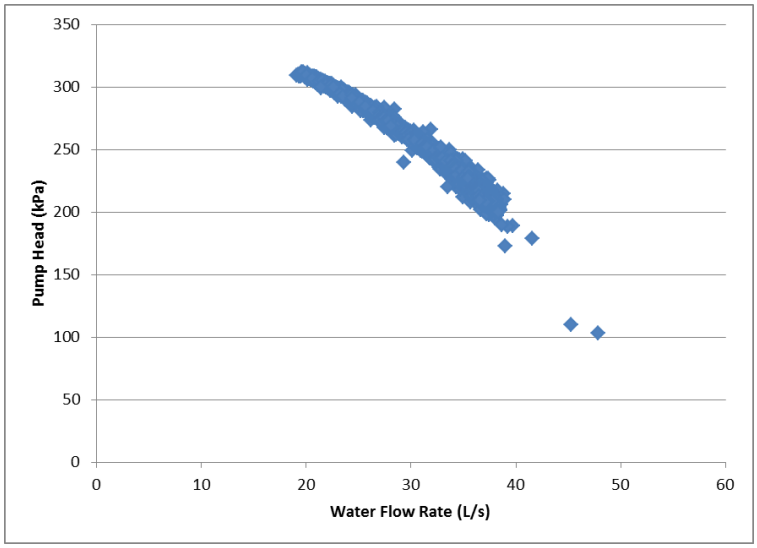


Figure 8.1: Converted pump head curve under full speed.

Then head (in kPa) versus water flow (in L/s) curve under the full speed is regressed as a second order polynomial, as shown by Equation (3.1) below:

$$H = -0.105Q^2 + 0.3432Q + 344.51 \qquad (8.1)$$

Then the water flow rate can be calculated based on discussion presented in Chapter 3 of this dissertation, under section 3.2, using the following equation:

$$Q = \frac{-a_1\omega_r - \sqrt{a_1^2 * \omega_r^2 - 4a_2[a_0\omega_r^2 - H]}}{2 * a_2} \qquad (8.2)$$

Flow rate error between measured actual rates and calculated rates using head-based virtual flow meter are shown in figure 8.2 below for full range of operating frequency.

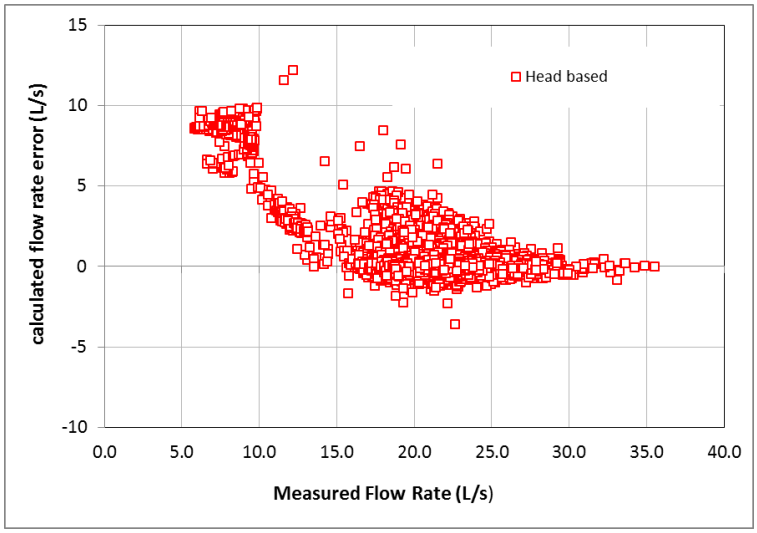


Figure 8.2: Calculated flow rate error versus measured flow rates

The coefficient of determination or R-square for the entire validation period for the pump-head-curve based water flow meter model was calculated to be 0.924. The validation period for this method of calculations included data gathered for operating frequencies ranging from 30 Hz to full load; data collected from operating frequencies lower than 30 Hz was ignored since the flow meter model based on measured head data did not yield accurate and reliable results. This outcome was consistent with studies previously conducted by others. As it can be seen on Figure 8.2, while the flow rate error for mid-to-high flow rates may average +/- 3 L/s, at lower frequencies, flow rate errors jump up to 10 L/s. This outcome confirms that the head-based virtual flow meter model is defficient at lower operating frequencies, corresponding to the flat section of the pump head curve.

## 8.2 Outcome of head-power based virtual flow meter model using pseudo pump efficiency

Head-Power based water flow meter based on pseudo pump efficiency model developed using VFD output power at an experiment site with a 20 HP chilled water pump and VFD system produced outcome with a coefficient of determination or R-square of 0.88, when validated using actual water flow measurements recorded by an ultrasonic water flow meter over the full range of operating frequencies. Figure 8.3 below represents the flow rate error based on this model compared to flow rate errors documented using the head-based virtual flow meter model discussed in section 8.1 above.

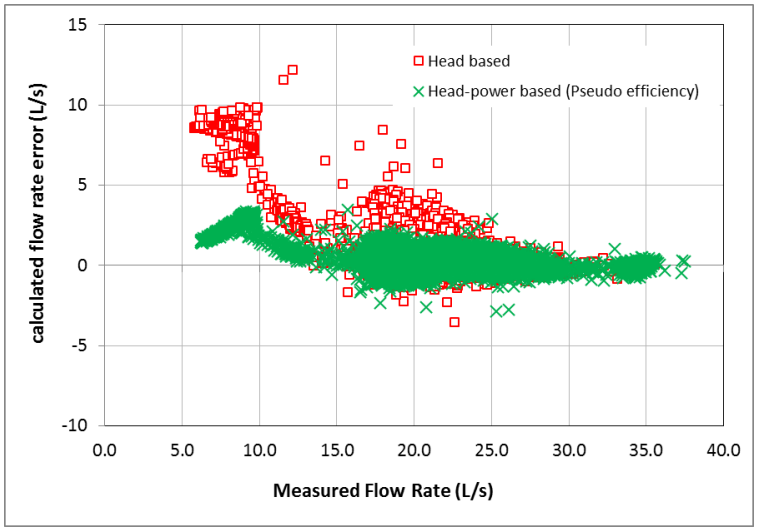


Figure 8.3: Calculated flow rate error versus measured flow rates for head-based and head-power based virtual flow meter models

The coefficient of determination or R-square for the entire validation period for the head-power based water flow meter model using pseudo pump efficiency was calculated to be 0.88. As it can be seen from Figure 8.3, the calculated flow rate error compared to

measured flow rates are +/- 2 L/s at mid to high flow range, and up to around 3.5 L/s at low frequency ranges. Based on these findings, it may be concluded that this model yields notably improved outcome for full range of operating conditions.

### 8.3 Outcome of head-power based virtual flow meter model with impact of harmonic-degraded efficiency using motor input power

Waterflow rate was calculated from the measured pump head, VFD output freqeuncy and voltage and the motor input power using Equation 7.11. The data during the validation period included 19,500 samples with a one-minute sample interval for the full range of operating frequencies. Figure 8.4 represents the water flow rate error based on comparison to values measured by the ultrasonic water flow meter installed at the experiment site along with comparison of head-power based virtual flow meter developed using pseudo pump efficiency, as discussed in section 8.2 above.

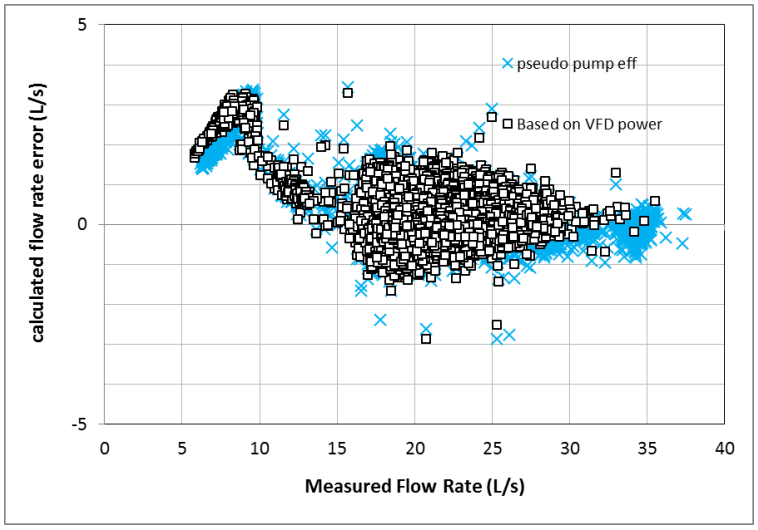


Figure 8.4: Calculated flow rate error with harmonic-degraded efficiency using motor input power compared to head-power based model using pseudo pump efficiency

Virtual water flow measurements obtained using this approach matched well with the measurements provided by the physical meter; the coefficient of determination or R-square for the entire validation period for this approach was calculated to be 0.91; the validation period included data gathered for full operating frequencies, ranging from 0.2 Hz to full load. As it can be seen from Figure 8.4, flow rate errors were +/- 2 L/s for mid- to high frequency ranges and up to 3 L/s at low frequency range. Compared to model outcomes summarized under sections 8.1 and 8.2 above, this model showed more reliable results for the full range of operating frequency.

### 8.4 Outcome of head-power based virtual flow meter model with impact of harmonic-degraded efficiency using VFD input power from power meter

Waterflow rate was calculated for head-power based virtual flow meter using Equation 7.14 with measured pump head, VFD output frequency, voltage and VFD input power measured by a power meter. This approach was carried out in order to establish if the VFD output readings may be considered as a reliable source for motor input power, and thus possibly eliminate the need for an independent power meter for the water flow meter development model. Flow rate errors between actual measured flow rates and flow rates calculated from head-power based virtual flow meter model with impact of harmonics degraded efficiency using VFD input power from a power meter are shown in Figure 8.5 below. A comparison of outcome against the virtual flow meter model discussed under section 8.3 above is also provided in Figure 8.5.

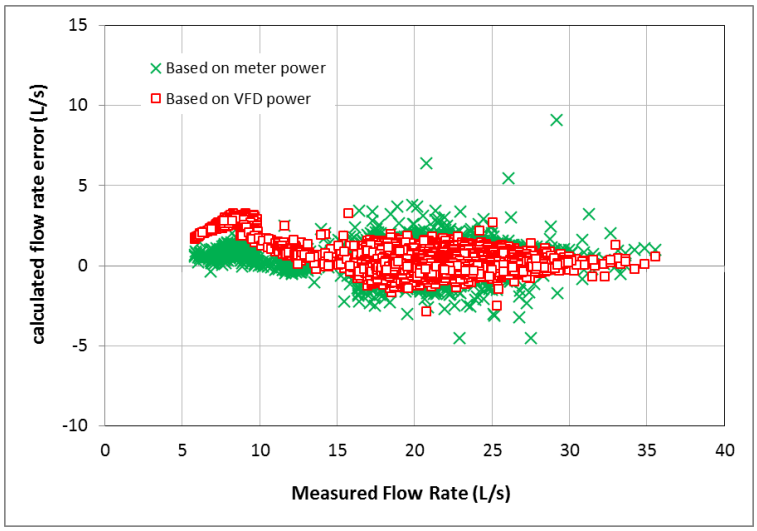


Figure 8.5 Calculated flow rate error with harmonic-degraded efficiency using VFD input power measured by a power meter compared to meter model based on motor input power from VFD.

Once again, consistent with other approaches, the data during the validation period included 19,500 samples with a one-minute sample interval. Figure 8.5 represents the calculated water flow rate error compared to actual flow rates measured by the ultrasonic water flow meter installed at the experiment site. Virtual water flow measurements obtained using this approach matched very well with the measurements provided by the physical meter; the coefficient of determination or R-square for the entire validation period for this approach was calculated to be 0.97; the validation period included data gathered for the full operating frequency range, from 0.2 Hz to full load. As it can be seen from Figure 8.5, flow rate errors were +/- 2 L/s for mid to high full rates and operating frequencies and an average of +/- 1 L/s for low frequency ranges. Based on this outcome, compared to all other model outcomes summarized in sections 8.1, 8.2 and 8.3 above, this model shows the most reliable and consistent results for the full range of operating frequencies.

Figure 8.6 below shows a more pronounced detail of the comparison of calculated flow rate errors from all virtural flow meter models studied and discussed in this chapter. While at higher frequency and flow ranges , the outcome from all of the virtual flow meter models developed have been demonstrated to be fairly consistant with actual flow measurements, the two head-power based virtual flow meter models developed with harmonic-degraded efficiency impact considered, performs best at lower range of operating frequencies compared to head-based model and head-power based model using pseudo pump efficiency.

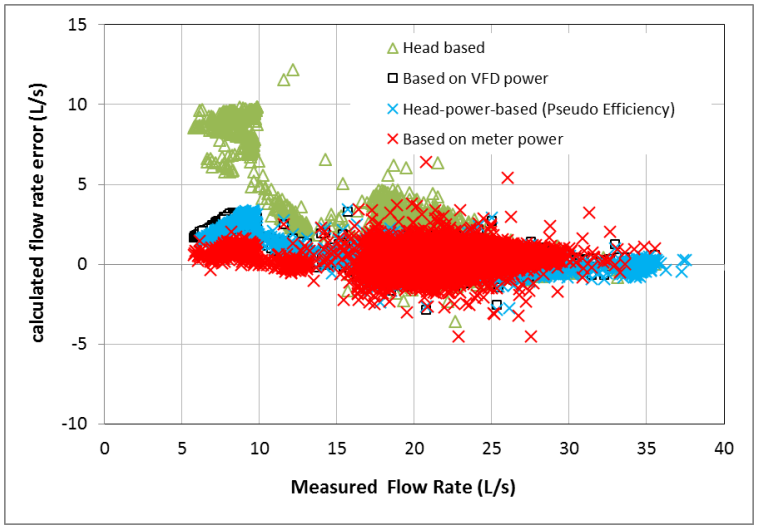


Figure 8.6 Comparison of calculated flow rate error for all developed virtual flow meter models

Furthermore, based on the data presented in Figure 8.6, head-power based virtual flow meter model with impact of harmonic-degraded efficiency using motor input power yields a greater error margin compared to head-power based virtual flow meter model with impact of harmonic-degraded efficiency using VFD input power from power meter.

This may be attributed to the error associated with the estimation of the harmonic-degraded efficiency in lower power range using a linear regression as discussed earlier in Chapter 7, which may also suggest that VFD analog output data for motor input power may not be a reliable source due to inaccuracies associated with VFD efficiency at lower frequency ranges.

Thereofore, it can be concluded that compared to model outcomes summarized under sections 8.1 , 8.2 & 8.3 above, the head-power based virtual flow meter model with impact of harmonic-degraded efficiency using VFD input power from power meter shows the most reliable results with the highest accuracy for the full range of operating frequencies.

# CHAPTER 9

# CONCLUSIONS AND SUGGESTIONS FOR FUTURE STUDY

## 9.1 Conclusions

The theory of virtual air and water flow meters with precise motor efficiency and fan/pump efficiency models are demonstrated. Flow rates can be virtually determined based on measured motor power, voltage and frequency, and pump head as well as the projected motor and pump efficiency models. Furthermore, it has been demonstrated that the power-head based virtual fan air flow and pump water flow models yield significantly more accurate and reliable results across full range of VFD frequencies, in comparison to head only based models previously developed by others.

The objectives outlined for this study has been achieved as summarized below:

**1.** A vitual airflow meter and a virtual water flow meter with consideration to impact of the VFD frequency on motor efficnecy using the motor equivalent circuit method were developed. All other uncertainties, including harmonic loss and fan/pump loss, were lumped into pseudo fan / pump efficiency,which was identified through a calibration process. The experiment results carried out for variable speed conditions using motor model with pseudo fan efficiency on a small fan-motor-VFD system show that the air flow rates determined by the virtual flow meter agrees well with the actual air flow measurements. The coefficient of determination or R-square for the entire validation period is 0.717. The fluctuations are observed for the virtual air flow measurement. The moving average can filter the fluactuation. With five minute moving average the R-square is improved to 0.813.

The virtual water flow meter experimentally tested and developed on a chilled water pump using the same motor model with pseudo pump efficiency on a medium size pump-motor-VFD system yielded even more accurate results. The water flow determined by the developed virtual water flow meter using VFD output data for motor input agrees well with the ultrasonic water flow meter measurement as indicated by the R-square of 0.86 for instant measurement. Based on this outcome it may be concluded that the use of VFD output data for motor power for larger motors may be considered as a viable option and warrants further investigation.

**2.** The water flow rates determined by the virtual water flow meter developed with impact of VFD induced harmonics degradation considered on motor and actual VFD efficiencies, proved to yield consistently reliable outcome for full range of operating speeds.

**3.** The water flow rates were determined by the virtual water flow meter developed with impact of VFD induced harmonics degradation considered on motor and actual VFD efficiencies using the VFD input power measured by a power meter and the motor input power read from the VFD contorl panel respectively. The experimental results show that the water flow rate determined by either of the virtual flow meters agrees well with the result from the installed ultrasonic water flow meter. The coefficient of determination or R-square for the entire validation period is 0.97 using the VFD input power and 0.91 using the motor input power. The standard deviation for the entire validation period is 0.60 L/s for both of the virtual pump flow meters. However, since the harmonic degraded efficiency obtained through application of linear regression cannot accurately represent

the efficiency when operating in low power range, the virtual flow rate obtained using the motor input power from the VFD control panel shows more errors in this range.

**4.** Upon verification and validation of the developed meter models based on the three objectives identified above, it can be further concluded that even though the VFD control panel provides an economic approach to obtain the motor power without the use of a power meter, the accuracy of the VFD power reading is uncertain when applied to systems where small motors are in use. The virtual airflow meter using the VFD input power produced consistently more accurate results. However, the motor input power from VFD control panel did not yield as accurate results since the power data from the VFD in use was limited to increments of 0.1 kW and the motor in use was small (3 HP). On the other hand, considering that with a larger pump motor (20 HP) used in the experimental development model for the virtual water flow meter developed with impact of VFD induced harmonics degradation considered using VFD output power, calculated water flow rates agreed well with the ultrasonic water flow meter measurement, (as indicated by the R-square of 0.97 for instant measurement), it can be concluded that this approach can be considered reliable.

### 9.2 Suggestions for future study

Experimental investigations carried out as part of this study for the development and validation of virtual air and water flow meters using a VFD-pump/fan-motor system have been based on two motors (3 HP fan motor and a 20 HP pump motor). While use of VFD output panel data for motor input power allows for the implementation of a simpler model, its' reliability has not been demonstrated and confirmed. Therefore, application of

the different meter models discussed in this study through additional experimental investigations using varying motor sizes with the VFD-fan/pump-motor systems is suggested. In addition, further investigation of VFD-motor system through additional experimental set ups using varying motor sizes with VFD bypass capability is warranted in order to detail and validate VFD related power losses and impact of such losses on VFD and motor efficiencies. Analysis of collected data outcome when VFD is in bypass mode of operation compared to projected power distribution profile with VFD in use, can quantify the significance of potential errors and their impact on virtual flow meter development model.

Furthermore, full design and development of the virtual air / water flow meters based on the theoretical development models presented in this study, setting the pathway for their practical implementation in industry applications may be anticipated in the future.

## REFERENCES


Andiroglu, E., Wang, G., Song, L., Kiamehr, K. 2015. Development of a Virtual Pump Water Flow Meter Using Power Derived from Comprehensive Energy Loss Analysis. Submitted to Science and Technology for the Built Environment section at ASHRAE.

Andiroglu, E., Wang, G., Song, L.2013. Development of a Virtual Water flow Meter using Pump Head and Motor Power. Zero Energy Mass Customization Housing (ZEMCH2013) International Conference, October 30-Nov 1, 2013, Miami, FL.

ANSI/AMCA Standard 99-10: Standards Handbook. 2003.

ASHRAE Handbook, Fundamentals, 2001: Measurement and Instruments, American Society of Heating, Refrigerating and Air Conditioning Engineers, Atlanta, 111.

ASHRAE 90.1-2010. Energy Standard for Buildings Except Low-Rise Residential Buildings.

ASHRAE 2009. 2009 ASHRAE Handbook-Fundamentals. Atlanta: American Society of Heating, Refrigeration and Air-conditioning Engineers, Inc.

ASHRAE. 2009. 2009 ASHRAE Fundamentals Handbook, Measurement and Instruments, American Society of Heating, Refrigerating and Air-conditioning Engineers, Inc., Atlanta, GA.

ASHRAE 1987. ASHRAE Standard 41.2-1987, Standard Methods for Laboratory Airflow Measurement. Atlanta: American Society of Heating, Refrigeration and Air-conditioning Engineers, Inc.

Boglietti, A., Cavagnino, A., Knight, A. M. 2008. Isolating the Impact of PWM Modulation on Iron Losses, Proceeding of IEEE-IAS'08 Annual Meeting, Edmonton, Canada.

Burt, C. M., X. Piao, F. Gaudi, B. Busch, and N. F. N. Taufik. 2008. Electric Motor Efficiency under Variable Frequencies and Loads. Journal of Irrigation and Drainage Engineering, V 134, n 2, p.129-136.

Carrier. 2005. Variable Frequency Drive. Carrier Corporation, Syracuse, New York

CCI. Clinton Climate Initiative, 2006. CLINTONFOUNDATION.ORG

CEATI. 2000. Energy Efficient Reference Guide: Variable Frequency Drives. CEATI International, Montreal, QC, Canada.

Celenza, L., Dell'Isola, M., Ficco, G., Palella, B., Riccio, G. 2015. Heat Accounting in Historical Buildings, Energy and Buildings, 95, 47-56.

Cisco, 2005, Cisco Connected Real Estate, http://www.builconn.com/downloads/CCRE-WP2.pdf

DOE. 2008. Improving Motor and Drive System Performance: A Sourcebook for Industry. U.S. Department of Energy, Office of Energy Efficiency and Renewable Energy, Washington, DC

DOE 2010. Operations and Maintenance Best Practices. The U.S. Department of Energy.

DOE. 2012a. Energy Tips: Motor Systems (Tip Sheet #11). The U.S. Department of Energy Advanced Manufacturing Office of Energy Efficiency and Renewable Energy, Washington, DC.

DOE. 2012b. Energy Tips: Motor Systems (Tip Sheet #14). The U.S. Department of Energy Advanced Manufacturing Office of Energy Efficiency and Renewable Energy, Washington, DC.

DOE. 2013. Energy savings potential and opportunities for high-efficiency electric motors in residential and commercial equipment. Washington DC: U.S. Department of Energy Building Office. Energy.gov/sites/prod/files/2014/02/f8/Motor Energy Savings Potential Report 2013-12-4.pdf.

Domijan, A., A. Abu-aisheh, and D. Czarkowski. 1997. Efficiency and Separation of Losses of an Induction Motor and its Adjustable-speed Drive at Different Loading/speed Combinations. ASHRAE Transactions, v 103, n 1, p. 228-234.

EIA 2010. The U. S. Energy Information Administration, Independent Statistics & Analysis. eia.gov

EPAct. Energy Policy Act of 2005. An Act to ensure jobs for our future with secure, affordable, and reliable energy. Enacted by the 109th United States Congress on August 8, 2005.

Federspiel, C. 2000. Predicting the Frequency and Cost of Hot and Cold Complaints in Buildings. HVAC & R Research 6(4):289-305.

Friedman, H., M. Shuman, D. Claridge, J. Curtain, and P. Haves. 2007. Building Commissioning: Innovation to Practice Technical Report. California Energy Commission, PIER Energy-Related Environmental Research Program. CEC-500-2008-074.

Gao, D.C., Wang, S., Sun, Y. 2011. A Fault-Tolerant and Energy Efficient Control Strategy for Primary–Secondary Chilled Water Systems in Buildings, Energy and Buildings, 43 (12) 3646-3656.

Gao, X., McInerny, S. A. and Kavanaugh, S. P. 2001. Efficiencies of an 11.2 kW Variable Speed Motor and Drive. ASHRAE Transactions, v 107, PART 2, p. 259-265.

Gragger, J. V., Haumer, A., Kral, C., Pirker, F. 2008. Efficient Analysis of Harmonic Losses in PWM Voltage Source Induction Machine Drives with Modelica. Proceedings of the 6th Modelica Conference 2008, Bielefeld, Germany.

Hughes, A. 2006. Electric Motors and Drives Fundamentals, Types and Applications, 3rd Edition. Burlington: Elsevier Ltd.

IEEE. 2004. IEEE Standard 112-2004, IEEE Standard Test Procedure for Polyphase Induction Motors and Generators. New York: IEEE Power Engineering Society.

ISO. 2012. Rotodynamic Pumps - Hydraulic Performance Acceptance Tests -- Grades 1, 2 and 3. International Standard (ISO 9906:2012).

Joo, Ik-Seong; Liu, Mingsheng; Liu, Guopeng. 2007. Application of Fan Airflow Stations in Air-Handling Units. Energy Engineering, 104(2):66-80.

Katipamula, S. and Brambley, M.R. 2005. Methods for Fault Detection, Diagnostics, and Prognostics for Building Systems – A Review, Part I. HVAC & R Research, 11(1):3-25.

Kueck, J. D., Olszewski, M., Casada, D. A., Hsu, J., Otaduy, P. J. and Tolbert, L. M. 1996. Assessment of Methods for Estimating Motor Efficiency and Load under Field Conditions. ORNL/TM-13165, Oak Ridge National Laboratory, Oak Ridge, TN.

LEED. U. S. Green Building Council. Leadership in Energy & Environmental Design is a green building certification program that recognizes best-in-class building strategies and practices.

Li, H and Braun, J.E. 2007a. Decoupling Features and Virtual Sensors for Diagnosis of Faults in Vapor Compression Air Conditioners. International Journal of Refrigeration, 30(3): 546-564.

Li, H and Braun, J.E. 2009a. Development, Evaluation and Demonstration of a Virtual Refrigerant Charge Sensor. HVAC &R Research, 15(1):117-136.

Li, H and Braun, J.E. 2009b. Virtual Refrigerant Pressure Sensors for Use in Monitoring and Fault Diagnosis of Vapor-Compression Equipment. HVAC & R Research, 15(3): 597-616.

Li, H., Yu, D., and J.E. Braun, 2011. A Review of Virtual Sensing Technology and Application in Building Systems. HVAC & R Research.

Liu, M., Claridge, D. E., Haberl, J. S. and Turner, W.D. 1999. Improving Building Energy Systems Performance by Continuous Commissioning. Energy Engineering, May.

Liu, G., Joo, I., Song, L., and Liu, M. 2003. Development of In-situ Fan Curve Measurement with One Airflow Measurement, Proceedings of the International Conference for Enhanced Building Operations (ICEBO), October 13-14, Berkley, California.

Liu, G. and Liu, M. 2005. Impact of Motor Slip and Belt Slip on Fan Air Flow Station for VAV AHU Systems, Proceedings of the SOLAR 2005 CONFERENCE (ISEC'05), August 6-12, Orlando, Florida.

Liu, G. and Liu, M. 2006. Determination of Building Load Condition in Dual Duct System, ICEBO 2006, November 6-8, 2006, Shenzhen, China.

Liu, G. and Liu, M. 2007. Application of the Pump Water Flow Station for Optimizing Pump Speed Control. ASHRAE Winter 2007, Dallas.

Liu M. 2002. Variable Speed Drive Volumetric Tracking (VSDVT) for Airflow Control in Variable Air Volume (VAV) Systems. Journal of Solar Energy Engineering, Transactions of the ASME, v 125, n 3, p 318-323.

Liu, M., Liu, G., Joo, I., Song, L. and Wang, G. 2005. Development of In Situ Fan Curve Measurement for VAV AHU Systems. Journal of Solar Energy Engineering, 127(2): 287-293.

Liu, Guopeng; Liu, Mingsheng; Wang, Gang. 2007a. Development of a Pump Water Flow Station in HVAC Systems. 2007 Energy Sustainability Conference.

Liu, Guopeng; Liu, Mingsheng; Wang, Gang. 2007b. Optimized Pump Speed Control Using Pump Water Flow Station for HVAC Systems. ASHRAE Transactions, 113(2):362-367.

Manz, L.B., Morgan, R. B. 1999. Mating New Variable Frequency Drives to Existing Motors. Electrical Construction and Maintenance. March, 1999

McIntosh, Ian B.D., Mitchell, John W. and Beckman, William A. 2000. Fault Detection and Diagnosis in Chillers-Part I: Model Development and Application. ASHRAE Transaction 106:268-282.

Milanese, Mario; Regruto, Diego; Fortina, Andrea. 2007. Direct Virtual Sensor (DVS) Design in Vehicle Sideslip Angle Estimation, 2007. American Control Conference: 3654-3658.

Plessis, G. E. D., Liebenberg, L., Mathews, E. H. 2013. The Use of Variable Speed Drives for Cost-Effective Energy Savings. Applied Energy 111 (2013) 16–27.

Prindle, W., Dietsch, N., Elliott, R.N., Kushler, M., Langer, T., and Nadel, S. (2003). Energy Efficiency's Next Generation: Innovation at the State Level (Publication No. E031). Washington, DC: American Council for an Energy-Efficient Economy.

Reddy, T. Agami 2007a. Formulation of a Generic Methodology for Assessing FDD Methods and its Specific Adaptation to Large Chillers. HVAC & R Research, 113(2):334-342.

Reddy, T. Agami 2007b. Development and Evaluation of a Simple Model-Based Automated Fault Detection and Diagnosis (FDD) Method Suitable for Process Faults of Large Chillers. ASHRAE Transactions, 113(2):27-39.

Saidura, R.; Rahim, N.A.; Ping, H.W.; Jahirul, M.I.; Mekhilefb, S.; Masjuki, H.H.;. 2009. Energy and Emission Analysis for Industrial Motors in Malaysia, Energy Policy 37 (2009)3650–3658

Seo, Donghyun; Huang, Joe; Krarti, Moncef. 2008. Development of Models for Hourly Solar Radiation Prediction. ASHRAE Transactions, 114(1):392-403.

Song, L., Joo, I., Wang, G. 2012. Uncertainty Analysis of a Virtual Water Flow Measurement in Building Energy Consumption Monitoring. International Journal of HVAC&R Research, DOI: 10.1080/10789669.2012.658137, 18:5, 997-1010.

Song, L., Wang, G., Brambley, M. R. 2013. Uncertainty Analysis for a Virtual Flow Meter Using an Air-Handling Unit Chilled Water Valve. International Journal of HVAC&R Research, in press.

Sousa, G.C.D., B.K. Bose, J. Cleland, R.J. Spiegel, and P.J. Chappell. 1992. Loss Modeling of Converter Induction Machine System for Variable Speed Drive. The 1992 International Conference on Industrial Electronics, Control, Instrumentation, and Automation, 114-20 vol.1

Swamy, A., Song, L., & Wang, G. 2012. A Virtual Chilled-Water Flow Meter Development at Air Handling Unit Level. ASHRAE Transactions 118(1): 1013-1020.

Venkataraman, B. Godsey, W. Premerlani, W., Shulman, E., Thaku, M., Midence, R. 2005. Fundamental of Motor Thermal Model and Its Application in Motor Protection, 58th Annual Conference for Protective Relay Engineers, pp 127-142, July 2005

Waide, P. and Brunner, C.U. 2011. Energy-Efficiency Policy Opportunities for Electric Motor-Driven Systems. Paris: International Energy Agency.

Wang, G., Song, L. 2012. Air Handling Unit Supply Air Temperature Optimal Control during Economizer Cycles, Energy and Buildings, 49, 310-316.

Wang, G., Andiroglu, E., Sprinkle, J. E. 2015. Experimental Investigation of Energy Performance of a Variable-Frequency Drive on a Drive-Motor-Pump System. Submitted for presentation at the ASHRAE Annual Conference in Atlanta. ASHRAE Transactions, Volume 121, Part 2.

Wang, G. and M. Liu. 2005. Development of Power-head Based Fan Airflow Station, Proceedings of International Conference for Enhanced Building Operations 2005, Pittsburgh, Pennsylvania.

Wang, G. and M. Liu. 2007. Development of Motor Power Based Fan Airflow Station, Proceedings of Energy Sustainability 2007, Long Beach, California.

Wang, G., M. Liu and D. E. Claridge. 2010. Demonstration of an Energy Meter Using a Pump Flow Station. ASHRAE Transactions, v 116, Part 2.

Wang, G., Song, L., Park, S. 2013. Estimation of Induction Motor Circuit Parameters and Efficiency under Variable Frequencies. ASHRAE Transactions. Volume 119, Part 2.

Wang, G., Song, L., Andiroglu, E., Shim, G. 2014. Investigations on a Virtual Airflow Meter using Projected Motor and Fan Efficiencies. HVAC&R Research. 20(2):1-10.

Wang, H., 2014. Water Flow Rate Models based on the Pipe Resistance and Pressure Difference in Multiple Parallel Chiller Systems, Energy and Buildings, 75, 181-188.

Wang, Shengwei and Cui, Jingtan 2006. Robust Fault Detection and Diagnosis Strategy for Centrifugal Chillers. HVAC & R Research; 12(3):407-427.

Ward, Matthew and Siegel, Jeffrey. 2005. Modeling Filter Bypass: Impact on Filter Efficiency: ASHRAE Transactions, 111(1):1091-1100.

WEG. 2010. Technical Guide – Induction Motors Fed by PWM Frequency Inverters. WEG ELECTRIC CORP. S.A. Brazil

Wichman, A. and Braun, J.E. 2009. A Smart Mixed-Air Temperature Sensor. HVAC & R Research 15(1):101-115.

Wildi, T. 2002. Electrical Machines, Drives and Power Systems, 5th ed. Upper Saddle River, NJ: Pearson Education.

World Energy Council. (2010). Energy Efficiency: A Recipe for Success – Executive Summary. London.

Yan, A.; Zhao, J.; An, Q.; Zhao, Y; Li, H.; Huang. Y.; 2013. Hydraulic Performance of a New District Heating Systems with Distributed Variable Speed Pumps in South African Mine Cooling Systems. Applied Energy 112 (2013) 876–885

Yang, M., Yu, D., Xiong, J. and Li, H. 2011. A Methodology of Virtual Calibration and Its Applications in Building Systems. HVAC & R Research.

Yu, D., Li, H. Yu, Y., and Xiong, J. 2011. Virtual Calibration of A Supply Air Temperature Sensor in Rooftop Air Conditioning Units. HVAC & R Research, 17(1):31.

Yu, D., Li, H., and Yang, M. 2010. A Virtual Supply Airflow Meter for Rooftop Air Conditioning Units. Building and Environment, 46(6): 1292-1302.

Yu, Daihong. 2011. Virtual Supply Airflow Rate Meter in Rooftop Air Conditioning Units, Architectural Engineering – Dissertations and Student Research, Paper 6; Digital Commons at University of Nebraska-Lincoln.

Zhao, X., Yang, M., Li, H. 2014. Field Implementation and Evaluation of a Decoupling-Based Fault Detection and Diagnostic Method for Chillers, Energy and Buildings, 72, 419-430.

Zhao, X. 2015. Lab Test of Three Fault Detection and Diagnostic Methods' Capability of Diagnosing Multiple Simultaneous Faults in Chillers, Energy and Buildings, 94, 43-51.